THE
PHYSICAL REVIEW
A Journal of Experimental and Theoretical Physics Established by E. L. Nichols in 1893
VOL. 60, NO. 1 JULY 1, 1941 SECOND SERIES

Extensive Cosmic-Ray Showers and the Energy Distribution of Primary Cosmic Rays

NORMAN HILBERRY
University of Chicago, Chicago, Illinois
(Received May 19, 1941)

An experiment is described which determines the variation in the number of extensive cosmic-ray showers per unit time with altitude from sea level up to 4300 m. The number of showers which should have been observed with the apparatus used is calculated on the basis of the cascade theory in which various power law energy distributions for the primary cosmic rays are assumed. Good agreement is obtained between the observations and the calculation at high altitudes for suitable choice of parameters; at low altitudes the observed excess is what would be expected from a mesotron component in the extensive showers. It is found that the same choice of parameters which will give good agreement with the extensive shower data will also describe cosmic-ray observations at much lower energies. It is pointed out that this offers strong support for the hypothesis that there is but one type of primary cosmic-ray particle. The effects of choosing the proton as this primary particle are discussed.

INTRODUCTION

THE prodigious energy associated with extensive cosmic-ray showers is one of their most thought-provoking aspects. Auger and his co-workers[1] have estimated this energy to be above 10^{13} ev. The entire energy of such a shower has been attributed to a single primary particle incident at the top of the atmosphere. The cascade theory[2–5] accounts for the development from a high energy primary of the very large number of ionizing particles observed in these showers. On the basis of scattering in the atmosphere, Euler and Wergeland[6] have derived expressions which determine the spatial distribution of the shower particles about the axis determined by the direction of the incident primary particle. A fairly complete quantitative description is thus given of the number and spatial distribution of the ionizing particles in the shower at different depths in the atmosphere. Obviously, if the cascade theory is correct, the primary particles with energies greater than 10^{13} ev must acquire their energies from some physical process hitherto unknown in kind or at least in order of magnitude. It seems important, therefore, to determine how well the cascade theory does describe the behavior of these extensive showers, and to determine the energy distribution of the incident primary particles as quantitatively as possible.

The simplest attack on the problem is a determination of the variation in the number of extensive cosmic-ray showers as a function of altitude. If the cascade theory is adequate, the energy requisite for a primary incident on the top

[1] Auger, Maze, Ehrenfest and Fréon, J. de phys. et rad. **10**, 39 (1939). Auger, Ehrenfest, Daudin, Robley and Fréon, Rev. Mod. Phys. **11**, 288 (1939).
[2] H. J. Bhabha and W. Heitler, Proc. Roy. Soc. **A159**, 432 (1937).
[3] J. F. Carlson and J. R. Oppenheimer, Phys. Rev. **51**, 220 (1937).
[4] H. Snyder, Phys. Rev. **53**, 960 (1938).
[5] R. Serber, Phys. Rev. **54**, 317 (1938).
[6] H. Euler and H. Wergeland, Naturwiss. **27**, 484 (1939).

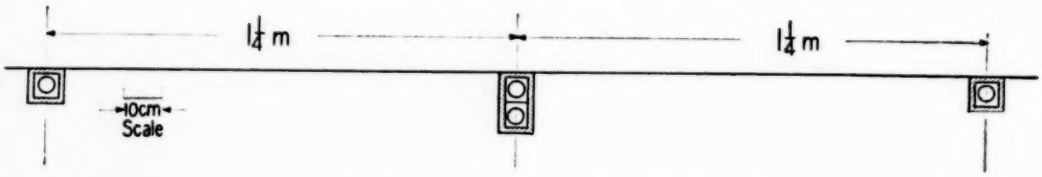

FIG. 1. Counter arrangement under the roof of the station wagon for the measurement of extensive cosmic-ray showers.

of the atmosphere to produce an observable shower at any given depth in the atmosphere is a sensitive function of that depth. Consequently, the number of extensive showers per unit time at any depth is a measure of the number of primary particles incident on top of the atmosphere with energies above a certain "cut-off" value. This latter is determined by the apparatus and by its depth in the atmosphere. Thus the variation of the number of showers with altitude should give definite information not only concerning the validity of the cascade theory but also a fairly quantitative determination of the energy distribution of the incident primary particles as well.

Since the number of showers observable with a given apparatus increases rapidly with decreasing depth in the atmosphere, it is important that the observations be extended to as high an altitude as possible. With this in mind, an experiment was so designed that observations could be made on the number of extensive showers over a range of altitudes from sea level at Chicago to 4300 meters at Mt. Evans, Colorado.

EXPERIMENT

To measure the number of these showers per unit time at various altitudes, a set of four argon and petroleum-ether filled Geiger-Müller tubes were mounted permanently just beneath the light wood and fabric roof of a Ford station wagon. All readings were taken in the open to eliminate any possibility of scattering from material above the counter set. Each counter was placed in an individual sheet-metal shielding can together with the first amplifier tube of the coincidence circuit. A one-half inch layer of Celotex was placed around each counter tube unit to furnish thermal insulation. One counter tube was mounted at the extreme forward end of the car, one at the extreme rear and the other two in vertical II-fold (twofold) coincidence midway between the extreme counters. The distance between the extreme counters was 2.5 meters (Fig. 1). Each counter had a diameter of 4 cm and an active length of 48 cm, giving an active area of 196 cm^2.

The counters were connected in fourfold coincidence by a conventional coincidence circuit and the usual precautions were taken to maintain constant working potentials on the G-M tubes and constant plate and grid potentials on the amplifier itself.

The counter tubes were mounted permanently in the station wagon to guarantee constant geometry throughout the experiment and thus facilitate alternation in the measurements at the various altitudes. The observational procedure was to take a run at one altitude for a period of from twelve to twenty-four hours; next, to take a run at a second station for a similar period; finally, to return to the first station for a final run to complete the set. This continual alternation of the observations at different altitudes with a fixed apparatus tends to eliminate errors due to slow variations in the cosmic-ray intensity or in the circuit itself. Actually, the latter effect was extremely small for the observations made in Chicago at the start of the expedition differed from those made after the return by less than the standard statistical deviation for the entire Chicago set.

The average depth below the top of the atmosphere for each observation station was determined by taking barometric readings for each run and averaging over the total counting interval.

The accidental counting rate was determined from the onefold counting rates for each G-M tube as measured with a scale 16 scaling circuit, from the twofold counting rate for the central pair and the twofold counting rate for the extreme G-M pair. The twofold rate for the

extreme pair was assumed to be entirely accidental, and this together with the onefold rate for each extreme counter gave the observed resolving time for the circuit. This procedure gives a maximum value and in all cases the value of the resolving time so measured was less than 10^{-4} sec. This resolving time was then used to compute the accidental counting rate for the present counter arrangement, which was treated as an effective threefold coincidence set with the onefold counting rates for the extreme counters and the vertical twofold rate of the central pair of counters as the onefold rate for a single effective central counter. In all cases the true fourfold accidental rate was completely negligible. The accidental rates so determined were, of course, also maximum values so that the accidental rate at Mt. Evans was less than the 0.1 count per hr. and that at Chicago was less than the 0.01 count per hr. computed for each respectively.

Table I gives the observed counting rates with their standard statistical deviations obtained by the above procedure.

Comparison with the Cascade Theory and Determination of the Energy Distribution

In order to interpret the experimental curve in terms of the validity of the cascade theory and to derive from it an expression for the energy distribution of the incident primary particles, it is necessary to carry through a complete calculation of the cascade process for all showers which can be detected by the counter system used. Since the validity of any conclusions based upon such a calculation depend upon the way in which the calculation is carried out, the method followed in the computation will be outlined in detail.

The computation is separable into three major parts: (1) the cascade computation itself for the development of the showers arising from a single incident primary particle of energy E, (2) the introduction of an energy distribution which will give the variation of counting rate with depth for vertically incident primary particles, and (3) the zenith angle calculation which then furnishes a quantitative description of the observed decrease of counting rate with depth in the atmosphere for a suitable choice of the parameters in the arbitrarily chosen energy distribution expression.

1. Cascade computation

(a) The first step in the cascade computation for a single incident ionizing particle is the solution of the cascade equations to determine the total number of ionizing particles, $n_{z,E}$ at a given depth z in the atmosphere, for a primary particle with a given incident energy E. For this purpose the cascade equations as given by Serber[5] and Snyder[4] were used. These equations express the number of ionizing particles as a function of the depth z below the surface of the atmosphere, the logarithm ϵ of the ratio of the incident energy to the critical energy in air, and an arbitrary parameter y. Values of the parameter ϵ were used corresponding to energies of the incident primaries of 1×10^{12} ev, 5×10^{12} ev, 1×10^{13} ev, $\cdots$, 1×10^{16} ev. The depth equation was then solved for each of these values of ϵ, to determine the values of the remaining parameter, y, corresponding to the depths 630 g/cm², 700 g/cm², 800 g/cm², $\cdots$, and 1100 g/cm². The equation for the number of ionizing particles, when solved for the above values of the parameters y and ϵ, yields the desired total numbers of ionizing particles, $n_{z,E}$ at each of the chosen depths due to incident primaries of each of the chosen energy values.

(b) *Determination of the spatial distribution* of the $n_{z,E}$ particles about the axis of the shower in the plane of observation. The axis of the shower is the direction of incidence of the primary particle. For this calculation the scattering formulas given by Euler[6] were used. While they are strictly valid only in the region of maximum development of the shower, the approximation is sufficiently good for the depths and energies here

Table I. *Extensive shower counting rate as a function of altitude.*

Place	Altitude Meters	Depth Below Top of Atmosphere in g/cm²	Counting Rate Counts/hr.
Mt. Evans	4320	628	24.1 ±0.3
Summit Lake	3900	658	20.5 ±0.5
Echo Lake	3100	709	14.0 ±0.5
Idaho Springs	2190	795	7.3 ±0.8
Denver	1610	854	5.0 ±0.4
Chicago	91	1025	1.47±0.15

considered. The values of the "half-width" of the shower in Euler's expression for the radial distribution were determined for each of the chosen depths and the expressions normalized to yield the proper values of $n_{z,E}$ when integrated over the entire plane of observation. These expressions then give the mean values of the surface densities of ionizing particles, $\rho_{z,E,r}$, at any distance r from the axis of a shower having a total number of particles at the depth z of $n_{z,E}$. Of course the actual distribution is statistical about this mean value.

(c) *Probabilities of observing extensive showers.* The probability ${}^{1}P_{z,E,r}$ that a single G-M counter tube of active area A will be struck by an ionizing particle when the counter tube is at any given distance r from the axis of the shower can be calculated readily from the mean particle density $\rho_{z,E,r}$. In the present case, the counter arrangement was not symmetrical about a vertical axis through its center. Consequently, to determine the probability of registering a threefold coincidence ${}^{III}P_{z,E,r}$ it was necessary to average over all orientations Φ of the counter set in the particle field. To do this the distance from the center of the counter arrangement to the axis of the shower was kept fixed at some value of r and the distances to each counter then determined for orientations of 0°, 30°, 60° and 90° between the radius vector from the counter set to the shower axis and the axes of the G-M tubes. The threefold coincidence probability was then calculated as:

$$ {}^{III}P_{z,E,r}=[{}^{1}P_{z,E,r'}]\times[{}^{1}P_{z,E,r}]\times[{}^{1}P_{z,E,r''}] $$

for each orientation, and the mean of these values (determined by a Simpson's rule calculation of the area under the ${}^{III}P_{z,E,r}(\phi)$ curve when necessary) gave the mean value of ${}^{III}P_{z,E,r}$. This orientation average was carried out in all cases for values of r of $\frac{1}{2}$, 1, 2, 3, 4 and 5 meters. For greater values of the radius the effect of the orientation was in general negligible and except in a few cases no appreciable error was introduced by computing ${}^{III}P_{z,E,r}$ as $[{}^{1}P_{z,E,r}]^{3}$. The orientation calculation was made for larger values of r in those cases where any sensible error would be introduced by the omission. The values of ${}^{III}P_{z,E,r}$ were extended in this fashion for values of r of 10, 15, 20, $\cdots$ out to 100 m in the case of the high energy primaries.

This means, of course, that there is a definite probability that a shower whose axis falls a distance r from the center of the counter arrangement will register a threefold coincidence. There is thus an "area of incidence" at the top of the atmosphere over which an incident particle of energy E will be effective in producing coincidences, and this area increases with the energy of the incident primary.

If, now, there are incident vertically on the top of the atmosphere N_E particles of energy E per cm² per sec., their contribution to the threefold counting rate of this counter set when incident at a distance between r and $r+dr$ will be

$$ N_E\,{}^{III}P_{z,E,r}\times 2\pi r dr $$

and the total contribution to the threefold counting rate will be

$$ {}^{III}R'_{z,E}=N_E\int_0^\infty {}^{III}P_{z,E,r}\times 2\pi r dr. $$

Since the integrand is an empirical function, this integration was carried out by a Simpson's rule determination of the area under the curve of ${}^{III}P_{z,E,r}2\pi r$ as a function of r. These numerical integrations were extended out to such values of r that contributions for still greater values of the radius were negligible. For the low energies the calculation could be stopped at 5 m or 10 m, while for the high energy primaries it was necessary to carry the calculation out to 90 m.

This process was repeated for each of the values of E at each depth z. The families of curves of ${}^{III}R'_{z,E}$ as a function of E for each z, and of ${}^{III}R'_{z,E}$ as a function of z for each E, were plotted as a check for possible arithmetical errors. Also, from these families of curves, values of ${}^{III}R'_{z,E}$ were interpolated for values of E intermediate between the values for which the computation had been carried out. The nature of the curves was such as to make this readily possible and sufficiently accurate. Thus the cascade computation has yielded a set of values of ${}^{III}R'_{z,E}$ for each of the energies (1, 2, 3, 4, 5, 6.25, 7.50, 8.75) $\times 10^{12}$ ev, (1, $\cdots$)$\times 10^{13}$ ev (1, $\cdots$)$\times 10^{14}$ ev, (1, $\cdots$)$\times 10^{15}$ ev, 1×10^{16} ev at each of the

chosen depths. The above values of the intermediate energies were chosen to facilitate a Simpson's rule integration over the energy intervals from 1×10^{12} ev-5×10^{12} ev, 5×10^{12} ev -1×10^{13} ev, $\cdots5\times10^{15}$ ev-1×10^{16} ev at the next stage of the computation.

2. Vertical counting rate *vs.* depth curves

For this it is necessary to make some assumption concerning the nature of the energy distribution of the incident primary particles. The usual form was adopted, that is

$$dN'_{0,\alpha}=N'_{0,\alpha}E^{-\alpha}dE,$$

where $dN'_{0,\alpha}$ represents the number of particles per sec. with energies between E and $E+dE$ incident vertically on each cm^2 of surface at $z=0$, the top of the atmosphere. $N'_{0,\alpha}$ and α are arbitrary parameters to be chosen to give the best possible quantitative description of the experimental observations. Various values have been used for α in the literature under various circumstances. In the present calculation, values of dE/E^{α} were computed for all of the above energies, including the interpolated values, for each value of α. The values of α chosen were 2.5, 2.6, $\cdots$3.0.

The total vertical extensive shower counting rate at each depth is now

$$^{III}R'_{z,\alpha}=N'_{0,\alpha}\int_0^{\infty}{}^{III}R'_{z,E}E^{-\alpha}dE.$$

Again the integrand is an empirical function and the integration was carried out by using a Simpson's rule determination of the area under the curve of $^{III}R'_{z,E}N'_{0,\alpha}E^{-\alpha}$ as a function of E. The calculation was extended to a value of E of 5×10^{15} ev which was sufficiently large to make the contributions from still higher energy groups negligible for the present counter arrangement.

3. Zenith angle computation

The calculation to this point gives a set of relationships between the vertical counting rate, $^{III}R'_{z,\alpha}$ and the depth z, for each of the chosen values of the exponent α. These relationships do not represent the variation of total counting rate with depth, however. The above relationships show that the variation of counting rate with depth is extremely rapid, so that a given change of zenith angle at small depths will produce a much smaller change of counting rate than the same change of zenith angle at a relatively great depth. Consequently, it is essential to make a computation of the zenith angle effect. This calculation is complicated for the present counter arrangement since the entire upper hemisphere of incidence is not open to threefold coincidences due to the fact that unless a single particle can produce a twofold coincidence in the central pair a true fourfold rather than a threefold coincidence is required in order to register a count. The geometry is simple, however, so that it is possible to determine the effective depths corresponding to any zenith angle across any chosen zone on the hemisphere of incidence, and the fraction of each such total zone which is open to threefold coincidences. For the present counter arrangement and depths, the contributions due to fourfold coincidences were negligible from the portion of the hemisphere of incidence closed to threefolds.

At the depth corresponding to the summit of Mt. Evans, the hemisphere of incidence was broken into zones at zenith angles of 0°, 21°6′, 30°, 36°58′, 42°57′, 48°19′ and 53°16′. The depth corresponding to this last zenith angle is 1050 g/cm^2 and the contribution from greater depths is negligible. Each of the first two zones was completely open to the threefold arrangement. Sixty-seven percent of the third zone was open, as was 48 percent of the fourth, 38 percent of the fifth and 31 percent of the sixth. At the 1000 g/cm^2 depth the contributions from zones beyond the second were negligible.

The contribution to the total counting rate from each zone was now determined from the vertical counting rate curves and the effective values of z sec θ across the zone. Again this was done by a Simpson's rule computation of the mean value. This mean value was multiplied by the value of the solid angle for that part of the zone open to the threefold arrangement and this gave the contribution from that zone to the total counting rate. The sum of these contributions from the various zones then gave the total counting rate at that depth. This, of course,

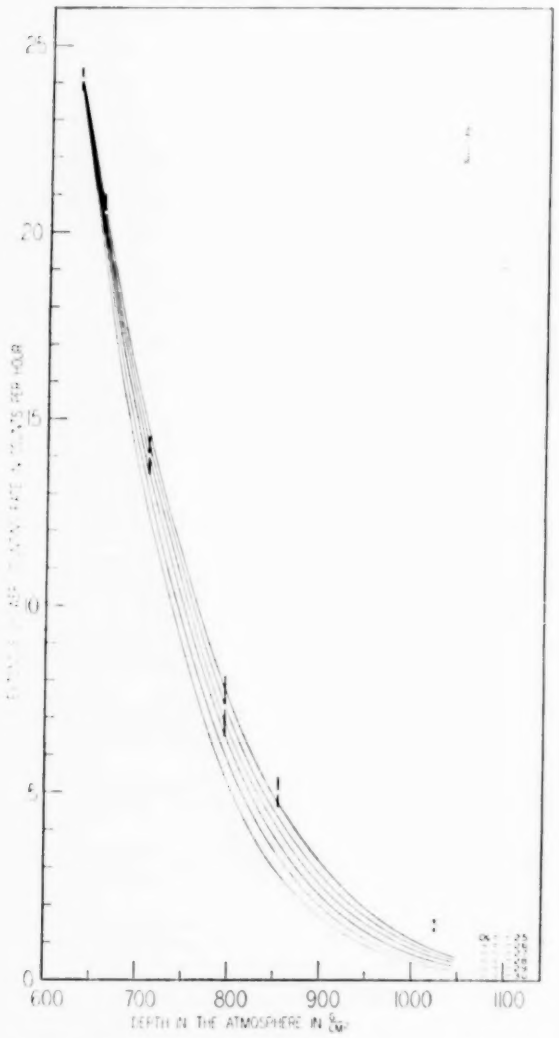

FIG. 2. The variation in the number of extensive cosmic-ray showers per unit time with depth in the atmosphere. The curves give the calculated variation for various choices of the power law exponent.

assumes that the primary particles are isotropically distributed in angle at the top of the atmosphere, which should be justified for the energies here involved ($>10^{13}$ ev).

Six such sets of values of counting rate as a function of depth were determined, one for each value of α used. Each contains a single undetermined constant, $N_{0,\alpha}$, which now represents the number of particles per cm² per sec. per unit solid angle incident at the top of the atmosphere. This constant was then adjusted so that the counting rate at Mt. Evans was the experimentally observed value of 24.1 counts per hr. These curves for ${}^{111}R_{z,\alpha}$ as a function of z for the various values of the exponent are shown in Fig. 2.

Discussion of Results

It will be seen from Fig. 2 that there is excellent agreement between the cascade computation and the experimental observations at the high altitudes, that is at Summit Lake and at Echo Lake, for values of the exponent lying between 2.6 and 2.8. At the lower altitudes, particularly at Chicago, there is definite disagreement for all values of the exponent. As pointed out in a recent note,[7] this discrepancy can be explained qualitatively on the basis of a mesotron component accompanying these extensive showers. With this in mind, the choice of the best value of the exponent must be made from the high altitude observations. Here the electron-photon component is most fully developed and consequently the relative contribution of the mesotron component to the total spatial distribution of ionizing particles in the shower is very small. The Echo Lake observation is at an altitude sufficiently high for the mesotron correction to be small and yet far enough below Mt. Evans for the differences between the calculations for the different values of the exponent to become appreciable. Basing the choice, therefore, on this point, the best value of the exponent would appear to be 2.70 or somewhat larger, although any value from 2.6 to 2.8 is permissible.

The selection of a particular value of the exponent based on the present data alone is not as well defined as could be desired. On the other hand, the value of the coefficient which must be associated with any given choice of the exponent is much more precisely determined. This arises from two facts; first, that the Mt. Evans observation is the best determined of the experimental counting rates; and second, that the cascade computation itself is most completely valid at high altitudes where the showers are most fully developed. The relationship between the coefficient and the exponent as determined by the present data and computations is

$$\log_{10}(N_{0,\alpha}) = 12.146 + 14.55(\alpha - 2.5) - \tfrac{1}{2} \times 1.1 \times (\alpha - 2.5)(\alpha - 2.4) \quad 2.5 \leqq \alpha \leqq 3.0.$$

[7] N. Hilberry, Phys. Rev. **59**, 763 (1941).

If numerical agreement with the extensive shower observations at the top of Mt. Evans is to be obtained, this expression must be satisfied for any choice of the exponent. To obtain good agreement with the Echo Lake observations α is limited to the range between 2.6 and 2.8.

Figure 3 shows in the full curve the graph of $d(NE)/dE$ over the energy range up to 5×10^{10} ev as predicted by this energy distribution expression with α equal to 2.75. It should be emphasized that this expression has been derived from observations involving primary particles chiefly in the energy range from 5×10^{13} ev to 5×10^{15} ev. In this case, the energy distribution expression becomes:

$$dN = 5.4_5\times10^{15}E^{-2.75}dEd\omega.*$$

The dotted curve in Fig. 3 is that published by Bowen, Millikan and Neher[8] and the blocks represent their experimental observations. The broken curve in Fig. 3, for energy values less than 1.0×10^{10} ev, has been obtained in the same manner as that of Bowen, Millikan and Neher by adjusting it so that the areas under the curve are kept equal to those of the corresponding blocks. As will be seen, the present curve fits the experimental observations remarkably well. In obtaining it, it has been assumed that over the major part of the observed energy range the particles are isotropically distributed at the top of the atmosphere.

Integration of the energy distribution expression to determine the energy per cm^2 per sec. carried into the top of the atmosphere from all directions by particles in various energy bands gives a value of 9.7×10^8 ev for those particles with energies above 1.7×10^{10} ev as compared with the Bowen, Millikan and Neher observation of 9.4×10^8 ev. In the band from 0.67×10^{10} ev to 1.7×10^{10} ev, the present expression gives 9.8×10^8 ev as compared with the experimental observation of 8.7×10^8 ev. Since the observed distribution has already dropped well below the power law in the lower part of this energy range, this agreement is also satisfactory.

If 2.74 is used for α, the energy which should be carried in by particles with energies above 1.7×10^{10} ev drops to 9.0×10^8 ev but it then becomes very difficult to fit a smooth curve to the experimental observations below 1.0×10^{10} ev. On the other hand, the choice of 2.76 for α makes possible a smooth fit below 1×10^{10} ev but the energy which particles above 1.7×10^{10} ev should carry in then becomes 10.5×10^8 ev and this is definitely in poorer agreement with the observations than the result given by the expression with $\alpha=2.75$.

It would seem, therefore, that a single power law expression is capable of describing the distribution of the number of primary cosmic-ray particles per unit energy range from energies of 10^{16} ev down to energies of 10^{10} ev.

The question immediately arises as to why a deviation from this power law should set in at 1×10^{10} ev, since this is a very high energy value to be affected by the solar magnetic field.[9] A *Letter to the Editor* by Carlson and Schein[10] now in press suggests that a large amount of energy is carried away by neutrinos in the disintegration of the mesotrons. If some such hypothesis is correct, the present power law may be valid down to energies even lower than 1×10^{10} ev. Thus if the total energy carried into the top of the atmosphere at Omaha be computed from the present

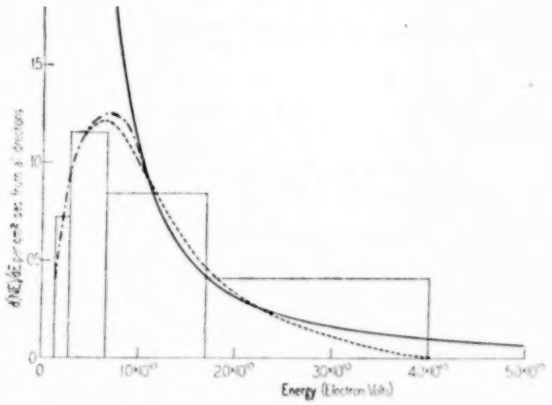

FIG. 3. The energy distribution curve in the region of 10^{10} ev. The full curve gives the present power law expression. The dotted curve is the curve of Bowen, Millikan and Neher and the blocks represent their experimental observations. The broken curve is the present power law distribution adjusted below 10^{10} ev to fit the experimental observations.

* The value of the coefficient, 5×10^{15} given in the previous note[7] was taken from a linear logarithmic graph of coefficient against exponent. In re-evaluating the coefficient-exponent relationship, the more precise formulation seemed justified.

[8] Bowen, Millikan and Neher, Phys. Rev. **53**, 855 (1938).

[9] P. Epstein, Phys. Rev. **53**, 862 (1938).

[10] J. F. Carlson and M. Schein, Phys. Rev. **59**, 840 (1941).

expression, the value is 3.54×10^9 ev per cm^2 per sec. from all directions as compared with the experimental observation of Bowen, Millikan and Neher of 2.25×10^9 ev per cm^2 per sec. There is then a discrepancy of 37 percent between the energy carried into the atmosphere as calculated and that observed, as compared with the loss of approximately 40 percent given by Carlson and Schein for the neutrino loss in the same energy range. On this basis it would seem possible that the power law given here may hold down to an energy considerably below 10^{10} ev.

The validity of a single energy distribution expression over an energy range from 10^{16} ev to 10^{10} ev or lower indicates strongly that there is but one predominant type of primary cosmic-ray particle. The recent experiments of Schein, Jesse and Wollan[11] indicate that these particles are protons. This suggestion has been made previously by R. Gunn[12] and W. F. G. Swann.[13] Others[14,15] have emphasized protons as responsible for the penetrating component. It must now be determined whether or not primary protons obeying the energy distribution given here are capable of accounting for the soft component of cosmic rays, the observed mesotron energy distribution and the extensive shower phenomena. The recent discussions by Swann[13] and by Carlson and Schein[10] describe the way in which the soft component can arise from such incident protons, and the mean energies used in their calculations are in good agreement with those computed from the present expression.

As pointed out in the previous note,[7] this energy distribution is capable of accounting qualitatively, likewise, for the mesotron distribution observed by V. C. Wilson[16] in his deep mine measurements.

The choice of the proton as the primary cosmic-ray particle has also certain advantages[7] from the point of view of the mesotron component in extensive showers. On the other hand, for the analysis presented here to furnish a valid description of the primary energy distribution, it is essential that practically the entire energy of a primary proton in the range above 10^{13} ev be transferred to electrons and photons very near the top of the atmosphere. It is possible that the radiation cross section of the proton in this energy range may prove to be sufficiently large to account for this energy transfer directly. If, however, the hypothesis of the explosive production of mesotrons by protons[12,10] proves to be justified, it would seem possible that it is this process which forms the first step in the genesis of an extensive shower. In the latter case, a large multiplication with a consequent large division of energy occurs in a single event practically at the top of the atmosphere. This would leave a group of extremely high energy mesotrons very near the top of the atmosphere as the second stage in the development of an extensive shower.

The next phase in the growth of the shower would depend on the behavior of the mesotron at these extremely high energies. Little is known with certainty from the theoretical standpoint concerning the nature of the mesotron. Experimentally, however, some information can be deduced from the absorption curves of V. C. Wilson.[16] If the decrease in intensity of the mesotrons with depth is due mainly to ionization loss as is almost certainly true, Wilson's absorption curve gives the integrated energy distribution for the very energetic mesotrons and, as pointed out before, this agrees well with the present primary proton distribution assuming a fairly constant production cross section at these high energies. There is a sudden change in this mesotron energy distribution, however, at a depth of about 250 m water equivalent, corresponding to an energy in the neighborhood of 10^{11} ev. For greater depths, the change of intensity with depth is much more rapid. The actual exponents for Wilson's absorption curve are -1.77 corresponding to energies less than 10^{11} ev and -2.52 for energies greater than this value. This marked break in the mesotron energy distribution indicates either that many fewer mesotrons are formed above this energy value or else that those formed in this range lose energy rapidly until they fall below this critical value.

[11] Schein, Jesse and Wollan, Phys. Rev. **59**, 615 (1941).
[12] R. Gunn, Terr. Mag. **38**, 247 (1933).
[13] W. F. G. Swann, Rev. Mod. Phys. **11**, 251–254 (1939); Phys. Rev. **58**, 200 (1940).
[14] A. H. Compton and H. A. Bethe, Nature **134**, 734 (1934).
[15] T. H. Johnson, Rev. Mod. Phys. **10** (1938); **11**, 208 (1939).
[16] V. C. Wilson, Phys. Rev. **53**, 337 (1938); Rev. Mod. Phys. **11**, 230 (1939).

There appears to be no reason why mesotrons should not be formed at high energies unless the radiation cross section of the proton in this energy range becomes large in comparison with the mesotron production cross section, which itself must be very great. In such a case the radiation of the mesotron would not be required as an intermediate process in the transfer of the energy from the proton to the shower particles. The proton itself would then be the shower-producing particle.

If the high energy mesotrons are formed abundantly, radiation from those with energies over 10^{11} ev must be assumed. This is in accord with the conclusion arrived at by Christy and Kusaka[17] in their analysis of bursts. The value of the radiation cross section must become large above approximately 10^{11} ev to account for the magnitude of the break in Wilson's energy distribution. On this basis, the third step in the formation of an extensive shower would be the transfer of energy from the energetic mesotrons to photons by successive radiation until the mesotron energy has dropped below the 10^{11} ev value. Since the minimum initial energy of the mesotrons in the present case would have been above 5×10^{12} ev this means that all but one or two percent of the energy of the softest mesotrons entering into extensive shower production would go into photons and electrons. This would mean that even for the lowest energy protons which make any appreciable contribution to the counting rates observed in the present experiment, all but some ten percent of the energy of the initial proton eventually would go into typically developing shower particles. For the majority of the protons, the energy carried off by the mesotrons would be very much smaller.

It is probably true that a certain fraction of the photon energy is also converted back into slow mesotrons,[18–20] but this again should have but a relatively small effect upon the total energy appearing in shower particles at high altitudes, and consequently in the total number of ionizing particles reaching the plane of observation.

It would thus seem quite possible for a primary proton to generate an extensive shower which would differ from an electron generated shower of the same initial energy at depths of sixteen or more cascade radiation units below the top of the atmosphere by less than the errors in the present observations and those inherent in cascade computations of the kind here carried out. Consequently, it would still appear justifiable to assume that the expression here given does represent approximately the energy distribution of the primary protons in the energy range from 10^{16} ev to 10^{10} ev.

In conclusion, the author wishes to express his indebtedness to Professor A. H. Compton for his advice and encouragement throughout the progress of this work, and to thank Professor Bruno Rossi for his advice on the arrangement of the experiment and for discussion of results during the expedition. To Professor Joyce Stearns of Denver University, whose unfailing thoughtfulness and assistance play such a large part in the success of any Mt. Evans expedition, the author is deeply grateful.

[17] R. F. Christy and S. Kusaka, Phys. Rev. **59**, 414 (1941).

[18] M. Schein and V. C. Wilson, Rev. Mod. Phys. **11**, 292 (1939).

[19] Schein, Jesse and Wollan, Phys. Rev. **57**, 847 (1940).

[20] L. Janossy and P. Ingleby, Nature **145**, 511 (1940).

On the Angular Distribution of Alpha-Particles Produced in the Li^7-Proton Reaction

CHARLES L. CRITCHFIELD*
Princeton University and the Institute for Advanced Study, Princeton, New Jersey

AND

EDWARD TELLER
George Washington University, Washington, D. C.

(Received April 28, 1941)

The angular distribution of the alpha-particles ejected in the reaction, $Li^7+H^1\rightarrow 2\,He^4$, is discussed. It is assumed that the Li^7-nucleus is odd, that the incident proton is in a P state and that a broad and a sharp nuclear resonance level participate in the reaction. The angular momentum 0 and 2 $\hbar$ are assigned to the broad and to the sharp levels, respectively. The constants entering into the theory could be determined only by extending the measurements on angular dependence to proton energies higher than 400 kev. The results are in qualitative agreement with the dependence on energy of the reaction yield and of the angular distribution observed so far.

INTRODUCTION

RECENT experiments[1] have revealed a marked departure from spherical symmetry in the distribution of alpha-particles created by the transmutation

$$Li^7+H^1\rightarrow 2He^4. \qquad (1)$$

In these experiments a thin film of lithium was bombarded by protons of energy ranging from 100 to 400 electron kilovolts. The emitted alpha-particles have a total of about 17 Mev kinetic energy. The relative number of alpha-particles was determined at angles of eight different cosines and for eight different energies of the incident protons.

In the center of mass coordinate system the relative number of alpha-particles per unit solid angle is represented very well by the factor $1+A(E)\cos^2\theta$; here θ is the angle between the direction of the emerging particles and the direction of the incident proton beam. The coefficient which gives the departure from spherical symmetry, $A(E)$, is positive and small at 100 kev, rises to a value of $\frac{1}{3}$ at 300 kev and then rises rapidly to about $\frac{3}{4}$ at 350 and 400 kev. A plot of $A(E)$ is reproduced in Fig. 1.

It is greatly to be desired that the experiments be carried out for proton energies greater than 400 kev.

As was pointed out by those who did the experimental work the behavior of $A(E)$ suggests an approach to a resonance level of the compound, Be^8, nucleus. In the present paper the expected theoretical behavior of the angular distribution of alpha-particles in the neighborhood of such a resonance is examined in detail. It is assumed that the alpha-particles which are ejected at energies outside the apparent resonance region are due to a second, but very much broader, resonant level of the compound nucleus.

The energy-dependence of the *yield* curve[2]

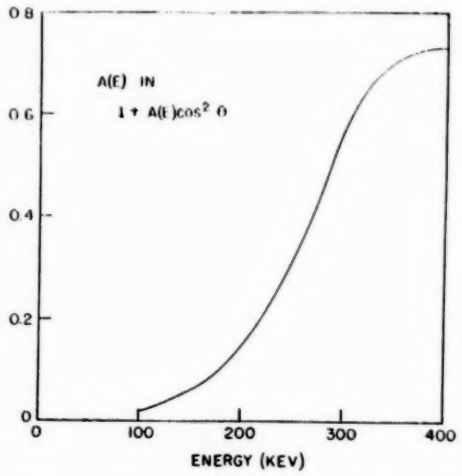

FIG. 1. The variation with bombarding energy of $A(E)$ in the factor, $1+A(E)\cos\theta$, which represents the experimental results on the angular distribution of alpha-particles.

* National Research Fellow.

[1] V. J. Young, A. Ellett and G. J. Plain, Phys. Rev. **58**, 498 (1940).

[2] L. H. Rumbaugh, R. B. Roberts and L. R. Hafstad, Phys. Rev. **54**, 657 (1938).

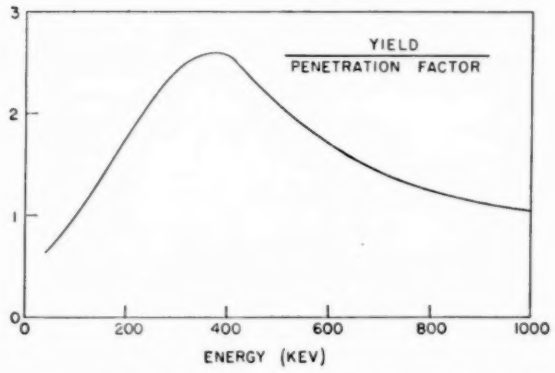

FIG. 2. The ratio of experimentally found yield to the calculated penetration factor as a function of the bombarding energy. Experimental results for energies above 350 kev were taken from reference (2), those between 150 kev and 350 kev from the paper of Herb, Parkinson and Kerst, Phys. Rev. **48**, 118 (1935), and those below 150 kev from the letter of Heydenburg, Zahn and King, Phys. Rev. **49**, 100 (1936). These three sets of results were joined to form a smooth curve on an arbitrary scale. The penetration factor used here is F_1^2/ρ in the notation of reference (3).

measured for alpha-particles ejected at right angles to the incident protons corroborates the presence of two processes giving rise to the emission of the alphas. Figure 2 shows the ratio of the yield and the penetration factor for protons (in arbitrary units). The penetration factor was calculated from the tables of Yost, Wheeler and Breit[3] by assuming a P wave and an effective collision radius of 4×10^{-13} cm (the last two assumptions are of minor importance in determining the shape of the curve). The figure shows the presence of a process that depends on the energy practically only through the penetration factor and a second process which has a resonance around 400 kev. As will appear later we shall associate the former process with a $J=0$ compound state, the latter with a $J=2$ state. The parallelism of the yield curve with the energy dependence of the angular distribution is striking. In view of our conclusions to be given below it would be more satisfactory if the maximum in Fig. 2 occurred at higher energy than the maximum deviation from spherical symmetry. But too much reliance must not be placed upon conclusions based on the ratio in Fig. 2. The resonance in this figure extends over so wide an energy range that the slowly varying influence of the energy on the yield may cause a difference between the position of the apparent maximum and the position of the resonance.

The angular distribution of ejected alpha-particles will thus depend upon the simultaneous influence of two nuclear levels. Under this condition the relative phase of the particles coming from the two resonance levels will be of importance. In most of the considerations involving dispersion theory, intensities alone were important; but in at least one example, the scattering of neutrons by He, phase relations had to be taken into account.[4] In the subsequent discussion the superposition of outgoing alpha-rays with different phases will lead in general to a sigmoid dependence of the quantity $A(E)$ (from the factor $1+A(E)\cos^2\theta$) on the energy of incident protons. This sigmoid dependence is not unlike the dispersion curve in optics. The shape of both curves is due to essentially similar resonance denominators in the dispersion formula and the similarity of the curves helps to emphasize that the dispersion theory of nuclear reactions and the dispersion theory in optics have more in common than a name.

STATISTICS AND PARITY

The disintegration (1) in the energy range involved permits of a fairly simple theoretical discussion. Alpha-particles obey Einstein-Bose statistics so that a pair of them can be produced only in states of even orbital angular momentum and even parity; since the spin is zero the allowed states may be designated ^1S, ^1D, $^1G\cdots$. Furthermore the ground state of Li^7 is well known to have a nuclear spin of $\frac{3}{2}$, whereas the parity of this state has not been experimentally determined. Theoretical predictions both from the individual particle model and the alpha-particle model are that the ground state of the Li^7 nucleus is odd. In this case only P, F, $\cdots$ states of the incident proton will be able to form the even compound nucleus Be^8. Computing the intensities of P and F "regular" solutions to the Schroedinger equation in a Coulomb field[3] it is found that the P wave is over 1000 times stronger than the F wave for particles of 200 kev. Even up to 1 Mev the F wave is inappreciable so if the parity of the

[3] F. L. Yost, J. A. Wheeler and G. Breit, Terr. Mag. 443 (December, 1935).

[4] F. Bloch, Phys. Rev. **58**, 829 (1940).

Li^7 nucleus is odd only the P wave need be taken into account. The relatively small yield of reaction (1) also points to the process being due to an incident proton in a P wave rather than in an S wave.[5]

If it is assumed that the reaction (1) is produced by protons in a P wave the experimental angular distribution, $1+A(E)\cos^2\theta$, can be readily understood. Since the bombarded nuclei are completely unpolarized and since the spins of the incident protons are also unpolarized the emitted beam cannot show more complicated transformation properties under rotation of coordinates than those of the orbital motion in the incident beam. Thus the emitted beam may contain a part which behaves as a vector and gives a $\cos^2\theta$ term but no higher powers of $\cos\theta$ if the incident wave function transforms like a vector, i.e., if it is a P wave. The Bose statistics of the alpha-particles excludes odd powers of $\cos\theta$ so that in fact $1+A(E)\cos^2\theta$ is the most general angular dependence to which incident P waves can give rise.

Although there are many indications that Li^7 nuclei are odd the possibility that they are even is not to be overlooked. In this case the incident proton must have an even wave function and an even angular momentum. In the angular distribution of the alpha-particles the term $A(E)\cos^2\theta$ might be explained as due mainly to an interference term produced by an incident S wave and a less effective incident D wave. The square of the amplitude of the outgoing alpha-particle wave function produced by the incoming D wave contains in general a term proportional to $\cos^4\theta$. But if the incoming D wave is relatively ineffective in producing the reaction, the $\cos^4\theta$ term may have too small a coefficient to be observed experimentally. The $\cos^2\theta$ term depending linearly on the small amplitudes produced by the incident D wave would in fact be much more noticeable than the $\cos^4\theta$ term depending quadratically on the same amplitude. On the basis of present experimental evidence it is not quite impossible that Li^7 nuclei are even and the $1+A(E)\cos^2\theta$ angular dependence is produced by joint action of incident S and D waves. But in principle it is possible to establish the odd parity of the Li^7 nucleus by eliminating experimentally in the reaction products the $\cos^4\theta$ terms to a high accuracy thus demonstrating that the angular dependence is not produced by an incident D wave.

It will be assumed in the following calculations that the Li^7 nucleus is odd and it will be shown that the experimental data obtained so far may be understood with this assumption. The incident proton P wave has a total angular momentum of $\frac{3}{2}h$ at most and this combined with the $\frac{3}{2}h$ of the nucleus can give rise to all integral angular momenta from 0 to $3h$ for the compound nucleus. Outgoing alphas are therefore either in ^1S or ^1D states. From the shape of the experimental curve for $A(E)$ one would judge that a resonance in one or the other of these states is approached as the proton energy increases. Below the apparent resonance, *e.g.*, at 100 kev, the angular distribution approaches spherical symmetry. Barring very special types of interaction which would make the angular distribution due to a compound nucleus of $J=2$ spherically symmetric it appears that the alpha-particles of low bombarding energies are ejected from a compound nucleus of $J=0$.

Dispersion Formula

In view of the probable applicability of the simple conditions discussed above we have calculated the expected angular distribution of alpha-particles in reaction (1). For this purpose the dispersion formula of wave mechanics as presented by Breit and Wigner[6] and Bethe and Placzek[7] has been used. According to the dispersion theory as applied to the calculation of the cross section $\sigma^P{}_Q$ of the nuclear transformation $P\rightarrow Q$

$$\sigma^P{}_Q=4\pi^3\lambda^2\left|\sum_r \frac{H^P{}_r H^r{}_Q}{E_P-E_r+\frac{1}{2}i\gamma_r}\right|^2. \qquad (2)$$

In Eq. (2) $H^P{}_r$ is the matrix element of the Hamiltonian which couples the initial state P with the compound (resonant) state r; $H^r{}_Q$ is the same thing for the final state Q. Both P and Q may be degenerate, and there are many levels r. E_P is the energy of the initial state, E_r the energy of the intermediate state and γ_r is the level

[5] M. Goldhaber, Proc. Camb. Phil. Soc. **30**, 561 (1934).

[6] G. Breit and E. Wigner, Phys. Rev. **49**, 519 (1936).

[7] H. A. Bethe and G. Placzek, Phys. Rev. **51**, 450 (1937).

width.[8] In calculating γ_r one must take into account all possible modes of decay of the state r. In the present problem the most probable method is just the emission of two alpha-particles and in this case

$$\gamma_r \cong 2\pi \sum_Q |H^r{}_Q|^2, \tag{3}$$

where the summation extends over the degenerate states Q.

We are interested in intermediate states, r, of two different angular momenta, 0 and $2h$, which have resonances in the region of the experimental results and which are eigenstates of the angular momentum. The initial state P is a Li^7 nucleus with a total angular momentum $\frac{3}{2}h$ plus an incident proton with an orbital angular momentum h and a spin momentum $\frac{1}{2}h$. Thus the initial state does not appear as an eigenstate of the total angular momentum. By proper linear combinations of the initial states with various orientations of angular momentum (including the three possible orientations of the P wave) one can construct eigenstates of the total angular momentum which we shall call X_r. The subscript r indicates that X_r has the same transformation properties with regard to rotation as the intermediate state r. It will be seen that two functions can be constructed with angular momentum $J=2$. We shall call X_2 that linear combination of them to which the intermediate state r with $J=2$ responds most strongly. The orthogonal linear combination is then not coupled at all with the compound nucleus. The construction of the state X_0 (which is invariant under rotations) is unique.

The matrix element $H^P{}_r$ in the numerator of Eq. (2) may then be written in the form

$$H^P{}_r = \varphi'(E)\alpha'_r(P, X_r). \tag{4}$$

Here (P, X_r) is the transformation coefficient from the state P to the state X_r. The matrix element connecting X_r and r has been written as a product of two factors: the energy independent complex number α'_r and the energy dependent $\varphi'(E)$. We shall assume $\varphi'(E)$ to be the same function for all intermediate states involved. This assumption is probably approximately valid over the relatively narrow energy region of the resonance. Actually the most important reason for the energy dependence of $\varphi'(E)$ is the variation of the penetration factor. This variation will not depend greatly on the nature of the intermediate state ($J=0$ or 2) over a narrow resonance region as long as the angular momentum of the initial wave (which is a P wave) is the same.

The final state Q is represented by two alpha-particles the wave function of which can be regarded as plane waves which describe the ejection of those alphas in a definite direction characterized by the angle θ. This final state will again not be an eigenstate of the angular momentum. We may introduce an eigenstate Z which can be obtained by superposition of the final states corresponding to various directions θ. The matrix element $H^r{}_Q$ can then be written

$$H^r{}_Q = \alpha''_r\varphi''(E)(Z, Q), \tag{5}$$

where the symbols have a similar significance as in Eq. (4). The transformation coefficient (Z, Q) is proportional to the surface harmonic (normalized Legendre polynomials) $Y_r(\theta)$. Here the index r refers to the intermediate state and is meant to specify both the angular momentum J and its component, m, around the direction of the incident protons. The surface harmonic $Y_r(\theta)$ can be assumed to be normalized since we still carry the numerical coefficient α''_r. The energy dependence of $\varphi''(E)$ is negligible in the region of resonance due to the high energy of the ejected alpha-particles. It follows from the same reason that according to Eq. (3) we may replace γ_r by an energy-independent quantity Γ_r. The equation for angular distribution then becomes

$$1+A(E)\cos^2\theta \sim \left|\sum_r \frac{\alpha_r(P, X_r)Y_r(\theta)}{E_P - E_r + \frac{1}{2}i\Gamma_r}\right|^2. \tag{6}$$

Here $\alpha'_r\alpha''_r$ has been set equal to α_r and the factors $\varphi'(E)\varphi''(E)$ common to all terms on the right-hand side have been dropped.

Spin-Orbit Coupling

The incident proton is assumed to have orbital angular momentum $L=1$ for the reasons given in the introduction. There is certainly no component of this orbital angular momentum about

[8] As has been shown by G. Gamow, *Atomic Nuclei and Nuclear Transformations* (Cambridge, 1937), p. 96, the energy of the unstable state r may be considered to be the complex value $E_r - \frac{1}{2}i\gamma_r$; the $\frac{1}{2}i\gamma_r$ gives the exponential decrease of the amplitude in that state with time.

the direction of bombardment so the states X_r cannot be obtained as a direct superposition of the initial states. From the $j=\frac{3}{2}$ of the Li^7 nucleus and the spin of the incident proton we may compose two states: a threefold degenerate state, P_3, in which the proton spin is opposite to the Li spin and a fivefold degenerate state, P_5, in which the proton spin is parallel to the Li spin. The plane wave describing the proton appears as a factor in both P_3 and P_5. It is evident that only P_3 can form a compound nucleus of $J=0$ and contribute to the resulting S wave. Both P_3 and P_5 are able to form compound states with $J=2$. Thus two intermediate states with $J=2$ can be constructed.

If there is no significant spin-orbit interaction, i.e., if the splitting caused is smaller than the level width it would seem most likely from experimental results on magnetic moment that the ground state of Li^7 nuclei can be described as $^2P^\circ_{1\frac{1}{2}}$. In this case the spin of the odd nuclear particle is parallel to the orbital angular momentum and then P_3 alone can contribute to the ^1D wave of alpha-particles; for the spin in the P_5 is parallel to that in $^2P^\circ_{1\frac{1}{2}}$ and in the absence of spin-orbit interaction the compound nucleus would remain in the triplet state. The two resonant energy levels with $J=2$ coincide when there is no spin-orbit interaction but only P_3 gives rise to alpha-particles.

We shall define strong spin-orbit interaction to be strong enough to separate the two levels with $J=2$ by an amount large compared with the level width. Resonance with one of these levels will be considered as important in the energy range around 400 kev. The more general case in which the levels are separated only by an energy comparable to their widths will not be presented. For the problem at hand the neglected level may be at higher energy than the one revealed so far in the experiments or it may be at negative bombarding energy and thus unattainable in the reaction. Further consideration will be limited to resonance with two compound states, one with $J=0$ which will be designated r_0 and one with $J=2$ which will be called r_2.

As has been stated above, the resonant state r_2 responds most strongly to the linear combination X_2. To any orthogonal linear combination r_2 will not respond at all. In the next section we shall construct two states with $J=2$ which we shall call $X_2^{(3)}$ and $X_2^{(5)}$. The state $X_2^{(3)}$ is constructed to be orthogonal to P_5 and $X_2^{(5)}$ orthogonal to P_3. We may express X_2 as a linear combination of these two states

$$X_2=X_2^{(3)}\cos\xi+X_2^{(5)}\sin\xi,$$

where ξ is a real number.[9] The state

$$X_2^{(3)}\sin\xi-X_2^{(5)}\cos\xi$$

will not be coupled with r_2. It may be noted that the case of no spin-orbit coupling is represented by $\xi=0$. In this case a nuclear state interacting with $X_2^{(5)}$ is present in the resonance region but this state does not disintegrate into two alpha-particles. For strong spin-orbit coupling $\xi=0$ is also possible but in this case a nuclear state interacting with $X_2^{(5)}$, though it can disintegrate into two alphas, falls into a region sufficiently far removed from the one under consideration.

Since P_3 alone is coupled with the nuclear state with $J=0$ one may substitute (P_3, X_0) for (P, X_0) in Eq. (6). Similarly $X_2^{(3)}\cos\xi+X_2^{(5)}\sin\xi$ is alone responsible for the excitation of the nuclear state with $J=2$. Substituting this expression in those terms of Eq. (6) which contain the second surface harmonic we obtain

$$\begin{aligned}1+A(E)\cos^2\theta \sim{}& \sin^2\xi\sum_{m=-2}^{2}\left|\frac{\alpha_2(P_5, X_2^{(5)m})\,Y_2^m(\theta)}{E_P-E_2+\frac{1}{2}i\Gamma_2}\right|^2 \\ &+\sum_{m=-1}^{1}\left|\frac{\alpha_0(P_3, X_0)\,Y_0(\theta)}{E_P-E_0+\frac{1}{2}i\Gamma_0}\right. \\ &\left.+\cos\xi\,\frac{\alpha_2(P_3, X_2^{(3)m})\,Y_2^m(\theta)}{E_P-E_2+\frac{1}{2}i\Gamma_2}\right|^2, \qquad (7)\end{aligned}$$

where the magnetic quantum number m is made explicit. Since waves of different m values and P_3 and P_5 have no phase relation, mixed products containing different m values and P_3 and P_5 are omitted. Terms $(P_3, X_2^{(5)})$ and $(P_5, X_2^{(3)})$ have been omitted because of the assumed orthogonality relations.

[9] There is no phase relation between the initial states P_3 and P_5 so that interference terms between P_3 and P_5 do not occur. Thus only absolute values of the coefficients of $X_2^{(3)}$ and $X_2^{(5)}$ matter and we can use the sine and cosine of a real number for these coefficients without loss of generality.

TABLE I. *Transformation coefficients.*

m	$(P_3, X_2^{(3)})$	$(P_5, X_2^{(5)})$	ANGULAR DEPENDENCE
2	0	$-\frac{1}{3}\sqrt{6}$	$(15/8)^{\frac{1}{2}}e^{2i\varphi}\sin^2\theta$
1	$\frac{1}{2}\sqrt{2}$	$-\frac{1}{6}\sqrt{6}$	$(15/2)^{\frac{1}{2}}e^{i\varphi}\sin\theta\cos\theta$
0	$\frac{1}{3}\sqrt{6}$	0	$(5/4)^{\frac{1}{2}}(1-3\cos^2\theta)$
-1	$\frac{1}{2}\sqrt{2}$	$\frac{1}{6}\sqrt{6}$	$(15/2)^{\frac{1}{2}}e^{-i\varphi}\sin\theta\cos\theta$
-2	0	$\frac{1}{3}\sqrt{6}$	$(15/8)^{\frac{1}{2}}e^{-2i\varphi}\sin^2\theta$

CALCULATION OF MATRIX ELEMENTS

Let "a" represent the normalized wave function of the nucleus. It is fourfold degenerate having components $a_{1\frac{1}{2}}$, $a_{\frac{1}{2}}$, $a_{-\frac{1}{2}}$, $a_{-1\frac{1}{2}}$. Similarly let b_1, b_0, b_{-1} describe the normalized incident P wave of the proton and $s_{\frac{1}{2}}$, $s_{-\frac{1}{2}}$ the spin state of the incident proton. The subscripts give the z component of the angular momentum of each state. We take the direction of bombardment as the z axis so that the only component of b which appears in P_3 and P_5 is b_0.

Incident waves P_3 and P_5 are then described as follows:

$$\begin{gathered}\tfrac{1}{2}[a_{\frac{1}{2}}s_{\frac{1}{2}}-\sqrt{3}a_{1\frac{1}{2}}s_{-\frac{1}{2}}]b_0,\\ \frac{1}{\sqrt{2}}[a_{-\frac{1}{2}}s_{\frac{1}{2}}-a_{\frac{1}{2}}s_{-\frac{1}{2}}]b_0,\\ \tfrac{1}{2}[\sqrt{3}a_{-1\frac{1}{2}}s_{\frac{1}{2}}-a_{-\frac{1}{2}}s_{-\frac{1}{2}}]b_0,\\ a_{1\frac{1}{2}}s_{\frac{1}{2}}b_0,\end{gathered}\qquad (P_3)$$

$$\begin{gathered}\tfrac{1}{2}[\sqrt{3}a_{\frac{1}{2}}s_{\frac{1}{2}}+a_{1\frac{1}{2}}s_{-\frac{1}{2}}]b_0,\\ \frac{1}{\sqrt{2}}[a_{-\frac{1}{2}}s_{\frac{1}{2}}+a_{\frac{1}{2}}s_{-\frac{1}{2}}]b_0,\\ \tfrac{1}{2}[a_{-1\frac{1}{2}}s_{\frac{1}{2}}+\sqrt{3}a_{-\frac{1}{2}}s_{-\frac{1}{2}}]b_0,\\ a_{-1\frac{1}{2}}s_{-\frac{1}{2}}b_0.\end{gathered}\qquad (P_5)$$

The functions X_0, $X_2^{(3)}$ and $X_2^{(5)}$ can be constructed from the same waves, a, b and s:

$$\begin{gathered}\frac{1}{2\sqrt{3}}\{-\sqrt{3}a_{-1\frac{1}{2}}b_1s_{\frac{1}{2}}+\sqrt{2}a_{-\frac{1}{2}}b_0s_{\frac{1}{2}}+a_{-\frac{1}{2}}b_1s_{-\frac{1}{2}}-a_{\frac{1}{2}}b_{-1}s_{\frac{1}{2}}-\sqrt{2}a_{\frac{1}{2}}b_0s_{-\frac{1}{2}}+\sqrt{3}a_{1\frac{1}{2}}b_{-1}s_{-\frac{1}{2}}\},\\ \tfrac{1}{2}[a_{\frac{1}{2}}b_1s_{\frac{1}{2}}-\sqrt{3}a_{1\frac{1}{2}}b_1s_{-\frac{1}{2}}],\\ \tfrac{1}{4}[2a_{-\frac{1}{2}}b_1s_{\frac{1}{2}}+\sqrt{2}a_{\frac{1}{2}}b_0s_{\frac{1}{2}}-2a_{\frac{1}{2}}b_1s_{-\frac{1}{2}}-(6)^{\frac{1}{2}}a_{1\frac{1}{2}}b_0s_{-\frac{1}{2}}],\end{gathered}\qquad (X_0)$$

$$\begin{gathered}\frac{1}{2(6)^{\frac{1}{2}}}\{\sqrt{3}a_{-1\frac{1}{2}}b_1s_{\frac{1}{2}}+2\sqrt{2}a_{-\frac{1}{2}}b_0s_{\frac{1}{2}}-a_{-\frac{1}{2}}b_1s_{-\frac{1}{2}}+a_{\frac{1}{2}}b_{-1}s_{\frac{1}{2}}-2\sqrt{2}a_{\frac{1}{2}}b_0s_{-\frac{1}{2}}-\sqrt{3}a_{1\frac{1}{2}}b_{-1}s_{-\frac{1}{2}}\},\\ \tfrac{1}{4}[(6)^{\frac{1}{2}}a_{-1\frac{1}{2}}b_0s_{\frac{1}{2}}+2a_{-\frac{1}{2}}b_{-1}s_{\frac{1}{2}}-\sqrt{2}a_{-\frac{1}{2}}b_0s_{-\frac{1}{2}}-2a_{\frac{1}{2}}b_{-1}s_{-\frac{1}{2}}],\\ \tfrac{1}{2}[\sqrt{3}a_{-1\frac{1}{2}}b_{-1}s_{\frac{1}{2}}-a_{-\frac{1}{2}}b_{-1}s_{-\frac{1}{2}}],\\ -\frac{1}{2\sqrt{3}}[\sqrt{3}a_{\frac{1}{2}}b_1s_{\frac{1}{2}}-2\sqrt{2}a_{1\frac{1}{2}}b_0s_{\frac{1}{2}}+a_{1\frac{1}{2}}b_1s_{-\frac{1}{2}}],\end{gathered}\qquad (X_2^{(3)})$$

$$\begin{gathered}\frac{1}{4\sqrt{3}}\{2\sqrt{3}a_{-\frac{1}{2}}b_1s_{\frac{1}{2}}-(6)^{\frac{1}{2}}a_{\frac{1}{2}}b_0s_{\frac{1}{2}}+2\sqrt{3}a_{\frac{1}{2}}b_1s_{-\frac{1}{2}}-4a_{1\frac{1}{2}}b_{-1}s_{\frac{1}{2}}-\sqrt{2}a_{1\frac{1}{2}}b_0s_{-\frac{1}{2}}\},\\ \frac{1}{2\sqrt{2}}[a_{-1\frac{1}{2}}b_1s_{\frac{1}{2}}+\sqrt{3}a_{-\frac{1}{2}}b_1s_{-\frac{1}{2}}-\sqrt{3}a_{\frac{1}{2}}b_{-1}s_{\frac{1}{2}}-a_{1\frac{1}{2}}b_{-1}s_{-\frac{1}{2}}],\\ \frac{1}{4\sqrt{3}}\{\sqrt{2}a_{-1\frac{1}{2}}b_0s_{\frac{1}{2}}+4a_{-1\frac{1}{2}}b_1s_{-\frac{1}{2}}+(6)^{\frac{1}{2}}a_{-\frac{1}{2}}b_0s_{-\frac{1}{2}}-2\sqrt{3}a_{-\frac{1}{2}}b_{-1}s_{\frac{1}{2}}-2\sqrt{3}a_{\frac{1}{2}}b_{-1}s_{-\frac{1}{2}}\},\\ \frac{1}{2\sqrt{3}}[-a_{-1\frac{1}{2}}b_{-1}s_{\frac{1}{2}}+2\sqrt{2}a_{-1\frac{1}{2}}b_0s_{-\frac{1}{2}}-\sqrt{3}a_{-\frac{1}{2}}b_{-1}s_{-\frac{1}{2}}].\end{gathered}\qquad (X_2^{(5)})$$

One easily verifies that $(P_3, X_2^{(5)})=(P_5, X_2^{(3)})=(X_2^{(3)}, X_2^{(5)})=0$. The transformation coefficients $(P_3, X_2^{(3)})$ and $(P_5, X_2^{(5)})$ and the normalized angular dependence of the surface harmonics for the different values of magnetic quantum number are given in Table I. $(P_3, X_0)=\frac{1}{3}\sqrt{3}$.

Substituting the results of Table I into Eq. (7) and summing up the coefficients of α_0^2, $\alpha_0\alpha_2$ and α_2^2 one obtains

$$\sigma \sim \frac{1}{3}\left|\frac{\alpha_0^2}{(E_P-E_0+\frac{1}{2}i\Gamma_0)^2}+\frac{2(5/2)^{\frac{1}{2}}\alpha_0\alpha_2(1-3\cos^2\theta)\cos\xi}{(E_P-E_0+\frac{1}{2}i\Gamma_0)(E_P-E_2+\frac{1}{2}i\Gamma_2)}\right. \tag{8}$$

$$\left.+\frac{(5/2)\alpha_2^2[(1+3\cos^2\theta)\cos^2\xi+3\sin^2\xi(1-\cos^2\theta)]}{(E_P-E_2+\frac{1}{2}i\Gamma_2)^2}\right|.$$

As has been anticipated in the introduction only the zeroth and second power of $\cos\theta$ appear in this formula.

Theoretical Angular Dependence

It is assumed for the reasons given above that the sharp rise of $A(E)$ with increasing energy is due to an approach to resonance with a state of $J=2$. The spherically symmetrical contribution below resonance then comes from a broad resonance to a state of $J=0$. In Eq. (8) we accordingly assume $\Gamma_0 \gg E_P-E_0$ and neglect the dependence of the $J=0$ resonance on energy. The unknown quantities α_2, α_0, Γ_0 and Γ_2 can be lumped into one complex number, $\beta e^{i\delta}$ which is conveniently defined as

$$\beta e^{i\delta} \equiv \tfrac{1}{2}(10)^{\frac{1}{2}}\alpha_2\Gamma_0/\alpha_0\Gamma_2. \tag{9}$$

β and δ are real. Since $\frac{1}{2}\Gamma_2$ is unknown it is expedient to choose it as the energy unit and instead of the energy difference E_P-E_2 we shall use ϵ,

$$\epsilon \equiv (E_P-E_2)/\tfrac{1}{2}\Gamma_2. \tag{10}$$

With the notations defined in Eqs. (9) and (10) we get

$$1+A(\epsilon)\cos^2\theta \sim 1+\epsilon^2+2\beta(1-3\cos^2\theta)(\epsilon\cos\delta+\sin\delta)\cos\xi$$

$$+\cos^2\xi\beta^2(1+3\cos^2\theta)+3\sin^2\xi\beta^2(1-\cos^2\theta) \tag{11}$$

from which follows at once

$$A(\epsilon)=3\frac{\beta^2\cos 2\xi-2\beta(\epsilon\cos\delta+\sin\delta)\cos\xi}{1+\epsilon^2+2\beta(\epsilon\cos\delta+\sin\delta)\cos\xi+\beta^2(1+2\sin^2\xi)}. \tag{12}$$

The denominator of the right-hand side of Eq. (12) is positive and vanishes only under the particular conditions: $\sin\xi=0$, $\beta\sin\delta\cos\xi=-1$. This means that the emission in the direction of the beam does not vanish at any bombarding energy unless these conditions are fulfilled or unless $A=-1$.[10] In general $A(\epsilon)$ has one real root which occurs for the value $\epsilon=\epsilon_0$, with

$$\epsilon_0=-\tan\delta+\tfrac{1}{2}\beta\sec\delta\cos 2\xi\sec\xi. \tag{13}$$

At the energy corresponding to ϵ_0 the angular distribution is spherically symmetrical. In terms of ϵ_0, $A(\epsilon)$ becomes

$$A(\epsilon)=6\beta\cos\delta\cos\xi\frac{\epsilon_0-\epsilon}{\epsilon^2+1+2(\epsilon-\epsilon_0)\beta\cos\delta\cos\xi+2\beta^2}. \tag{12'}$$

[10] It is interesting to note that if $A(\epsilon)$ falls below -1 in a certain energy range there will be no emission at those angles θ for which $\cos^2\theta=1/|A|$. Thus in this range there will be a cone of zero alpha-particle intensity the opening angle of which rises from zero to a certain maximum value and falls back to zero again as the bombarding energy is increased.

The plot of $A(\epsilon)$ against ϵ is clearly a sigmoid curve asymptotic to the ϵ axis at large absolute values of ϵ and crossing the axis at ϵ_0. There is one maximum and one minimum to this curve and these lie at ϵ_m

$$\epsilon_m = \epsilon_0 \pm (\epsilon_0^2 + 1 + 2\beta^2)^{\frac{1}{2}}. \quad (14)$$

It is characteristic of this theory that the maximum and the minimum occur at equal energy differences from ϵ_0. Substituting Eq. (14) into Eq. (12′) we find the extreme values of $A(\epsilon)$

$$A(\epsilon_m) = -3\beta \cos\delta \cos\xi/(\epsilon_m + \beta \cos\delta \cos\xi). \quad (15)$$

It will be noted that in general the maximum values of A are not equal in absolute value. If, for instance, the energy corresponding to ϵ_0 does not lie in the resonance region ($|\epsilon_0| \gg 1$), one of the extreme values of A will differ from zero insignificantly. From Eqs. (15) and (10)

$$3/A_{\max} - 3/A_{\min} = -(E_{\max} - E_{\min})/\tfrac{1}{2}\Gamma_2\beta \cos\delta \cos\xi, \quad (16)$$

where $E_{\max}$ and $E_{\min}$ are the E values at which the maximum and minimum occur. Thus the measured values of A and E at the maximum and minimum determine $\frac{1}{2}\beta\Gamma_2 \cos\delta \cos\xi$ at once. The resonant energy E_2 is then related to the energy at which $A=0$, E^0, by

$$E_2 = E^0 + \tfrac{1}{4}\Gamma_2\beta \cos\delta \cos\xi[2 + 3/A_{\max} + 3/A_{\min}]. \quad (17)$$

Actually it is not at all certain that the shape of the $A(E)$ curve has a sigmoid appearance. As has been pointed out above in one-half of the sigmoid curve the value of $A(E)$ may be very small. In fact if the energy corresponding to ϵ_0 should happen to lie at negative energies of the incident protons one-half of the sigmoid curve is missing. Thus in appearance, or even in fact, the dependence of A on the energy may reduce to a simple hump. The observed dependence of the yield of alpha-particles on energy makes it more likely that A as a function of E has a simple maximum rather than a sigmoid behavior. In fact if $A(E)$ would become negative above 400 kev and yet within the resonance region one would expect the maximum in Fig. 2 to lie at higher energies than 400 kev. This is so because a negative value of $A(E)$ within the resonance region would enhance particularly strongly the number of alpha-particles ejected at right angles to the incident beam and the experiments on which Fig. 2 is based were made with just such a geometrical arrangement.

Though in the present calculations explicit assumptions about the nuclear model have been avoided some simplifications had to be introduced. In particular we assumed that only two compound nuclei are involved in the process and we also neglected the energy dependence of the matrix elements involved within the resonance range. It seems however that it is not worth while to make more refined calculations at present. Extension of the measurements on angular dependence to higher energies will probably indicate to what extent the basis of the present calculations should be modified or extended.

The Scattering of Slow Neutrons by Molecular Gases

R. G. SACHS* AND E. TELLER
The George Washington University, Washington, D. C.

(Received April 18, 1941)

It has been shown by Fermi that the cross section for the scattering of slow neutrons by protons is four times greater for protons strongly bound to an infinite mass than it is for free protons initially at rest. A simple generalization of this factor of four can be given for the scattering of neutrons by molecular gases if the neutron energy is great as compared to the energy differences of the rotational levels of the scattering molecule but small compared to the quanta of molecular vibration. In this case, the proton may be replaced by a freely moving hypothetical mass point whose mass is a tensor depending on the mass and structure of the molecule. On this basis the total cross section for the scattering of slow neutrons by H_2 and by CH_4, NH_3 and H_2O at low temperatures has been calculated as a function of the ratio of the neutron energy to the thermal energy of the scattering gas. The possibility of applying the theory to a determination of the neutron-proton scattering cross section is discussed.

1. INTRODUCTION

THE problem of the scattering of slow neutrons by bound protons was first treated by Fermi[1] and then in somewhat more detail by Arley.[2] Fermi showed that for sufficiently slow neutrons the scattering cross section σ may be calculated by substituting a relatively wide and shallow neutron-proton interaction potential for the actual narrow and deep potential. Then the Born approximation may be applied to this shallow potential. The width of this potential must be small compared to the wave-length of the neutron (relative to the proton). The effect of the substitute potential is essentially the same as that of a delta-function interaction between neutron and proton since the neutron wave function varies but little over its width.

If the proton is elastically bound to an infinite mass the scattering cross section depends on the ratio of vibrational quantum to neutron energy. For neutrons of energy less than a vibrational quantum, only elastic collisions are possible and it has been shown[1,2] that the cross section is nearly independent of the vibrational proper functions. If such be the case, then according to perturbation theory the transition probability depends only on the density of energy states into which the neutron can be scattered. This density is proportional to p^2dp/dE, where p is the momentum of the neutron in the center of gravity coordinate system and E is the relative kinetic energy. In terms of E, $p^2dp/dE \sim \mu^{\frac{3}{2}}E^{\frac{1}{2}}$ where μ is the reduced mass of the neutron plus proton-system (i.e., the system of the proton and all the particles to which it is bound). If the proton is initially at rest, E is related to the initial kinetic energy, E_0, of the neutron in the laboratory system by $E=(\mu/m)E_0$. Thus the transition probability, and therefore the scattering cross section, is proportional to μ^2. Since we are considering a proton-system of infinite mass, μ is equal to the mass, m, of the neutron. The cross section for this case will be called σ_x.

For the scattering by a free proton at rest the cross section is again proportional to μ^2, but in this case the reduced mass is $\mu=m/2$ and the cross section is $(\frac{1}{4})\sigma_x$. Thus we are led to the well-known factor of $\frac{1}{4}$ for the ratio of the cross section for a free proton to the cross section for a proton rigidly bound to an infinite mass.

In the case of the scattering of neutrons by hydrogen-containing molecules (in the gaseous state) the proton may be treated as free if the neutron energy is very great compared to both rotational and vibrational quanta (i.e., h times rotational and vibrational frequencies) of the molecule. When the neutron energy is much smaller than both of these energies, only the translational motion of the molecule as a whole is affected by the neutron impact so the cross section may be calculated as above with μ determined by $1/\mu=1/m+1/M$ where M is the

* Now at Purdue University, Lafayette, Indiana.
[1] E. Fermi, Ricerca Scient. **7**, No. 2, 13 (1936).
[2] N. Arley, Kgl. Dansk. Vid. Selsk. **16**, 1 (1938).

total mass of the molecule. The cross section is then $(M/m+M)^2\sigma_x$ (as long as interference effects may be neglected).

In the intermediate case for which the neutron energy is great compared to a rotational quantum but too small to excite molecular vibrations, the situation is somewhat more complicated. For, if it is assumed that the rotational-translational motion of the molecule can be treated classically, the effective mass of a proton in the molecule during the collision depends on the direction of the initial and final momentum of the neutron. For example, a neutron in a head-on collision with one of the protons of the H_2 molecule will feel an effective proton mass of $2m$ if it is moving parallel to the H-H axis and a mass m if its path is perpendicular to this axis. In general, there will be a linear relation between the change in velocity of the proton and the change in momentum of the neutron due to the collision. Therefore we may associate with the proton a hypothetical mass point which moves with the velocity of the proton but whose mass is a tensor which depends on the mass and structure of the molecule.

In order to calculate the transition probability for the scattering of neutrons with energy that is great compared to the rotational quanta of the molecule, the rotational wave function in the final state can be replaced by a rotating wave packet which is a combination of neighboring rotational states since many rotational quanta will be excited by the collision. By making the packet sufficiently small the rotational wave function within it may be approximated by a plane wave. The molecular wave function is a product of the rotational and translational wave functions of the molecule multiplied by a vibrational wave function which in this case serves only to limit the position of the proton with respect to the other atoms in the molecule. Taking into account the fact that the translational wave function of the molecule is a plane wave, we see that the relevant part of the molecular wave function after collision may be treated as a plane wave which describes the properties of the wave packet under translation and infinitesimal rotation.

Insofar as the calculation of the matrix element for the transition is concerned, the initial rotational state may also be replaced by a plane wave since its only contribution to this matrix element is in the region of the wave packet. Therefore, just as in the case of free protons, the matrix element serves only to guarantee the conservation of momentum and angular momentum and the transition probability depends only on the density of final energy states into which the neutron can be scattered. By the conservation laws, the density of the neutron states is equal to the density of the permissible final states for the molecule. However this density will now depend on the reduced mass that is associated with the mass of the neutron and the mass tensor of the hypothetical mass point described above.

Since the quantum calculations are essentially concerned with small wave packets moving under the influence of constant or slowly varying potentials and since the only quickly varying interaction—that between the neutron and proton—leads to matrix elements that merely represent conservation laws, the entire calculation can be carried out according to classical mechanics. The meaning of the mass tensor as the linear relation between velocity and momentum vectors is the same in the classical and quantum treatment. Instead of the density of energy levels the volume of momentum space per unit energy interval will enter into the classical theory.

The condition that the energy of the neutron be greater than the separation between rotational states is roughly $\lambda < r_0$, where λ is the neutron wave-length and r_0 is a measure of the linear dimensions of the molecule. Therefore, under this condition, interference between the scattering from two different protons in the molecule may be neglected.

2. The Mass Tensor

Since the hypothetical mass point has only three degrees of freedom and the molecule (treated as rigid) has five or six, the motion of the molecule cannot be described completely by the motion of the mass point.

We separate the infinitesimal displacements of the molecule into the set of two or three displacements for which the proton remains fixed

and the set for which the angular momentum about the proton is zero. In a collision with a thermal (S) neutron the angular momentum around the proton is unchanged. Therefore the change in motion suffered by the molecule involves only displacements of the latter type. The velocities associated with these displacements are uniquely determined by the velocity components of the proton so the behavior of these displacements can be equivalently described by the motion of the mass point to be associated with the proton.

It will be shown below that the two sets of displacements described above are orthogonal in the sense that the kinetic energy of the molecule can be written as the sum of two terms depending on the first and second types of displacement, respectively.

The molecular motion is usually described by means of its angular velocity $\mathbf{w}$ about the center of gravity, and the velocity $\mathbf{V}_c$ of the center of gravity. In order to obtain for the displacements per unit time the two types described above we write $\mathbf{w}$ and $\mathbf{V}_c$ as the sum of two terms:

$$\mathbf{w}=\mathbf{w}'+\mathbf{w}'', \quad \mathbf{V}_c=\mathbf{V}_c'+\mathbf{V}_c'',$$

where the set $(\mathbf{w}', \mathbf{V}_c')$ satisfies

$$[\mathbf{w}'\times\mathbf{r}]+\mathbf{V}_c'=0 \tag{1}$$

and the set $(\mathbf{w}'', \mathbf{V}_c'')$ satisfies

$$\mathbf{I}\mathbf{w}''-M_0[\mathbf{r}\times\mathbf{V}_c'']=0, \tag{2}$$

if $\mathbf{r}$ is the vector drawn from the center of gravity of the molecule to the proton, M_0 is the mass of the molecule, and $\mathbf{I}$ is the moment of inertia tensor of the molecule. Equation (1) corresponds to the condition that the proton be at rest and (2) to the condition that the angular momentum about the proton be zero. Thus we have written the original displacement described by $\mathbf{w}$ and $\mathbf{V}_c$ as the sum of two displacements $(\mathbf{w}', \mathbf{V}_c')$ and $(\mathbf{w}'', \mathbf{V}_c'')$ which satisfy the conditions for the displacements of the first and second type.

The kinetic energy of the molecule is

$$\begin{aligned}2E_M&=(\mathbf{w}\cdot\mathbf{I}\mathbf{w})+M_0V_c^2\\&=(\mathbf{w}'\cdot\mathbf{I}\mathbf{w}')+M_0V_c'^2+(\mathbf{w}''\cdot\mathbf{I}\mathbf{w}'')+M_0V_c''^2\\&\quad+2[(\mathbf{w}'\cdot\mathbf{I}\mathbf{w}'')+M_0(\mathbf{V}_c'\cdot\mathbf{V}_c'')]\end{aligned}$$

and the condition for orthogonality,

$$(\mathbf{w}'\cdot\mathbf{I}\mathbf{w}'')+M_0(\mathbf{V}_c'\cdot\mathbf{V}_c'')=0. \tag{3}$$

To verify Eq. (3) we make use of Eq. (2) and find that

$$\begin{aligned}(\mathbf{w}'\cdot\mathbf{I}\mathbf{w}'')&=M_0(\mathbf{w}'\cdot[\mathbf{r}\times\mathbf{V}_c''])\\&=M_0([\mathbf{w}'\times\mathbf{r}]\cdot\mathbf{V}_c'').\end{aligned}$$

Then by Eq. (1) the condition (3) is satisfied.

We now wish to describe the part of the motion corresponding to $(\mathbf{w}'', \mathbf{V}_c'')$ by the motion of the hypothetical mass point. Assume that the momentum of the mass point is equal to the momentum of the molecule,

$$\mathbf{P}=M_0\mathbf{V}_c''. \tag{4}$$

Conservation of momentum will then be satisfied for the molecule if it is satisfied for the mass point since the motion $(\mathbf{w}', \mathbf{V}_c')$ is unaffected by the collision; and, for the same reason, the angular momentum around the proton will be conserved.

Since the mass point is defined as having a velocity $\mathbf{V}$ equal to the velocity of the proton, the inverse mass tensor is defined by $\mathbf{V}=\mathbf{M}^{-1}\mathbf{P}$. Now $\mathbf{V}=[\mathbf{w}''\times\mathbf{r}]+\mathbf{V}_c''$, so Eqs. (2) and (4) give

$$\mathbf{V}=[\mathbf{I}^{-1}[\mathbf{r}\times\mathbf{P}]\times\mathbf{r}]+M_0^{-1}\mathbf{P}, \tag{5}$$

which is the desired linear relation between $\mathbf{V}$ and $\mathbf{P}$.

It immediately follows from Eqs. (2), (4), and (5) that the kinetic energy of the mass point is equal to that part of the molecular kinetic energy due to $(\mathbf{w}'', \mathbf{V}_c'')$; that is,

$$\tfrac{1}{2}(\mathbf{P}\cdot\mathbf{V})=\tfrac{1}{2}(\mathbf{w}''\cdot\mathbf{I}\mathbf{w}'')+\tfrac{1}{2}M_0\mathbf{V}_c''^2.$$

Finally, the expression (5) written in terms of components is

$$V_i=\left(\frac{r_j^2}{I_k}+\frac{r_k^2}{I_j}+\frac{1}{M_0}\right)P_i-\frac{r_ir_j}{I_k}P_j-\frac{r_ir_k}{I_j}P_k,$$

where the subscripts i, j, k refer to the directions of the principal axes of inertia and r_1, r_2, r_3 are the coordinates of the proton under consideration with respect to the center of gravity. Therefore, the inverse mass tensor is

$$(M^{-1})_{ii}=\left(\frac{r_j^2}{I_k}+\frac{r_k^2}{I_j}+\frac{1}{M_0}\right), \quad (M^{-1})_{ij}=-\frac{r_ir_j}{I_k}. \tag{6}$$

It is seen that the tensor is symmetric, a fact which can be proved directly from Eq. (5); thus it can be transformed to diagonal form.

It will be convenient to introduce the dimensionless tensor $\mathbf{n}=m\mathbf{M}^{-1}$. In the following paragraphs we shall calculate the characteristic values n_1, n_2, n_3 of $\mathbf{n}$ for a few cases.

H_2

For the hydrogen molecule, the principal axes of inertia and mass coincide. As stated in Section 1, the mass perpendicular to the H-H axis is m and that parallel to the axis is $2m$. Thus $n_1=n_2=1$, $n_3=\frac{1}{2}$ for both protons.

CH_4

In methane the moment of inertia ellipsoid is a sphere so the axes of inertia may be chosen in such a way that one of them passes through the proton under consideration. These axes are then the principal axes of mass for this proton. The mass along the axis that passes through the proton and the center of gravity of the molecule is the total mass of the molecule; thus the corresponding component of $\mathbf{n}$ is $n_1=\frac{1}{16}$. The other two components of $\mathbf{n}$ are $n_2=n_3=\frac{7}{16}$.

NH_3

The principal axes of mass do not coincide with those of the moment of inertia for ammonia, but one of them is the line joining the given proton with the center of gravity; another is perpendicular to this and in the plane determined by the proton, the nitrogen atom, and the center of gravity; and the third is perpendicular to these two. The mass for the first of these directions is again the total mass of the molecule so $n_1=\frac{1}{17}(=0.0589)$. In sufficient approximation one can set the HNH angle in ammonia equal to the HCH angle in methane (109° 28′). Under this assumption, the other two characteristic values of $\mathbf{n}$ are given by $n_2=0.604$ and $n_3=0.439$.

H_2O

One principal axis of the mass tensor for water is, as usual, the line joining the proton with the center of gravity. The other two are perpendicular to this (and to each other) and one of them lies in the plane of the molecule. If the HOH angle is taken to be 106°, the results for the components of $\mathbf{n}$ are $n_1=\frac{1}{18}(=0.0555)$, $n_2=0.535$, $n_3=1$.

3. Scattering Cross Section

The collision of a slow neutron with a proton in the molecule gives rise to changes in $\mathbf{w}$ and $\mathbf{V}_c$ which are represented by vectors of the type $(\mathbf{w}'', \mathbf{V}_c'')$. The density of final neutron states, and therefore the transition probability, is then independent of motions of the molecule of the type $(\mathbf{w}', \mathbf{V}_c')$ and depends only on the motion of the mass point.

If the mass $\mathbf{M}$ of the hypothetical mass point has the characteristic values M_1, M_2, M_3, the position of the center of gravity of the neutron-mass point system is defined by $(m+M_i)\bar{x}_i = mx_i+M_i\xi_i$, $i=1, 2, 3$. Here, x_i are the coordinates of the neutron and ξ_i those of the mass point. The velocity, momentum and kinetic energy of the two particles in the center of gravity system may now be calculated in the usual way. The total kinetic energy E_0 separates into the sum of the kinetic energy of the center of gravity $\bar{E}$, and the relative kinetic energy E.

The density of final states for the neutron is proportional to $d\tau/dE$, where τ is the volume in momentum space contained within a surface of constant relative energy (E). That is,

$$\tau=\int\int\int_{E=\text{const.}} dp_1dp_2dp_3$$

where (p_1, p_2, p_3) is the final momentum of the neutron in the center of gravity coordinate system. E is the sum of the kinetic energy of the neutron and the kinetic energy of the mass point (both taken in the center of gravity system). The former energy is $(\mathbf{p}\cdot\mathbf{p})/2m$ and the latter is $(\frac{1}{2})(\mathbf{p}\cdot\mathbf{M}^{-1}\mathbf{p})$ since $\mathbf{p}=(p_1, p_2, p_3)$ is also the negative momentum of the mass point in the C.G. system. Therefore the surface of constant energy is given by

$$2mE=(\mathbf{p}\cdot\mathbf{p})+(\mathbf{p}\cdot\mathbf{np})=(\mathbf{p}\cdot\boldsymbol{\mu}^{-1}\mathbf{p})=\text{const.},$$

where $\boldsymbol{\mu}^{-1}=\mathbf{1}+\mathbf{n}$. The tensor $\boldsymbol{\mu}$ can be considered as the reduced mass tensor measured in units of the mass of the neutron. When $\boldsymbol{\mu}$ is in diagonal form, the energy surface is the ellipsoid

$$2mE=\mu_1^{-1}p_1^2+\mu_2^{-1}p_2^2+\mu_3^{-1}p_3^2$$

TABLE I. *The limits of validity of Eq. (7) are given by* $E_n > E_{\text{rot}}$, $E_n > (E_{\text{rot}}kT)^{\frac{1}{2}}$, *and* $E_n < E_{\text{vib}}$ *where* E_n *is the neutron energy and* T *is the temperature of the scattering gas.*

MOLECULE	H_2	CH_4	NH_3	H_2O
E_{rot}(ev)	0.015	0.001	0.002	0.006
E_{vib}(ev)	0.5	0.15	0.1	0.2

and the volume, τ, is $\tau = 4\pi/3(2mE)^{\frac{3}{2}}(\mu_1\mu_2\mu_3)^{\frac{1}{2}}$ so that

$$d\tau/dE = 2\pi(2m)^{\frac{3}{2}}(\mu_1\mu_2\mu_3)^{\frac{1}{2}}E^{\frac{1}{2}}.$$

The transition probability is therefore proportional to $(\mu_1\mu_2\mu_3)^{\frac{1}{2}}E^{\frac{1}{2}}$. Now, by conservation of energy, $E = E_0 - \bar{E}$, where E_0 and $\bar{E}$ are the total energy and the energy of the center of gravity before collision. If $\mathbf{P}_n$ and $\mathbf{P}$ are the momenta of the neutron and mass point in the laboratory system before collision,

$$2mE_0 = P_n^2 + (\mathbf{P}\cdot\mathbf{nP})$$

and

$$2m\bar{E} = (\mathbf{P}\cdot\mathbf{n}\mu\mathbf{P}),$$

where $\mathbf{P} = \mathbf{P} + \mathbf{P}_n$ is the total momentum. Taking the difference between these equations we obtain

$$2mE = [\mu^{\frac{1}{2}}(\mathbf{P}_n - \mathbf{nP})]^2.$$

Thus in terms of the components of momentum along the principal axes of mass of the molecule the transition probability is proportional to

$$(\mu_1\mu_2\mu_3)^{\frac{1}{2}}\{\textstyle\sum_i \mu_i(P_{ni} - n_iP_i)^2\}^{\frac{1}{2}}.$$

The scattering cross section is given by the transition probability divided by the initial velocity of the neutron in the laboratory system. Consequently

$$\sigma = c(\mu_1\mu_2\mu_3)^{\frac{1}{2}}\left\{\frac{1}{P_n^2}\sum_i \mu_i(P_{ni} - n_iP_i)^2\right\}^{\frac{1}{2}},$$

where c is the constant of proportionality. When the proton is rigidly bound to an infinite mass, $n_1 = n_2 = n_3 = 0$ and $\mu_1 = \mu_2 = \mu_3 = 1$, so the cross section is $\sigma_\infty = c$.

If the vector with components $n_i^{\frac{1}{2}}P_i$ has the magnitude ρ and the direction cosines β_i, then the energy of the mass point is given by $2mE_\rho = \sum_i n_iP_i^2 = \rho^2$. The cross section σ may be expressed in terms of ρ and β_i, and in terms of the magnitude P_n, and the direction cosines α_i of the initial momentum of the neutron by the equation

TABLE II. *Scattering cross sections per proton in the given molecules as a function of neutron energy* E_n *and the temperature* T *of the molecular gas. The last column gives the region over which the formulae are valid. In addition* E_n *must satisfy the conditions given in Table I. The total cross section per molecule is obtained by multiplying* $\bar{\sigma}$ *by the number of protons in the molecule and adding* $\bar{\sigma}_h$ *(Eq. (14)).*

MOLECULE	CROSS SECTION PER PROTON	LIMITS OF VALIDITY
CH_4	$\bar{\sigma}/\sigma_H = 2.7 + 0.42kT/E_n$	$0 \leq kT/E_n < 0.1$
NH_3	$\bar{\sigma}/\sigma_H = 2.18 + 0.39kT/E_n$	$0 \leq kT/E_n < 0.1$
H_2O	$\bar{\sigma}/\sigma_H = 1.855 + 0.46kT/E_n$	$0 \leq kT/E_n < 0.05$

$$\sigma = \sigma_\infty(\mu_1\mu_2\mu_3)^{\frac{1}{2}}\left\{\sum_i \mu_i\left(\alpha_i - \frac{\rho}{P_n}n_i^{\frac{1}{2}}\beta_i\right)^2\right\}^{\frac{1}{2}}. \quad (7)$$

This equation is then the generalization of the proportionality of the cross section to the square of the reduced mass. For use in specific problems such as the calculation of the mean scattering cross section or the mean free path, expressions obtained from (7) have to be averaged over the angles α_i and β_i, over the velocity distribution of the molecules, and often over the neutron velocities. In order to carry out these calculations, it is necessary to know the experimental conditions. We shall first calculate the mean cross section for the scattering of monochromatic neutrons. This quantity is connected with the diminution in intensity of a neutron beam in passing through a sufficiently small amount of gas. The effective cross section will also be calculated for a neutron current distribution of the form $P_n^2\exp(-P_n^2/2mkT_n)dP_n$. Although this distribution is difficult to realize experimentally, we will make use of it since it leads to relatively simple results.

It has been pointed out in the introduction that the formula (7) can be expected to hold only if the neutron energy is large compared to the separation between rotational states and small compared to any vibrational quantum. In Table I are given the values of $E_{\text{rot}} = \hbar^2/I_{\min}$ and $E_{\text{vib}} = h\nu_{\min}$ for those molecules which will be considered below. $I_{\min}$ is the smallest moment of inertia of the molecule and $\nu_{\min}$ the smallest vibrational frequency. The condition that the neutron energy be large compared to the separation between rotational states is then: $E_n > E_{\text{rot}}$, $E_n > (E_{\text{rot}}kT)^{\frac{1}{2}}$, where T is the temperature of the molecular gas under consideration. In order that E_n be small compared to a vibrational quantum we have $E_n < E_{\text{vib}}$.

4. Mean Cross Section for Monochromatic Neutrons

The direction cosines α_i, β_i are given with respect to axes fixed in the molecule. Therefore, in order to obtain the mean cross section, the expression (7) must be averaged over all possible orientations α_i, β_i of the molecule. For the purpose of carrying out this average, let

$$\gamma_i=\left\langle\left(\alpha_i-\frac{\rho}{P_n}n_i^{\frac{1}{2}}\beta_i\right)^2\right\rangle_{Av}$$

and

$$X_i=\left(\alpha_i-\frac{\rho}{P_n}n_i^{\frac{1}{2}}\beta_i\right)^2-\gamma_i,$$

where the average is taken over α_i, β_i. Then σ is given by

$$\sigma=\sigma_x(\mu_1\mu_2\mu_3)^{\frac{1}{2}}(\textstyle\sum_i\gamma_i\mu_i)^{\frac{1}{2}}\{1+\sum_j\mu_jX_j/\sum_i\gamma_i\mu_i\}^{\frac{1}{2}}.$$

If the quantity $X=\sum_j\mu_jX_j/\sum_i\gamma_i\mu_i$ is less than one, the square root may be expanded in powers of X and then averaged. Thus

$$\sigma_{Av}=\sigma_x(\mu_1\mu_2\mu_3)^{\frac{1}{2}}(\textstyle\sum_i\gamma_i\mu_i)^{\frac{1}{2}}\{1-\frac{1}{2}\langle X\rangle_{Av}-\frac{1}{8}\langle X^2\rangle_{Av}+\frac{1}{16}\langle X^3\rangle_{Av}+\cdots\}. \tag{8}$$

The conditions under which this expansion is valid will be discussed below. The ranges of values of kT E_n for which it holds are given in the last column of Table II.

Now making use of the averages

$$\langle\alpha_i^{2n}\rangle_{Av}=\frac{1}{2n+1},\quad \langle\alpha_i^2\alpha_j^{2n}\rangle_{Av}=\frac{1}{(2n+1)(2n+3)},\quad \langle\alpha_1^2\alpha_2^2\alpha_3^2\rangle_{Av}=\frac{1}{105},$$

we find

$$\textstyle\sum_i\gamma_i\mu_i=\mu+(1-\mu)\rho^2/P_n^2,\quad X_{Av}=0,$$

$$(\textstyle\sum_i\gamma_i\mu_i)^2\langle X^2\rangle_{Av}=\frac{4}{45}\{a_1(1+\rho^4/P_n^4)+a_2\rho^2/P_n^2\},$$

$$(\textstyle\sum_i\gamma_i\mu_i)^3\langle X^3\rangle_{Av}=\frac{8}{945}\{b_1(1-\rho^6/P_n^6)+b_2(1-\rho^2/P_n^2)\rho^2/P_n^2\},$$

where

$$\begin{aligned}
\mu&=\tfrac{1}{3}\textstyle\sum_i\mu_i,\\
a_1&=\tfrac{1}{2}\textstyle\sum_{i>j}(\mu_i-\mu_j)^2,\\
a_2&=5\textstyle\sum_i n_i\mu_i^2,\\
b_1&=\tfrac{1}{21}(2\textstyle\sum_i\mu_i^3-3\sum_{i\neq j}\mu_i^2\mu_i+12\mu_1\mu_2\mu_3),\\
b_2&=2\textstyle\sum_j\mu_j^3n_j-\sum_{i\neq j}\mu_i^2\mu_jn_i.
\end{aligned} \tag{9}$$

In obtaining these expressions, use has been made of the relation $1/\mu_i=n_i+1$. With $a=1/\mu-1$, the average of the cross section over α_i, β_i becomes

$$\sigma_{Av}=\sigma_x(\mu_1\mu_2\mu_3\mu)^{\frac{1}{2}}(1+a\rho^2/P_n^2)^{\frac{1}{2}}\left\{1-\frac{a_1(1+\rho^4/P_n^4)+a_2\rho^2/P_n^2}{90\mu^2(1+a\rho^2/P_n^2)^2}+\frac{b_1(1-\rho^6/P_n^6)+b_2(1-\rho^2/P_n^2)(\rho^2/P_n^2)}{90\mu^3(1+a\rho^2/P_n^2)^3}+\cdots\right\}. \tag{10}$$

If the scattering molecules are at a temperature[3] T, their energy distribution is proportional to $\exp(-E_M/kT)$ times the element of volume in momentum space. The kinetic energy E_M of the

[3] It is assumed throughout the paper that the temperature T is not high enough to excite molecular vibrations.

molecule is the sum of E_p (kinetic energy of the mass point) and a kinetic energy that is independent of the motion of the mass point. The element of volume in the molecular momentum space is the product of an element of volume in the momentum space of the mass point and a second volume element that is independent of the momentum of the mass point. Therefore the number of molecules for which $(2mE_p)^{\frac{1}{2}}$ lies between the values ρ and $\rho+d\rho$ is proportional to $\exp(-\rho^2/2mkT)\rho^2 d\rho$. The expression (10) must now be averaged over this distribution. If we let $\eta=\rho/P_n$, this average is

$$\bar{\sigma}=\sigma_x(\mu_1\mu_2\mu_3\mu)^{\frac{1}{2}}(T_0+T_1+T_2+\cdots), \tag{11}$$

where

$$T_0=\int_0^\infty (1+a\eta^2)^{\frac{1}{2}}\exp[-(E_n/kT)\eta^2]\eta^2 d\eta \Big/ \int_0^\infty \exp[-(E_n/kT)\eta^2]\eta^2 d\eta,$$

$$T_1=-\frac{1}{90\mu^2}\int_0^\infty (1+a\eta^2)^{-\frac{1}{2}}\exp[-(E_n/kT)\eta^2](a_1\eta^2+a_2\eta^4+a_1\eta^6)d\eta \Big/ \int_0^\infty \exp[-(E_n/kT)\eta^2]\eta^2 d\eta,$$

$$T_2=\frac{1}{90\mu^3}\int_0^\infty (1+a\eta^2)^{-5/2}\exp[-(E_n/kT)\eta^2]$$
$$\times(b_1\eta^2+b_2\eta^4-b_2\eta^6-b_1\eta^8)d\eta \Big/ \int_0^\infty \exp[-(E_n/kT)\eta^2]\eta^2 d\eta.$$

These integrals may be put into a convenient form by writing

$$I_0=\frac{4\vartheta^{\frac{1}{2}}}{\sqrt{\pi}}\int_0^\infty (1+x^2)^{\frac{1}{2}}x^2\exp[-\vartheta x^2]dx$$

and

$$I_{pq}=\frac{4\vartheta^{\frac{1}{2}}}{\sqrt{\pi}}\int_0^\infty (1+x^2)^{-(p+\frac{1}{2})}x^{2q}\exp[-\vartheta x^2]dx,$$

where

$$\vartheta=E_n/akT.$$

Then the terms T_0, T_1, T_2 become

$$\begin{aligned} T_0&=I_0,\\ T_1&=-(a_1I_{11}+a_2I_{12}/a+a_1I_{13}/a^2)/90\mu^2,\\ T_2&=(b_1I_{21}+b_2I_{22}/a-b_2I_{23}/a^2-b_1I_{24}/a^3)/90\mu^3. \end{aligned} \tag{12}$$

Unfortunately, the integrals I_0, I_{pq} could not be carried out explicitly so that it has been necessary to evaluate them numerically. A rough evaluation of I_0 has been carried out as follows: In the range $0\leq x\leq 0.5$, the expression $(1+x^2)^{\frac{1}{2}}$ may be expanded in power series and the resulting expression integrated. Similarly, from $x=2$ to ∞, $(1+1/x^2)^{\frac{1}{2}}$ may be expanded and the direct integration carried out. Then in the range from 0.5 to 2 the integration has been done numerically.

The integrals I_{1q} have been treated similarly, except that in this case the ranges chosen were $0\leq x\leq 0.1$ and $10\leq x\leq\infty$, because of the slower convergence of $(1+x^2)^{-\frac{1}{2}}$. Only upper limits have been obtained for I_{2q} in order to check the convergence of the expression for the scattering cross section.

The values of n_i may be taken from Section 2 and the corresponding values of μ_i, μ, a, a_1, a_2, b_1, b_2 may be calculated from them by Eqs. (9). The results for the T_i are then given by Eq. (12) and $\bar{\sigma}$ may finally be obtained from Eq. (11).

The final result for the scattering of slow neutrons with energy E_n by one of the protons in H_2 is given in Fig. 1 for $0.1 \leq E_n/kT \leq 10$. The ordinate in this figure is $\bar{\sigma}$ divided by the cross section, σ_H, of a free proton at rest ($\sigma_H = \frac{1}{4}\sigma_x$). The abscissa is $\log_{10} E_n/kT$ where T is the temperature of the molecules. In computing these curves T_2 and all higher terms have been neglected, which is a rather good approximation for H_2. The broken part of the curve was interpolated with the help of rough integrations of I_0 and I_{pq}.

The validity of this curve depends upon the convergence of the expansion (8). In the case of H_2, it turns out that for all values of E_p/E_n (E_p is the energy of the mass point), the quantity X in Eq. (8) is less than one in absolute value so the expansion can be expected to converge in this case. However, for other molecules such as CH_4, NH_3, and H_2O, X is less than one only for a restricted range of values of E_p/E_n. In these regions, the quantities $\bar{\sigma}/\sigma_H$ are, to a very good approximation, linear functions of kT/E_n. Formulae for the scattering cross sections per proton in the molecules CH_4, NH_3 and H_2O and their limits of validity are given in Table II. It is to be noted that the conditions given in the last column of Table II indicate that these results may only be applied to gases at low temperatures if the limits on E_n given in Table I are taken into account.

The scattering cross section per proton for H_2 in the range $0 \leq kT/E_n \leq 0.1$ is also an approximately linear function of kT/E_n. It may be expressed by the equation

$$\bar{\sigma}/\sigma_H = 1.22 + 0.86 kT/E_n. \tag{13}$$

The total cross section per molecule is given by $\bar{\sigma}$ multiplied by the number of protons in the molecule plus the cross section for the heavy nucleus in the molecule. This latter cross section may again be computed by associating a mass tensor with the motion of the heavy nucleus. The characteristic values of the mass tensor will lie between the mass of the molecule and the mass of the heavy nucleus. In CH_4, the symmetry of the molecule causes the mass tensor to be spherically symmetrical and to be equal to the molecular mass. For H_2O and NH_3 the mass tensors are still nearly spherical and they may be sufficiently approximated by using a spherical mass tensor the characteristic values of which are chosen equal to the average of the characteristic values of the correct mass tensor. This gives an effective mass of 16 m for the nucleus C^{12} in CH_4, an effective mass 16.6 m for the nucleus N^{14} in NH_3, and an effective mass of 17.06 m for the nucleus O^{16} in H_2O. If we designate the actual mass of the nucleus by M and its effective mass by M_e, then integration over the motion of the mass point representing the heavy nucleus yields[4]

$$\bar{\sigma}_h = \sigma_X \left(\frac{M+m}{M_e+m}\right)^2 \left(\frac{M_e}{M}\right)^2 \left[\left(1+\frac{1}{2\xi^2}\right)\Phi(\xi) + \frac{\pi^{-\frac{1}{2}}}{\xi^3}\exp[-\xi^2]\right], \tag{14}$$

where

$$\xi^2 = \frac{M_e E_n}{mkT} \quad \text{and} \quad \frac{\sqrt{\pi}}{2}\Phi(\xi) = \int_0^\xi \exp[-x^2]dx.$$

σ_X is the scattering cross section for the heavy nucleus when it is initially at rest.

The total cross sections (σ_T) per molecule are given in Table III for very low temperatures, that is, for $kT/E_n \approx 0$.

5. Effective Cross Section for Neutrons with a Maxwell-Like Distribution

We now assume that the number of neutrons with momentum between P_n and $P_n + dP_n$ passing through unit surface per unit time is proportional to $P_n^2 \exp(-P_n^2/2mkT_n)dP_n$, where the effective temperature T_n is not in general equal to the temperature T of the scattering gas. Then the expression (10) for σ_h must be averaged over this distribution as well as the velocity distribution of the mass point. When the expansion (8) is valid (cf. Table II) the average cross section may again be written

[4] Compare J. Schwinger, Phys. Rev. **58**, 1004 (1940).

in the form

$$\bar{\sigma}=\sigma_s(\mu_1\mu_2\mu_3\mu)^{\frac{1}{2}}(T_0'+T_1'+T_2'+\cdots) \tag{11'}$$

with

$$T_0'=\int_0^{'}\int_0^{'}(1+a\rho^2/P_n^2)^{\frac{1}{2}}\exp\left[-\frac{1}{2mk}\left(\frac{P_n^2}{T_n}+\frac{\rho^2}{T}\right)\right]P_n^2\rho^2dP_nd\rho\Big/$$

$$\int_0^{'}\int_0^{'}\exp\left[-\frac{1}{2mk}\left(\frac{P_n^2}{T_n}+\frac{\rho^2}{T}\right)\right]P_n^2\rho^2dP_nd\rho, \tag{12'}$$

$$T_1'=-\frac{1}{90\mu^2}(a_1J_1+a_2J_2+a_1J_3),$$

etc., where J_1, J_2, J_3 are integrals of the form

$$J_q=\frac{16}{\pi}\lambda^{\frac{1}{2}}(2mkT_n)^{-3}\int_0^{'}\int_0^{'}(P_n^2+a^2\rho^2)^{-\frac{1}{2}}\exp\left[-\frac{1}{2mkT_n}(P_n^2+\lambda\rho^2)\right]P_n^{7-2q}\rho^{2q}dP_nd\rho \quad\text{and}\quad \lambda=T_n/T.$$

These integrals can be evaluated explicitly and the result[5] for $\lambda>a^2$ is

$$T_0'=\frac{2\lambda^{\frac{1}{2}}}{\pi(\lambda-a^2)}\left\{\frac{a}{\lambda^2}(\lambda-2a^2)+(\lambda-a^2)^{-\frac{1}{2}}\operatorname{arccot}(\lambda/a^2-1)^{\frac{1}{2}}\right\},$$

$$J_1+J_3=\frac{2\lambda^{\frac{1}{2}}}{\pi(\lambda-a^2)^3}\left\{(\lambda^2-8\lambda a^2-8a^4-15)(\lambda-a^2)^{-\frac{1}{2}}\operatorname{arccot}(\lambda/a^2-1)^{\frac{1}{2}}\right.$$

$$\left.+\frac{1}{a\lambda^2}(a^2\lambda^3+14a^4\lambda^2+8\lambda^2+9\lambda a^2-2a^4)\right\},$$

$$J_2=\frac{2\lambda^{\frac{1}{2}}}{\pi(\lambda-a^2)^3}\left\{3(\lambda+4a^2)(\lambda-a^2)^{-\frac{1}{2}}\operatorname{arccot}(\lambda/a^2-1)^{\frac{1}{2}}-\frac{a}{\lambda}(13\lambda+2a^2)\right\}.$$

For $\lambda<a^2$ all of the terms $(\lambda-a^2)^{-\frac{1}{2}}\operatorname{arccot}(\lambda/a^2-1)^{-\frac{1}{2}}$ are to be replaced by

$$(a^2-\lambda)^{-\frac{1}{2}}\operatorname{arccoth}(1-\lambda/a^2)^{-\frac{1}{2}}.$$

6. Application to Experiment

In applying the foregoing calculations to experiments a number of limitations, most of which have been previously mentioned, must be borne in mind. First, the entire theory is limited to neutron energies satisfying the conditions $E_n>E_{\text{rot}}$, $E_n>(E_{\text{rot}}kT)^{\frac{1}{2}}$, and $E_n<E_{\text{vib}}$, where E_{rot} and E_{vib} are given in Table I. In addition, the particular approximate methods applied in Sections 4 and 5 are limited in every case except that of H_2 by the conditions given in the last column of Table II. In the particular case of H_2 the cross sections have been roughly interpolated in the part of Fig. 1 which is indicated by a broken curve.

The greatest difficulty arises from the fact that the neutron current distribution is not known. It has been assumed in Section 5 that it is of the form $P_n^2\exp(-E_n/kT_n)dP_n$. This is the distribution that one might expect if the neutrons leave the free surface of a slowing down material in which the time required for the neutrons to reach the Maxwell distribution is small compared to the lifetime of the neutrons in the material. On the other hand, a distribution of the form $P_n^3\exp(-E_n/kT_n)$ would be expected if the neutrons behave like a gas at thermal equilibrium escaping through an opening of linear dimensions small compared to the mean free path. It is probable that the usual experimental situation corresponds to a condition that is between the two. However only the first case

[5] Cf. N. Arley, reference 2 (note 6), for a discussion of one of the integrals of this type.

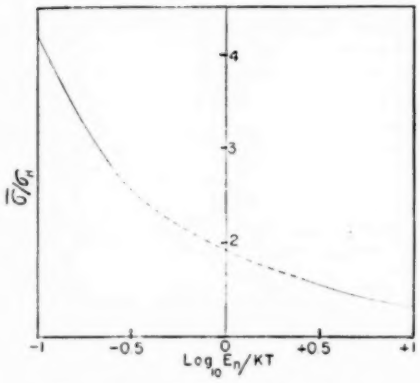

FIG. 1. Cross section for the scattering of neutrons with energy E_n by one of the protons in H_2 gas at temperature T. σ_H is the cross section for a free proton initially at rest. The broken part of the curve was interpolated with the help of rough calculations. In the range $0 \leq kT/E_n \leq 0.1$ the cross section is given by Eq. (13).

was treated here because the second apparently involves a double numerical integration.

Preliminary experiments on the scattering of 300°K neutrons by H_2 and CH_4 at room temperature have been carried out by Carroll and Dunning.[6] According to Table II, we see that the present theory cannot be applied to the experiments on CH_4 since $E_n/kT \approx 1$. In the case of H_2, the neutron energy, $\frac{3}{2}kT_n$, is approximately equal to the limiting energy E_{rot} given in Table I, so we can only expect a rough agreement.

This experimental value of the cross section per proton for scattering by H_2 is given in the first column of Table IV. In the second column the theoretical value of $\bar{\sigma}/\sigma_H$ is given on the assumption that the neutrons have a Maxwell-like distribution (Section 5). The third column contains the value of σ_H obtained from the first two columns. In the fourth column is the experimental value of σ_H found by Cohen, Goldsmith and Schwinger[7] and by Hanstein,[8]

[6] H. Carroll and J. R. Dunning, Phys. Rev. **54**, 541 (1938).
[7] V. W. Cohen, H. H. Goldsmith and J. Schwinger, Phys. Rev. **55**, 106 (1939).
[8] H. B. Hanstein, Phys. Rev. **57**, 1045 (1940); **59**, 489 (1941).

TABLE III. *σ_T is the total cross section per molecule for the scattering of monochromatic neutrons if the thermal energy of the molecules is much smaller than the energy of the neutrons ($kT/E_n \approx 0$). σ_H, σ_C, σ_N, and σ_O are the scattering cross sections for the free nuclei* H, C, N and O *when they are initially at rest.*

MOLECULE	σ_T	MOLECULE	σ_T
H_2	$2.44\sigma_H$	NH_3	$6.55\sigma_H+1.02\sigma_N$
CH_4	$10.8\sigma_H+1.04\sigma_C$	H_2O	$3.72\sigma_H+1.01\sigma_O$

TABLE IV. *The first column contains the experimental values of $\bar{\sigma}$ obtained by Carroll and Dunning,[6] the second gives the theoretical value of $\bar{\sigma}/\sigma_H$ assuming a neutron current distribution of the form $P_n^2 \exp(-P_n^2/2mkT_n)dP_n$. σ_H has been calculated from these two. $\sigma_H^{(1)}$ is the value given by Cohen, Goldsmith and Schwinger[7] and by Hanstein,[8] and $\sigma_H^{(2)}$ is the value given by Schwinger.[4, 9]*

EXPERIMENTAL $\bar{\sigma}$	THEORETICAL $\bar{\sigma}/\sigma_H$	σ_H	EXPERIMENTAL $\sigma_H^{(1)}$	EXPERIMENTAL $\sigma_H^{(2)}$
32×10^{-24} cm^2	1.69	18.9×10^{-24}	21×10^{-24}	16.6×10^{-24}

and the last column gives the value obtained by Schwinger[4] from the experiments of Alvarez and Pitzer[9] with very slow (20°K) neutrons.

If it had been assumed that the neutron current distribution was of the form $P_n^3 \exp(E_n/kT)dP_n$ rather than $P_n^2 \exp(E_n/kT)dP_n$, then greater weight would have been given to higher values of E_n in calculating the theoretical cross section. It can be seen from Fig. 1 that this would tend to decrease the theoretical value of $\bar{\sigma}/\sigma_H$ and thus increase the value of σ_H given in Table IV.

It would be particularly interesting to measure the cross section for the scattering by H_2 of monochromatic neutrons with an energy somewhat greater than E_{rot} (Table I). If this measurement were carried out at different temperatures of the H_2 gas it would be a means of checking the theory and should yield a fairly accurate value of σ_H.

The authors take pleasure in thanking Professor Placzek for valuable discussions.

[9] L. W. Alvarez and K. S. Pitzer, Phys. Rev. **58**, 1003 (1940).

A Note on Nuclear Radii

R. D. PRESENT*
Research Laboratory of Physics, Harvard University, Cambridge, Massachusetts
(Received May 19, 1941)

Corrections to the nuclear radius and particle density arising from the neutron excess $N-Z$, from the electrostatic repulsion of the protons and from the surface tension forces, are calculated on the basis of the statistical model. The density throughout the interior of the heaviest nuclei is found to be about one-third less than in medium light nuclei ($A\sim 50$). The trend of $r_0=R/A^{\frac{1}{3}}$ from the lightest to the heaviest elements is discussed and compared with experiment.

INTRODUCTION

THE law that the nuclear volume is proportional to the total number of particles in the nucleus is an approximate theoretical consequence of the statistical treatment of nuclei with exchange-saturation type forces acting between the particles. Let R denote the radius of the sphere into which the particles are packed with constant density; then $R=r_0A^{\frac{1}{3}}$ where A is the mass number and r_0, representing the interparticle distance, depends only on the ratio N/Z of neutrons to protons. The monotonic increase of this ratio along the periodic table introduces a correction term to the density which, although constant within a given nucleus, will decrease slowly with increasing mass number. The kinetic energy part of this correction is due essentially to the exclusion principle and the potential energy part to the symmetry and saturation properties of the Hamiltonian, and both parts raise the energy and diminish the density as N/Z increases. The correction to the density depends on the nuclear compressibility which can be explicitly evaluated from the statistical model.

Through the introduction of surface effects due partly to the desaturation of the short-range forces near the boundary of the nucleus and partly to the diffuseness of the boundary associated with the uncertainty principle, the density throughout the nucleus will be altered. Omitting from consideration the lighter nuclei ($A\lesssim 50$), we can assume the same thickness of surface layer for all nuclei.[1] The density falls off continuously from the constant value in the interior over an effective distance approximately equal to the range a of nuclear forces. The "geometrical radius" of the nucleus, including the surface region, will differ from the "constant density radius" by approximately $a/2\sim\lambda\sim 10^{-13}$ cm. The surface tension forces uniformly contract the compressible nuclear matter and the resulting density in the interior is greater and the radius R smaller than their Majorana values. The correction to the density decreases with increasing mass number since the surface pressure is inversely proportional to the radius. Consequently, the density in the interior diminishes as A increases. For light nuclei ($A\lesssim 50$) the surface region can no longer be properly differentiated from the interior. If the density of particles be represented by a Gaussian distribution about the center of the nucleus, the nuclear radius can be defined in terms of the breadth of this distribution and the $A^{\frac{1}{3}}$ law will still hold approximately true.[2] In the transition to light nuclei, the increased density in the interior due to surface tension is compensated by the reduced density in the surface layer. Accordingly, one can even expect that the average density is less and the average r_0 (to be denoted by r_G) greater as one goes to *smaller* mass numbers.

A third correction to the $A^{\frac{1}{3}}$ law arises from the mutual electrostatic repulsion of the protons. This effect, which has already been considered by several authors,[3-5] obviously leads to an increase of r_0 with increasing Z. An additional effect of the Coulomb forces is to distort the

* On leave of absence from Purdue University.

[1] $A\sim 50$ marks the minimum of the packing fractions curve, where surface effects have become small compared to volume effects.

[2] S. Flügge, Zeits. f. Physik **96**, 459 (1935).

[3] K. Nakabayasi, Zeits. f. Physik **97**, 211 (1935).

[4] H. A. Bethe and R. F. Bacher, Rev. Mod. Phys. **8**, 82 (1936).

[5] E. Feenberg, Phys. Rev. **59**, 149 (1941).

constant density distribution: the proton density tends to increase toward the boundary of the nucleus and the correlated neutron density varies in a similar manner. This effect has been discussed by Feenberg[6] who has shown that although the departure from uniform density is appreciable, the associated energy correction is small and the correction to the radius negligible.

Save for light nuclei, all three corrections tend to increase r_0 with increasing A. The calculations to be described give for the constant density radii:

$$R=r_0A^{\frac{1}{3}}=r^*_0A^{\frac{1}{3}}\{1+0.8(N-Z)^2A^{-2} -0.3A^{-\frac{1}{3}}+0.010Z^2A^{-4/3}\}, \quad (1)$$

where the corrections in order represent the effects of $N\neq Z$, of surface tension and of electrostatic repulsion. The factor in brackets increases by 9 percent from Fe^{56} to Pb^{207}. The Gaussian radii for light nuclei are given by:

$$R_G=r_GA^{\frac{1}{3}}=r^*_GA^{\frac{1}{3}}\{1+0.7A^{-\frac{2}{3}}\}. \quad (2)$$

The factor in brackets has a 7 percent increase from Sc^{41} to N^{13}; when the effects of neutron excess and Coulomb repulsion are included, this is reduced to 5 percent. Values of r^*_0 and r^*_G may be determined empirically.

Calculations

Bethe and Bacher[4] have outlined the calculations of the statistical model, assuming Gaussian functions for the intranuclear forces. Their notation will be used as far as possible. The total energy E of the nucleus in its ground state is expressed as a function of the adjustable parameter x which is proportional to the cube root of the density:

$$E(x)=\alpha(x)A+\beta(x)(N-Z)^2A^{-1} +\gamma(x)A^{\frac{2}{3}}+\delta(x)Z^2A^{-\frac{1}{3}}. \quad (3)$$

The first term gives the main binding energy when $N=Z$, the second term the correction when $N\neq Z$, the third term the surface energy, and the fourth term the classical Coulomb energy of the protons.[7] The $A^{\frac{1}{3}}$ law for the nuclear radius is obtained when only the first term is taken; when this is minimized with respect to x, we obtain the standard density x_0^3. The inclusion of the three additional terms shifts the minimum of the energy from x_0 to x'_0. Let

$$x'_0=x_0\{1+c_\beta(N-Z)^2A^{-2} +c_\gamma A^{-\frac{1}{3}}+c_\delta Z^2A^{-4/3}\}, \quad (4)$$

where the c's are all small. Since $\alpha'(x'_0)=(x'_0-x_0)\alpha''(x_0)$, we obtain:

$$x_0c_\beta=-\frac{\beta'(x_0)}{\alpha''(x_0)};\quad x_0c_\gamma=-\frac{\gamma'(x_0)}{\alpha''(x_0)};\quad x_0c_\delta=-\frac{\delta'(x_0)}{\alpha''(x_0)}. \quad (5)$$

The quantity $x_0^2\alpha''(x_0)$ is inversely proportional to the compressibility of nuclear matter; in fact, we have for the compressibility

$$\kappa=12\pi r_0^3/x_0^2\alpha''(x_0). \quad (6)$$

From the statistical model with Gaussian potentials of interaction radius a, the following expressions are obtained:

$$\begin{aligned}\alpha(x)&=(3/10)T_0x^2-9A^*x^{-3}[2-3x^2 +(x^2-2)\exp(-x^2)+\pi^{\frac{1}{2}}x^3\Phi(x)],\\ \beta(x)&=(1/6)T_0x^2+(A^*/3x) \times[7x^2-9+(2x^2+9)\exp(-x^2)],\\ \gamma(x)&=(9/8)(3/\pi)^{\frac{1}{2}}(a/t)T_0x -(12/175)(3/\pi)^{\frac{1}{2}}(t/a)T_0x^3\\ &\quad+(27/5)(3/\pi)^{\frac{1}{2}}(t/a)A^*x^{-4} \times[x^4-4x^2+6-(2x^2+6)\exp(-x^2)],\\ \delta(x)&=(2/5)(3/\pi)^{\frac{1}{2}}(e^2/a)x,\end{aligned} \quad (7)$$

where

$$x=(3/2)(\pi/3)^{\frac{1}{2}}(a/r_0);\quad T_0=\hbar^2/Ma^2;\quad A^*=A/8\pi^{\frac{1}{2}}$$

and A is the depth of the Gaussian well potential $-A\exp[-(r/a)^2]$ for the ground state of the deuteron. $\Phi(x)$ represents the error integral. The symmetrical Hamiltonian with the Volz[8] conditions has been used in the expressions for $\alpha(x)$ and $\beta(x)$. The formula for $\gamma(x)$ has been given for the case that the auxiliary potential falls off linearly in the surface region over a distance t: the last two terms represent the corrections to the kinetic and potential energies due to the

[6] E. Feenberg, Phys. Rev. **59**, 593 (1941).

[7] The exchange part of the Coulomb energy has been omitted here, since its effect on the results is negligible.

[8] H. Volz, Zeits. f. Physik **105**, 537 (1937). The result for c_β depends only slightly on the special choice of constants in the Hamiltonian.

redistribution of the particles and the first term[9] corrects for the fact that the statistical model does not give an infinite kinetic energy for a sharp nuclear boundary. $\gamma(x)$ has to be minimized with respect to t.

The *ad hoc* constants of the statistical model (reference 4, Eq. (164)) were used to calculate the corrections to the nuclear radius. Since these constants give too strong an interaction between the nuclear particles, they may be expected to give too large results for quantities other than the main binding energy which depend on the strength of the forces. Thus $\beta(x_0)=32$ Mev and $\gamma(x_0)=17$ Mev compared with the semi-empirical values of 20 Mev and 13 Mev, respectively. The constants[10] determined from the hydrogen and helium isotopes and two-particle scattering experiments give too small results; in calculating the c's a suitable average was taken with less weight being put on the latter constants since they give probably too small a value for the inverse compressibility $x_0^2\alpha''(x_0)$. From the *ad hoc* constants we obtain $x_0^2\alpha''(x_0)=72$ Mev, in agreement with semi-empirical estimates of Feenberg.[5]

The values of c_β and c_γ have also been estimated in a quasi-classical way assuming that the $N-Z$ correction energy was inversely proportional to the nuclear volume and that the surface energy contained a surface tension factor which was independent of R. Substituting semi-empirical values for β, γ and κ, the resulting values for c_β and c_γ agreed within 20 percent with those calculated from the statistical model.

The calculations of Flügge[2] have been used to estimate the surface corrections for light nuclei. Assuming that the density of protons (and of neutrons similarly) could be represented by the Gaussian distribution

$$\rho=(2/\pi)^{\frac{3}{2}}(Z/R_G^3)\exp[-2(r/R_G)^2], \qquad (8)$$

he calculated the binding energy statistically with the "nuclear radius" R_G as an adjustable parameter. His results for a suitable choice of the constants lead to Eq. (2).

Applications

Since the nuclear radius can only be defined precisely in terms of the operations used to measure it and since these operations are widely different in character and theoretically unrelated except in a very approximate way at present, it is clear that the intercomparison of nuclear radii derived by different methods from different parts of the periodic table can be somewhat misleading. To obtain reliable evidence for the effects discussed in this paper, it is necessary to have at least one method for measuring nuclear radii which can be applied over the entire periodic table. Measurements of the cross sections for elastic and inelastic scattering of fast neutrons would provide two suitable methods. In view of the experimental uncertainties in the latter measurements, we shall consider only the evidence from elastic scattering experiments. As was pointed out by Placzek[11] and Bethe,[12] the elastic scattering of fast neutrons can be described by the formula for Fraunhofer diffraction around a spherical obstacle.[13] The differential cross section for the scattering is given by

$$\sigma(\theta)=[R'J_1(kR'\sin\theta)/\sin\theta]^2, \qquad (9)$$

where J_1 is a Bessel function of the first kind, k is the wave number of the incident neutrons, and R' the effective radius of the nucleus acting as a screen. Bethe[14] has shown that, because of the finite range of the forces extending beyond the nuclear boundary, the effective nuclear radius is increased for elastic scattering by about 10^{-13} cm. The difference between the "screening radius" of the elastic scattering experiments and the "constant density radius" of the statistical model is independent of mass number, and is approximately $R'-R\sim 2\times 10^{-13}$ cm. The experimental results of Wakatuki[15] on Fe and on Pb are well fitted by the diffraction formula (except for the measurements at 14°) with $R'(\text{Fe})=7.4\times 10^{-13}$ cm and $R'(\text{Pb})=11.3\times 10^{-13}$ cm. These two values are almost exactly in the ratio of the cube roots of the respective mass numbers; since $R'>R$, this provides direct

[9] C. v. Weiszäcker, Zeits. f. Physik **96**, 431 (1935).
[10] W. Rarita and R. D. Present, Phys. Rev. **51**, 788 (1937).
[11] I am indebted to Dr. Placzek for a discussion of the elastic scattering experiments.
[12] G. Placzek and H. A. Bethe, Phys. Rev. **57**, 1075A (1940).
[13] M. Born, *Optik* (J. Springer, Berlin, 1933), p. 160.
[14] H. A. Bethe, Phys. Rev. **57**, 1125 (1940).
[15] T. Wakatuki, Proc. Phys.-Math. Soc. Japan **22**, 430 (1940).

evidence for the calculated inflation effect ($r_0(\mathrm{Pb}) > r_0(\mathrm{Fe})$). The earlier data of Kikuchi, Aoki, and Wakatuki[16] are best fitted with $R'(\mathrm{Fe}) = 6.5\times10^{-13}$ cm and $R'(\mathrm{Pb}) = 10.2\times10^{-13}$ cm. Averaging the results of the two experiments, subtracting 2×10^{-13} cm and dividing by $A^{\frac{1}{3}}$, we obtain $r_0(\mathrm{Fe}) = 1.30\times10^{-13}$ cm and $r_0(\mathrm{Pb}) = 1.48\times10^{-13}$ cm; an increase of 13 percent compared with the theoretical estimate of 9 percent from Eq. (1). Actually it is somewhat questionable to apply the diffraction formula in this region where the neutron wave-length is still comparable with the nuclear radius ($\lambda\!\!\!^{-} \sim 2.5\times10^{-13}$ cm). Much interesting information about nuclear radii could be obtained by investigating the elastic scattering at higher neutron energies.

The evidence from the penetration of potential barriers is less certain.[17] Weisskopf and Ewing[18] have derived a value of $r_0 = 1.3\times10^{-13}$ cm from proton penetrabilities into elements with $A \sim 60$. It is unsatisfactory to compare this value with the r_0 derived from the spontaneous alpha-decay because of the uncertainties in the interpretation of the latter. The Weisskopf-Ewing radii, taken together with the trend of r_0 discussed in this paper, would indicate that the radii of the heaviest nuclei are close to the Gamow values; hence, the many-body correction and the correction for the finite radius of the alpha-particle must nearly cancel one another. Another method for estimating r_0 is from the Weizsäcker-Bethe semi-empirical formula with the constants adjusted to fit known mass defects. The Dempster[19] packing fractions for ${}_{22}\mathrm{Ti}^{48}$, ${}_{46}\mathrm{Pd}^{108}$, and ${}_{78}\mathrm{Pt}^{195}$ lead to a value of $r_0 = 1.2\times10^{-13}$ cm, whereas ${}_{46}\mathrm{Pd}^{108}$, ${}_{78}\mathrm{Pt}^{195}$, and ${}_{92}\mathrm{U}^{238}$ give $r_0 = 1.3\times10^{-13}$ cm. The increase in r_0 lies within the limits of error and need not be real.

The trend of r_0 from $A \sim 50$ down to very light nuclei is also rather uncertain. The data on elastic scattering of neutrons by Al nuclei cannot be used to get an accurate value of r_0 because the measurements are not much above the background; also the wave-length $\lambda\!\!\!^{-}$ and the correction $R' - R$ are almost as large as R itself. Values of r_0 can be obtained from the Coulomb energy differences between the light positron emitters and their stable isobars. Assuming either a constant density distribution of the protons, or else the Gaussian distribution (8), whose electrostatic energy is given by $(1/\sqrt{\pi})Z^2e^2/R_G$, or any similar distribution, the experimental results[20] from the positron spectra of elements between $A = 11$ and $A = 41$ indicate a remarkable constancy of r_0 or r_G over the entire region.[21] If the statistical estimate of the Coulomb exchange energy is included, the values of r_0 and r_G are found to increase slightly with increasing A in contrast to what is predicted by Eq. (2). It does not seem justifiable to make comparisons between the radii determined in this way and the "penetrability radii" of Weisskopf and Ewing.

I wish to express my appreciation of the hospitality of the Harvard Physics Department.

[16] Kikuchi, Aoki and Wakatuki, Proc. Phys-Math. Soc. Japan **21**, 410 (1939).

[17] The "penetrability radii" may be expected to be rather close to the "geometrical radii": although the Coulomb law breaks down somewhat beyond the nuclear boundary, the artificially sharp cut-off of the Coulomb potential assumed in calculating the penetration factor mostly compensates for this by giving too small a breakdown distance.

[18] V. F. Weisskopf and D. Ewing, Phys. Rev. **57**, 472 (1940).

[19] A. J. Dempster, Phys. Rev. **53**, 869 (1938).

[20] M. G. White, E. C. Creutz, L. A. Delsasso and R. R. Wilson, Phys. Rev. **59**, 63 (1941). D. R. Elliott and L. D. P. King, Phys. Rev. **59**, 403 (1941).

[21] Any smooth distribution in density of the form $\rho = \rho_0 f(r/R)$ will have an electrostatic energy proportional to Z^2e^2/R and will exhibit the same agreement with the $A^{\frac{1}{3}}$ law as the constant density distribution.

An Electron Lens Type of Beta-Ray Spectrometer*†

CLIFFORD M. WITCHER
Department of Physics, Columbia University, New York, New York

(Received April 21, 1941)

A beta-ray spectrometer utilizing the focusing action of the homogeneous magnetic field produced by a long solenoid is described. The theory of the action of an instrument of this type is considered in some detail for the case of a point source of beta-rays, and the extension of the theory to cover the case of an actual source of finite area is discussed. Details of design are given, together with a number of experimental tests which have been made on the instrument. These tests include measurements of the absorption of beta-rays in the Cellophane window of the G-M counter used for detection, measurement of the resolution and efficiency of the spectrometer, calibration of the instrument, and an examination of the beta-ray spectrum of radium E. The beta-spectra of phosphorus $_{15}P^{32}$ and iridium $_{77}Ir^{194}$ have been investigated. The forms of the distribution curves all agree better with the Fermi than the K-U theory. It is concluded that the spectrometer operates satisfactorily and possesses some definite advantages over the conventional designs.

INTRODUCTION

THE most common methods for investigating beta-ray energies which have been in use for the past three decades are: (1) absorption measurements, (2) measurements with a cloud chamber in a magnetic field, and (3) measurements with a magnetic spectrometer essentially like the type developed by Rutherford and Robinson[1] in 1913.

The suggestion that a large solenoid might be used as an electron lens to focus beta-rays of determinate energy upon some sort of detecting device appears to have been first made by Kapitza[2] in 1923. In 1924 an instrument of this type was built by Tricker.[3] More recently Klemperer[4] has constructed an electron lens type of spectrometer, using the focusing properties of a flat coil.[5]

If one considers the operation of a spectrometer utilizing the electron lens properties of a solenoid, it soon becomes evident that, if a satisfactory instrument of this type could be designed, it would possess several marked advantages compared to the conventional spectrometer,[6] among which might be mentioned the following: (1) The efficiency of the spectrometer can be relatively high, since a larger solid angle at the source can be utilized without sacrifice of resolving power. (2) Source material can be distributed over the surfaces of thin films of collodion or some similar substance, covering an area much larger than that generally possible in the conventional type of spectrometer. It is thus possible for an instrument of this type to furnish data on materials whose activity cannot be concentrated sufficiently for use in the usual type. (3) Only one layer of absorbing material (the window of the G-M counter) is present in the electron path. (4) The source can be located relatively far from any scattering material except that of the source holder itself. (5) The relatively large distance between source and detector, together with the large amount of absorbing material interposed by a central baffle system, should practically eliminate detection of gamma-rays.

THEORY OF SPECTROMETER

A. General considerations

The theory of the action of magnetic electron lenses has been treated at length by various workers.[4, 7, 8] The present discussion is confined to

* Submitted in partial fulfillment of the requirements for the degree of Doctor of Philosophy in the Faculty of Pure Science, Columbia University, New York, New York.

† Publication assisted by the Ernest Kempton Adams Fund for Physical Research of Columbia University.

[1] E. Rutherford and H. Robinson, Phil. Mag. **26**, 717 (1913).

[2] P. Kapitza, Proc. Camb. Phil. Soc. **22**, pt. 3.

[3] R. A. R. Tricker, Proc. Camb. Phil. Soc. **22**, 454 (1924).

[4] O. Klemperer, Phil. Mag. **20**, 545 (1935).

[5] A flat coil type of electron lens spectrometer has been constructed recently by M. Deutsch, Phys. Rev. **59**, 684A (1941).

[6] Witcher, O'Conor, Haggstrom and Dunning, Phys. Rev. **55**, 1135A (1939).

[7] W. Glaser, Zeits. f. Physik **109**, 700 (1938).

[8] J. H. McMillen and G. H. Scott, Rev. Sci. Inst. **8**, 288 (1937).

the simple treatment of a few of the relations which have the most direct bearing on the use of the uniform solenoid lens for the examination of beta-ray spectra.

We consider an electron which is initially projected with momentum p,

$$p=m_0\beta c/\sqrt{(1-\beta^2)}$$

in a direction making an angle α with the direction of a uniform magnetic field H. The electron's path will have the form of a circular helix of radius

$$\rho=(p/He)\sin\alpha \tag{1}$$

and pitch

$$L=(2\pi p/He)\cos\alpha. \tag{2}$$

If z denotes the displacement of the electron from the initial position in the direction of H, and r its displacement perpendicular to H, it is readily shown that:

$$r=(L/\pi)\tan\alpha\sin(\pi z/L). \tag{3}$$

To examine this equation it is convenient to introduce the variable

$$D=L/(\pi\cos\alpha)=2p/He,$$

whereupon (3) takes the form:

$$r=D\sin\alpha\sin[z/(D\cos\alpha)]. \tag{4}$$

With the condition that the field H is initially fixed, this equation indicates (1) how r varies with z along the path of any particular electron (D and α constant), or (2) how, at a specified distance z from the initial position of the electron, the displacement r varies with departure angle α for electrons of the same momentum (z and D constant), or (3) how, for fixed z and α, r varies with electron momentum.

The first case is obvious, and case (3) need not be considered in this discussion.

As α increases from 0 to $\pi/2$, z and D constant, r starts from 0 and oscillates between a succession of positive and negative maxima, these being located at the values of α for which $\partial r/\partial\alpha=0$. The zeros of $|r|$ lying between successive maxima are at the α values for which

$$z/(D\cos\alpha)=n\pi, \quad n=1,\ 2,\ \cdots.$$

Physically, this behavior of $|r|$ corresponds to the fact that electrons with the same momentum,

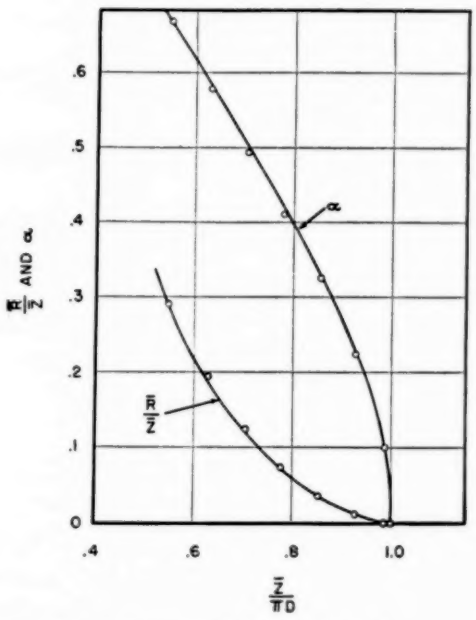

FIG. 1. Geometrical design functions.

but leaving the source with larger and larger departure angles, may cross the plane determined by z during the first, second, third, etc., turns of their helical paths. Further investigation indicates that the successive maxima of $|r|$ in the direction of increasing α are consecutively greater, approaching the limiting value D as α approaches $\pi/2$. Physically this expresses the fact that, as α increases, the pitch of the helix contracts, its diameter becoming correspondingly greater. For $\alpha=\pi/2$, the helix becomes a circle of diameter $D=2p/He$.

B. Intensity and resolution for a point source

It is difficult to obtain a general treatment of the problems of intensity and resolution when the source of electrons has a finite area in the plane perpendicular to the magnetic field. However, the treatment for a point source may be used to suggest the features of the more general problem.

Consider a source at the point $(r, z)=0$ emitting electrons with all possible momenta from 0 to some upper limit, the emission being assumed isotropic. We first wish to examine the distribution of the current arising from electrons whose momenta lie in the neighborhood of a given value p in the plane determined by assigning to z the value $\bar{z}$. From the analysis given above for the case z and D constant, it appears that at each

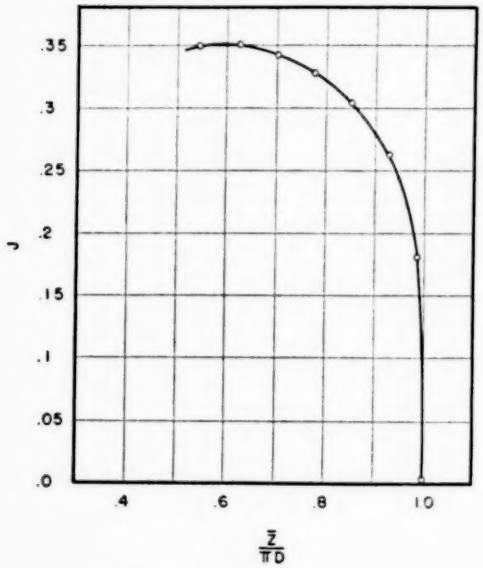

FIG. 2. Intensity function J.

value of r there will be contributions to the current arising from an infinite set of α values, extending from some definite lower limit to $\pi/2$. Let $I(r, \alpha)$ denote the contribution to the density of current at r due to any specified value of α from this set. Then $I(r, \alpha)$ must be proportional to $\sin\alpha$, and also to $\partial\alpha/\partial r$. It therefore follows that I will become infinite at the points where $\partial r/\partial\alpha = 0$, *viz.*, the maxima of $|r|$ as function of α considered previously. The current distribution due to electrons of the same momentum will therefore be characterized by the existence of a set of concentric "focal rings," upon which its density becomes infinite. The smallest ring will occur at the smallest value of r for which $\partial r/\partial\alpha$ vanishes. If this derivative vanishes concurrently with r, we may speak of a "point focus." We have, from (4):

$$\partial r/\partial\alpha = D\cos\alpha \sin[z/(D\cos\alpha)] + z\tan^2\alpha\cos[z/(D\cos\alpha)] = 0. \quad (5)$$

On setting $y = z/(D\cos\alpha)$, this gives:

$$\bar{\alpha} = \tan^{-1}\sqrt{[-(1/y)\tan y]}. \quad (6)$$

The symbol $\bar{\alpha}$ is used to identify the α value as that corresponding to a maximum of $|r|$. (It is convenient to consider y as a parameter in this and the succeeding two relations.) Combining the last relation with (4) and (5) and using $\bar{r}$ to denote the maximum value of r thus obtained, we have:

$$\bar{r}/\bar{z} = [(\sin y)/y]\tan\bar{\alpha}, \quad (7)$$

$$\bar{z}/\pi D = (1/\pi)y^{\frac{1}{2}}/\sqrt{(y - \tan y)}. \quad (8)$$

By use of the last three relations, with y as a parameter, the curves of Fig. 1 are obtained. These curves exhibit $\bar{\alpha}$ (corresponding to the *first* maximum of r) and $\bar{r}/\bar{z}$ as functions of $\bar{z}/\pi D$ from $\bar{z}/\pi D = 0.5$ to 1.0. ($\bar{\alpha}$ is plotted in radians, on the same scale as that of $\bar{r}/\bar{z}$.) If $\bar{z}$ is regarded as fixed, these curves indicate the variation of $\bar{\alpha}$ and of the radius of the first focal ring as functions of electron momentum. The first point focus occurs at $\bar{z}/\pi D = 1$, $\alpha = 0$. As $\bar{z}/\pi D$ decreases, this opens up into the first ring focus, as indicated in Fig. 1. For $\bar{z}/\pi D = 0.9$, $\bar{\alpha} = 15°$ approximately, and $\bar{r}/\bar{z} = 0.020$. For $\bar{z}/\pi D = 0.8$, $\bar{\alpha} = 22.5°$ and $\bar{r}/\bar{z} = 0.063$.

Intensity relations.—The current flowing through the annular area of radii $\bar{r} - \Delta r$ and $\bar{r}$ will be proportional to

$$\int_{\bar{\alpha}-\Delta\alpha_1}^{\bar{\alpha}+\Delta\alpha_2} \sin\alpha d\alpha \approx (\sin\bar{\alpha})(\Delta\alpha_1 + \Delta\alpha_2),$$

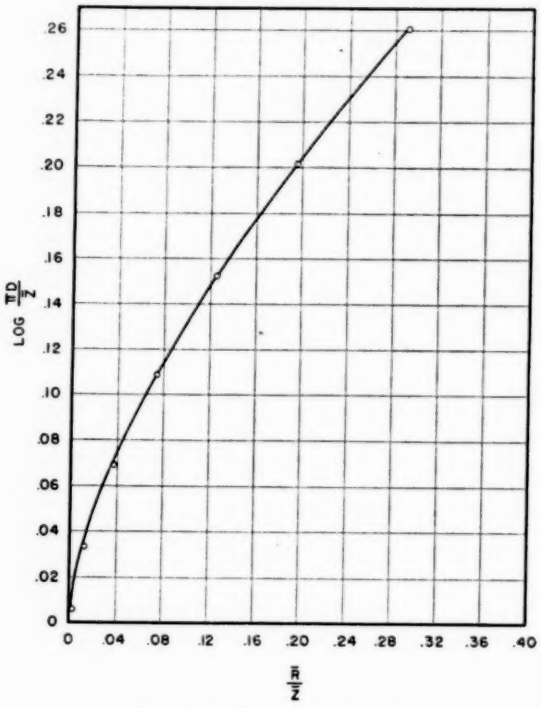

FIG. 3. Resolution function.

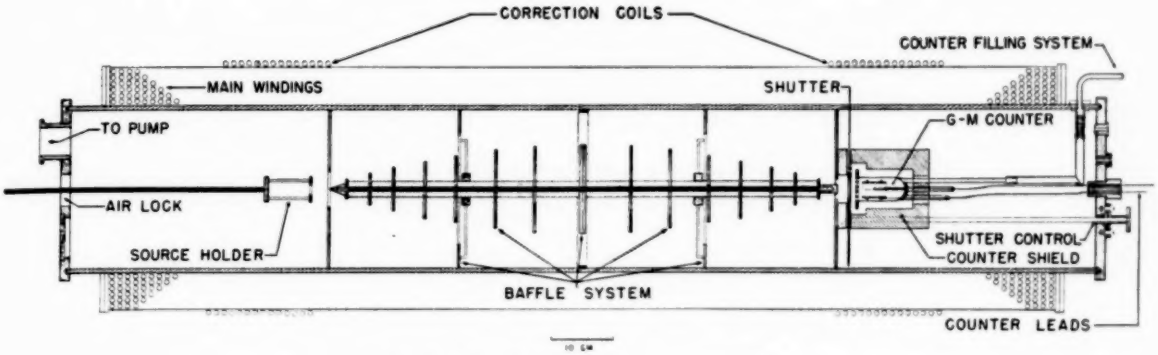

FIG. 4. Solenoidal beta-ray spectrometer.

where

$$\Delta\alpha_1+\Delta\alpha_2=2\sqrt{[-\Delta r/(\tfrac{1}{2})(\partial^2 r/\partial\alpha^2)_{\bar{\alpha}}]}. \quad (9)$$

The intensity function

$$J=\sin\bar{\alpha}/\sqrt{(-\partial^2 r/\partial\alpha^2)_{\bar{\alpha}}} \quad (10)$$

is plotted against $\bar{z}/\pi D$ in Fig. 2. This function gives an indication of the variation with $\bar{z}/\pi D$ of the current to be expected through a ring of constant width Δr and outer radius $\bar{r}$, $\bar{r}$ being the radius of the first focal ring. Note that J is a maximum at $\bar{z}/\pi D=0.6$, and that it begins to drop rather sharply above $\bar{z}/\pi D=0.85$.

Resolving power.—A convenient criterion of resolving power is the rate of variation of D (i.e., of electron momentum) with $\bar{r}$, expressed as a fraction of D itself. We accordingly consider

$$(1/D)(dD/d\bar{r})=(d/d\bar{r})(\log D). \quad (11)$$

In Fig. 3, $\log_{10}(\pi D/\bar{z})$ is plotted against $\bar{r}/\bar{z}$. The resolving power, as indicated by the slope of this curve, is greatest for $\bar{r}/\bar{z}=0$, decreasing rapidly until $\bar{r}/\bar{z}=0.10$, and then becoming approximately constant.

DESIGN OF SPECTROMETER

A. Design criteria

The utility of any beta-ray spectrometer will depend in general upon the following three criteria: (1) the range in energy over which the instrument can be used; (2) the sharpness of resolution; (3) the efficiency, as measured by the fraction actually detected of the beta-rays which leave the source with energies lying in the band passed by the instrument.

B. Maximum energy

Equation (2) in the form

$$HL/\cos\alpha=2\pi p/e$$

indicates that the maximum momentum (and hence the maximum energy) which it is possible to measure with an instrument of this type will depend on (1) the maximum obtainable field strength and (2) the length and diameter of the region in which the field can be considered uniform; i.e., the region between source and counter. In fact, the maximum energy increases with each of these factors.

C. Efficiency and resolution

From the theory outlined above, the electrons are brought to a focus at the plane $\bar{z}$ in a ring of radius $\bar{r}$. The geometry of the instrument may therefore be determined by a diaphragm provided with an annular slit of suitable radius and width equal to a small fraction of its radius, together with a baffle system which will allow only electrons with the correct angle of emergence $\bar{\alpha}$ to pass through the spectrometer.

The consideration of an extended beta-ray source in the form of a disk perpendicular to the magnetic field shows that the momentum values passed by the instrument are a function of (1) the distance from the axis to the initial position of the electron and (2) the azimuthal angle of its initial direction of motion. Since the resolving power decreases somewhat from the center of the source to its edge, the final design is a compromise between the resolution, the efficiency, and the area of the active material. Equation (4) and the curves in Figs. 2 and 3 permit approximate

selection of the actual geometrical design factors for a given resolution and efficiency.

Description of Apparatus

A. General features of spectrometer

The general features of the spectrometer as finally designed[6] are shown in Fig. 4. Essentially, it consists of a long solenoid having the source of beta-radiation placed on the axis near one end and a G-M counter for detection placed 90 cm distant in the analogous position near the other end. Between source and counter are interposed a series of Duralumin disks and rings, which serve to specify, within definite limits, the dimensions of the helical paths which the electrons may follow in passing from source to counter.

The dimensions of the instrument were primarily determined by the power supply, a 600-ampere 30-volt d.c. generator, which was available before design of the spectrometer was begun. The theoretical considerations outlined indicate that for a specified power supply, the solenoid should be designed for (1) maximum field strength, (2) maximum length of homogeneous field region, and (3) maximum ratio of diameter to length.

B. Solenoid

The solenoid was made by winding six layers of $\frac{1}{4}$-inch diameter copper tubing (0.035-inch wall thickness) on a brass tube 10.5 inches o.d., 10 inches i.d., and 66 inches long. The actual length of winding is 60 inches, and there are 220 turns per layer. The tubing for each layer was fabricated in one piece (lengths ranging up to 700 feet) by the manufacturers and has double cotton insulation 4.0 mils thick. All six layers of the winding are connected in parallel electrically by bus bars and also in parallel hydraulically by manifolds. The waterflow through the coil at 50 lb./in.^{2} pressure is adequate for cooling under full load conditions (18 kw). To improve the homogeneity of the field inside the solenoid, correcting coils consisting of 90 turns of No. 12 wire were wound 12 inches from each end of the main winding. These correcting coils, together with a rheostat, are connected across the main winding.

Careful comparison measurements with a standard solenoid showed that this solenoid gives a field of 1.859 oersteds/ampere, corresponding to a field of 1115 oersteds with 600 amperes through the coil. Investigation of field distribution showed that the homogeneity of the field at all points between the positions of source and counter is better than 1 percent.

C. Baffle system

The construction of the baffle system is shown in Fig. 4. The positions and diameters of the disks forming the central baffle were calculated so that the edges of the disks lie on a surface of revolution formed by rotating about the axis of the instrument a sine curve of amplitude 7.16 cm and half-period 90 cm, starting from the source position. The middle diaphragms have openings whose edges lie on a similar surface of amplitude 12.5 cm and half-period 90 cm and intersecting the instrument axis at the same points as the previous surface. The over-all length of the baffle system is 82 cm, there being a space of 4 cm between the source position and the annular opening in the first ring. The edges of the annular slit at the counter end also lie on the two surfaces of revolution previously described, and the slit is 3 cm o.d. and 2 cm i.d. The resolution and efficiency of the spectrometer for a source of 2-cm diameter are determined almost entirely by this final annular slit.

The central series of disks, together with their spacers, are held together by a Duralumin rod which passes through them. This central disk system is supported by the outer system of ring baffles through the two sets of radial rods. The baffle system was made of Duralumin to minimize electron scattering, and the further precaution was taken of painting all surfaces with thick colloidal graphite (Aquadag).

D. Source holder

The source holder is designed to minimize all possible scattering from the support and to permit quick introduction through an air lock. In this spectrometer, the radioactive material may be deposited on an area 2 cm in diameter without materially reducing the resolution, which permits the use of very thin sources. The thin collodion layer on which the source is deposited is mounted on a thin aluminum ring 3.5 cm in diameter, which is in turn supported by three thin alumi-

num rods attached by a plate to the end of a rod which enters the instrument through a Neoprene seal of the type described by Wilson and Kamen.[9] The gate valve air lock is essential to facilitate quick operation without destroying the vacuum, since the vacuum must be maintained at about 10^{-4} mm Hg by an oil diffusion pump in order to prevent discharges from occurring between the G-M counter leads.

E. The G-M counter

A single G-M counter is adequate for this type of spectrometer. Coincidence methods are unnecessary, since gamma-radiation from the source can contribute virtually nothing because of the large distance from source to counter and the interposed baffles.

The design of the counter used in this spectrometer has necessarily been somewhat unconventional: (1) because the window through which the beta-rays were to enter had to be placed at one end of the counter rather than in the side wall, and (2) because it was desired to construct a window which should be at least 3.0 cm in diameter and as thin as possible. The final design adopted is shown in Fig. 5. The cylindrical copper cathode is 3 cm i.d. and 4 cm long, and the central wire is 4-mil tungsten with a glass bead on the free end.[10] A glass sleeve covers the counter wire to within 1.5 cm of the end in order to minimize the active volume and reduce the background. The counter windows used thus far have been of Cellophane 0.5 mil thick (1.75 mg/cm^2), but considerably thinner films of collodion may be used to facilitate more accurate measurements at low energies. The window is clamped between a brass ring and a 1.6 mm thick brass grille, a very thin rubber gasket being interposed between the ring and the Cellophane. This assembly is cemented to the front end of the counter with picein. (Note that the grille is on the outside of the Cellophane.) The grille was made by drilling holes 0.32 cm in diameter in a brass plate, and its open area is 73 percent.

A mixture of 9 cm argon, and 1 cm ethyl alcohol[11] has proved satisfactory for operation

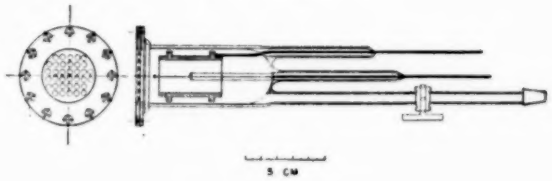

FIG. 5. G-M counter.

over periods as long as several weeks. The counter filling system with appropriate argon and alcohol reservoirs is permanently connected to the counter, but a stopcock operable through a Neoprene seal permits the counter to be isolated from the filling system.

While the geometrical proportions of the counter were necessarily bad, very satisfactory operation at high speeds was achieved by a capacitance coupled multi-vibrator quenching circuit which is a modification of that described by Getting.[12] An amplifier tube preceding a biased low impedance multi-vibrator circuit resulted in positive operation under all conditions. A scale-of-eight demultiplying circuit utilizing three pairs of 6SJ7 tubes permitted counting at high rates. It was observed that much more satisfactory quenching of the counter pulses was obtained when the metal grille was held at about $\frac{1}{3}$ the potential of the anode.

When shielded by lead 2.5 cm thick to minimize stray radiation effects, the natural background of the counter system was approximately 10 counts/min. The counter threshold was approximately 1300 volts, and the "plateau" about 300 volts broad with a slight positive slope. Counter operation was regularly checked with a small radium source placed in a standard position, but over periods of many weeks no deviations were observed beyond those expected statistically.

As shown in the drawing, a shutter operable from outside was placed in front of the counter. Four holes in the shutter permitted absorption measurements to be made on selected materials for electrons having any desired energy.

F. Spectrometer power supply

The current for the solenoid windings from the 600-ampere 30-volt d.c. generator is stabilized by a voltage regulator similar to the type described

[9] R. R. Wilson and M. D. Kamen, Phys. Rev. **54**, 1031 (1938).
[10] J. R. Dunning and S. M. Skinner, Rev. Sci. Inst. **6**, 243 (1935).
[11] A. Trost, Zeits. f. Physik **105**, 399 (1937).
[12] I. A. Getting, Phys. Rev. **53**, 103 (1938).

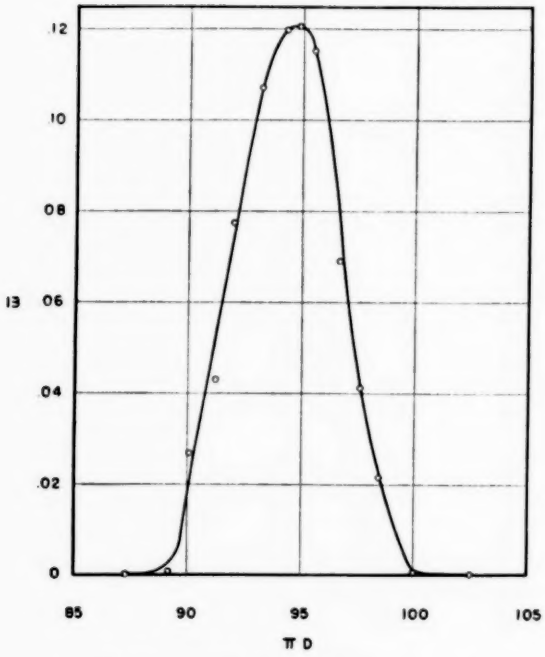

FIG. 6. Theoretical resolution curve and experimental points.

by Anderson, Dunning and Mitchell,[13] current fluctuations being not greater than 0.2 percent. Currents are measured by calibrated shunts connected to an ammeter or potentiometer.

EXPERIMENTAL TESTS OF INSTRUMENT

A. Test of resolving power—theoretical resolution

The *absolute* minimum and maximum values of πD (most convenient geometrical quantity for use in all discussions of resolution) can readily be calculated from Eq. (4), taking the source diameter as 2 cm and the baffle dimensions given previously. They are: $\pi D_{\min}=88.15$ cm, $\pi D_{\max}=100.19$ cm. The maximum and minimum starting angles for electrons are 23° 30′ and 12° 36′, respectively. What may be called the "resolution curve" of the instrument is obtained by a calculation of the effective solid angle $\bar{\omega}$, averaged over the entire source area, for electrons which pass through the baffle system as a function of πD over the range of this quantity. The ordinates on the theoretical resolution curve (Fig. 6) are the values (obtained by a process of numerical integration) of $\bar{\omega}$. The maximum value of $\bar{\omega}$ is approximately 0.122, giving a theoretical maximum efficiency of detection of approximately $0.122/4\pi=1$ percent. The value of πD at the peak of the curve is 94.7 cm. The estimated error in $\bar{\omega}$ introduced by numerical approximations does not exceed 1 percent in the neighborhood of the maximum of the curve and 4 percent near the extreme ends of the curve.

Experimental resolution.—To obtain an experimental test of the resolution of the instrument, the well-known beta-ray line of Th B+C+C′+C″ at $H\rho$1387.5 (mean value from the measurements of Ellis[14] and Wang[15]) was used.

The source was prepared by collecting recoil nuclei from thoron on a collodion film 1 to 2 microns thick. The deposit was confined to an area 2 cm in diameter by a diaphragm shield with a negatively charged collecting disk immediately behind the film, the holder itself being positively charged to minimize collection outside the desired source area.

The plotted points of Fig. 6 show the results of the experimental resolution measurements on the Th B line. The statistical error in $\bar{\omega}$ is approximately 1 percent at the peak, and the continuous beta-ray spectrum has been allowed for by subtracting its contribution, which is approximately 20 percent in the neighborhood of the line.

The agreement between the theoretical resolution curve and the experimental points (which have been matched at the peak) is seen to be very good. The total range of πD is about 12.5 percent of the mean value (94.7 cm), but 80 percent of the area of the experimental curve lies within a band extending about 3 percent on each side of the peak. Higher resolution may readily be obtained by redesigning the baffle system as suggested previously with smaller annular slits. The present baffle system, however, represents a good compromise between reasonably high resolution and large effective solid angle.

B. Test of spectrometer efficiency

The efficiency of the spectrometer was determined approximately by direct measurement in the following way. The number of α-particles

[13] Anderson, Dunning, and Mitchell, Rev. Sci. Inst. **8**, 497 (1937).

[14] C. D. Ellis, Proc. Roy. Soc. **138**, 318 (1932).

[15] K. C. Wang, Zeits. f. Physik **87**, 633 (1934).

emitted per second from a Th B source of the type described was first directly measured by counting, with a linear amplifier-ion chamber system, the number of particles emerging through a small foil-covered hole (of known diameter) at the end of a long evacuated tube which contained the source at a measured distance from the hole. The number of beta-particles emitted per second in the line $H\rho 1387.5$ could then be calculated by using the present accepted value for the coefficient of internal conversion for that line ($P\alpha = 0.25$). The number of electrons actually detected in the line when the source was placed in the spectrometer (after allowing for the opaque section of the brass counter grille) was then determined. These results gave a value for the effective solid angle in reasonably good agreement with the peak value of 0.12 shown in Fig. 6. The large solid angles for which the lens spectrograph should be effective were therefore achieved.

C. Correction for absorption in counter window

The absorption of electrons in the counter window was determined by making measurements of the transmission through 0, 1, 2, and 3 additional layers of 0.5-mil Cellophane, when these were interposed in front of the counter by means of the shutter system described. Figure 7 shows the correction factors by which the observed counting rates are to be multiplied, as obtained by extrapolation of the data for eight values of electron momentum to zero total absorber thickness. These correction factors should be fairly reliable down to $H\rho$ 854, but are probably not trustworthy below this value, although some electrons are still passing through the foils at $H\rho$ 640.

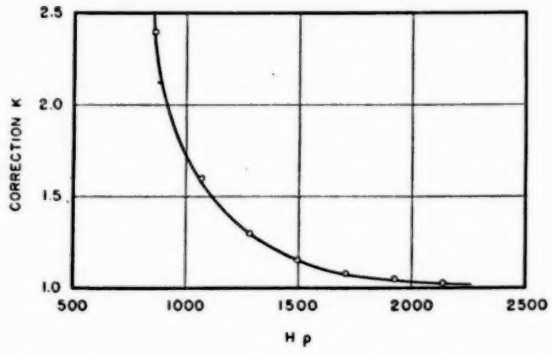

FIG. 7. Correction factor for counter window absorption.

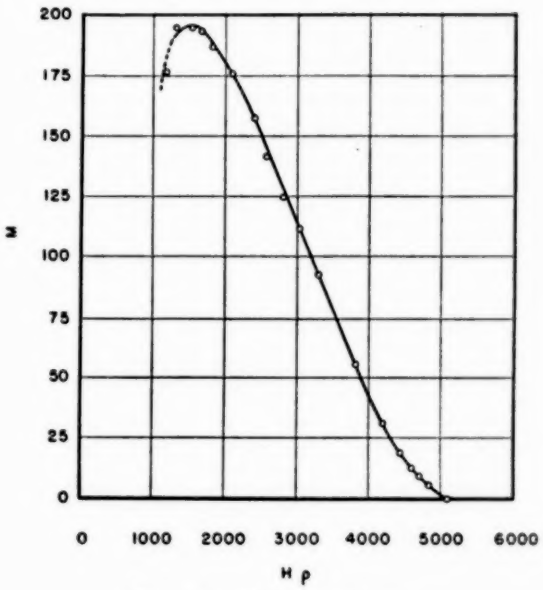

FIG. 8. Radium E spectrum.

There is little evidence for scattering in the baffle system. With zero field, no counts above background are observed.

D. Magnetic field measurements and calibration

Measurements of the field within the solenoid at various points, both on and off the axis, were made by a flip coil which had been calibrated previously with a standard solenoid. These measurements gave for the field at the center of the solenoid a value of 1.830 ± 2 percent oersteds/ampere. As stated previously, the homogeneity of the field was better than 1 percent throughout the region between source and counter.

If we take $\pi D = 94.7$ cm at the peak of the resolution curve and use 1387.5 for the $H\rho$ value of the Th B line, a comparison determination of the field may be obtained. If πD is assumed to be reliable to within ± 0.2 percent, the value of 1.859 ± 0.4 percent oersteds/ampere is obtained. This is considered to be reasonable agreement with the previous value.

The value 1.859 oersteds/ampere obtained from the Th B line has been used as a standard for the subsequent spectrometer measurements. The maximum field obtainable with the present power supply is thus 1115 oersteds at 600 amperes, corresponding to a beta-ray energy of 4.44 Mev.

It should be noted that in such an instrument the effect of the earth's field (or other stray fields) cannot be completely neglected in the very low energy region. The axis of the instrument has been placed in the direction of the horizontal component of the earth's field to minimize any effect due to this component. There is no evidence that the operation of the instrument is appreciably affected by the vertical component of the earth's field at the lowest energies so far used (100 kev.) However, a compensating coil for the vertical component is being installed for work down to 10 to 25 kev.

Investigation of Beta-Spectra

A. Measurements on radium E

The beta-spectrum of Ra E was selected for a general test of the spectrometer, since so many data are now available on it.

The Ra E source was prepared from a purified Ra D+E+F solution by successive deposition on Ni foil followed by successive solutions in hot HCl to insure freedom from Ra D. The final highly purified Ra E solution was distributed as uniformly as possible over a 2-cm diameter area in the center of a thin collodion film mounted on the source holder.

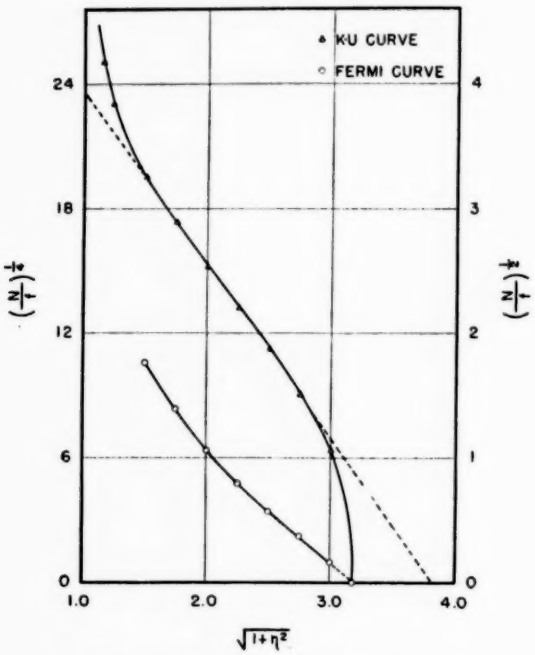

FIG. 9. Fermi and K-U plots for radium E.

Figure 8 shows the data obtained with such a source after correcting for counter window absorption. The individual points have a statistical error of 2 percent or less. Knowing the form of the resolution curve of the instrument, one can accurately determine the upper end point of any beta-spectrum by a process of successive approximations, provided that the source is reasonably strong. The value of the end point for the Ra E spectrum, after account is taken of the effect of the resolution curve, was computed to be $H\rho$ 5100 (1.11 Mev), corresponding to a total energy of 3.18 in m_0c^2 units. Plots of these data on the basis of the Fermi[16] and Konopinski-Uhlenbeck[17] theories are shown in Fig. 9. Neither theory is seen to give a straight line over the complete range of the data, but the Fermi plot is much better. The extrapolated K-U end point is at a total energy of $3.83m_0c^2$ units, in excellent agreement with the results of Flammersfeld,[18] Neary,[19] and other recent measurements.[20,21] These tests with Ra E indicate that the instrument can be regarded as reliable at least above $H\rho$ 1300 (135 kev).

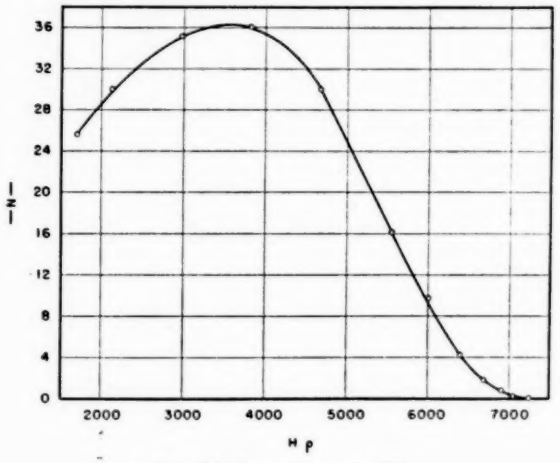

FIG. 10. Spectrum of $_{15}P^{32}$.

B. Beta spectrum of $_{15}P^{32}$

The source of $_{15}P^{32}$ was prepared by distributing a few drops of dilute Na_2HPO_4 solution

[16] E. Fermi, Zeits. f. Physik **88**, 161 (1934).
[17] E. J. Konopinski and G. E. Uhlenbeck, Phys. Rev. **48**, 7 (1935).
[18] A. Flammersfeld, Zeits. f. Physik **112**, 727 (1939).
[19] G. J. Neary, Proc. Roy. Soc. **175**, 71 (1940).
[20] L. H. Martin and A. A. Townsend, Proc. Roy. Soc. **A170**, 190 (1939).
[21] J. S. O'Conor, Phys. Rev. **52**, 303 (1937).

containing the active phosphorus over the source film, as in the case of Ra E. Some of the $_{15}P^{32}$ was kindly supplied by Professor E. O. Lawrence and his associates during a period when the Columbia cyclotron was not in operation. In all sources, the activity of the phosphorus was such that the total weight of the deposit over an area 2 cm in diameter was less than 0.5 mg.

The results of the measurements are shown in Fig. 10, where the statistical error of the points is

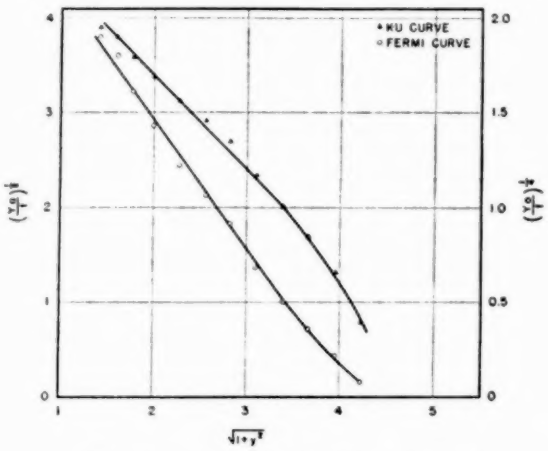

FIG. 11. Fermi and K-U plots for $_{15}P^{32}$.

less than 1 percent. The observed end point is at $H\rho$ 7357 (1.75±0.02 Mev). This is in good agreement with values since published, of Lawson[22] (1.72 Mev) and Lyman[23] (1.70±0.04 Mev).

The Fermi and K-U plots for $_{15}P^{32}$ are shown in Fig. 11. Again neither are straight lines over the entire range, although the Fermi plot is nearly so and shows less departure at the upper end.

C. Beta-spectrum of $_{77}Ir^{191}$

The source of $_{77}Ir^{194}$ was prepared through a concentration process of the Szilard-Chalmers[24] type developed by Dr. J. Steigman.[25] Approximately 5 g of Ir in the form of a Werner complex compound of iridium and ethylene diamine were irradiated with neutrons from the cyclotron. After separation of the active Ir as Ir metal with approximately 1 mg Ir as a carrier, the active material was deposited as a colloidal suspension on the source film.

[22] J. L. Lawson, Phys. Rev. **56**, 131 (1939).
[23] E. M. Lyman, Phys. Rev. **51**, 1 (1937).
[24] L. Szilard and T. A. Chalmers, Nature **134**, 462 (1934).
[25] J. Steigman, Phys. Rev. **59**, 498 (1941).

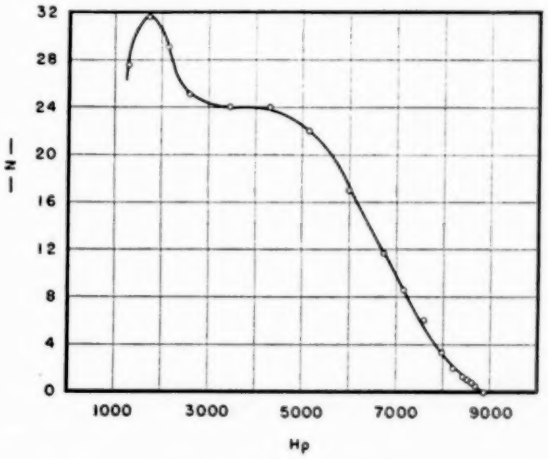

FIG. 12. $_{77}Ir^{191}$ spectrum.

The spectrum obtained is shown in Fig. 12, where the points have a precision of at least ±2 percent. The end point is concluded to be at $H\rho$ 8870 (2.18±0.04 Mev), in fair agreement with previous estimates by other methods.[26] The curve strongly suggests that the spectrum is complex. If only one weak lower energy group is assumed, its end point would correspond to 3000 to 3500 $H\rho$. Measurements of the half-life in various parts of the spectrum gave the same value, 19.5 hours, to within the limits of error.

The Fermi and K-U plots for Ir in Fig. 13 indicate the Fermi plot to be very straight in the upper region. A complex spectrum is likewise suggested by these plots.

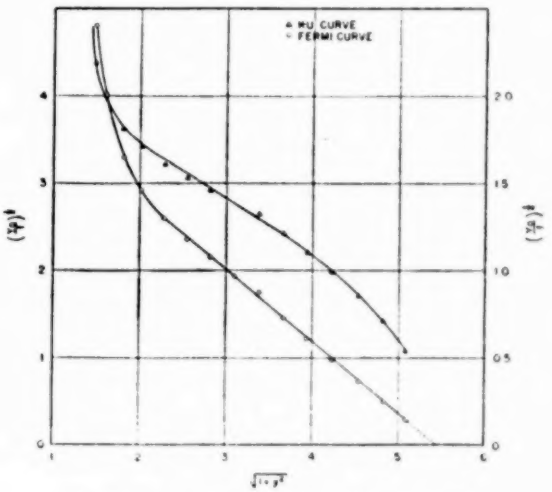

FIG. 13. Fermi and K-U plots for $_{77}Ir^{194}$.

[26] M. S. Livingston and H. A. Bethe, Rev. Mod. Phys. **9**, 359 (1937).

A series of measurements of the absorption of the Ir beta-rays in Al were made using an ion chamber with 1-mil aluminum window filled with Freon (CCl_2F_2) at 1 atmosphere, and which was connected to an FP-54 amplifier. The range obtained was 0.970 ± 0.030 g/cm^2. From Feather's empirical range-energy relation, as recently corrected by Widdowson and Champion,[27] we have energy (Mev) $=[0.165\pm$range (g/cm^2)$]/0.536$. This gives a value of 2.11 ± 0.07 Mev for the end point, in good agreement with the spectrometer value. The absorption curve gives evidence for the presence of a soft gamma-radiation almost completely stopped by 3-mm of Pb.

The author would like to express his sincere thanks to Professor J. R. Dunning for the suggestion of designing the lens spectrometer described here, and for his constant advice and encouragement. He is likewise indebted to Dr. C. J. Davisson of the Bell Telephone Laboratories for his invaluable contributions to the theory outlined. The cooperation of Mr. M. Hartley Dodge and Mr. W. W. Kelley in supplying the copper tubing and the brass cylinder for the spectrometer is gratefully acknowledged.

The author wishes to express his sincere appreciation of the assistance given him throughout the work by his co-workers Miss E. Haggstrom and Father J. S. O'Conor; of the aid given by Dr. J. Steigman and Dr. A. V. Grosse in the chemical processes, and to the many others in the Department of Physics who have helped in designing and building the instrument.

[27] E. E. Widdowson and F. C. Champion, Phys. Soc. Proc. **50**, 185 (1938).

JULY 1, 1941 PHYSICAL REVIEW VOLUME 60

The Scattering of One- to Three-Mev Protons by Helium

N. P. HEYDENBURG AND N. F. RAMSEY*
Department of Terrestrial Magnetism, Carnegie Institution of Washington, Washington, D. C.
(Received April 30, 1941)

The scattering of protons of from one- to three-Mev energy by helium has been experimentally examined for the existence of resonance scattering analogous to the neutron-helium resonance observed for one-Mev neutrons by Staub and Stephens. If *n-n* and *p-p* nuclear forces are equal, such a resonance should occur in *p*-He scattering for protons of approximately two Mev. The number of protons scattered through 140° were observed as a function of their energy. This number passed through a maximum at two Mev as expected, but the sharpness and height of the maximum were several times less than for the *n*-He resonance. However, this greater width and lesser intensity can be qualitatively justified. The number of protons scattered through 76° did not show the presence of a resonance scattering as the energy was varied. Observations of the angular distribution of the scattered protons for angles of scattering between 30° and 140° for proton energies of 1.0, 1.5, 2.0, 2.5 and 3.0 Mev, respectively, have been obtained.

Introduction

PROTON-helium scattering experiments for protons of energy one- to three-million electron volts are of especial interest because of the similarity of the proton-helium scattering problem to that of neutron-helium scattering. The dependence of the neutron-helium scattering cross section upon the neutron energy has been investigated experimentally by Staub and Stephens.[1] They have found that the ratio of the *n*-He cross section for the production of recoils to the similar *n-p* cross section is a maximum for neutrons of about one-Mev energy. This maximum they attribute to a resonance in the compound He^5 nucleus. The existence of this large amount of scattering of one-Mev neutrons by He has since been confirmed by a number of workers,[2]

* Formerly Research Fellow of Carnegie Institution of Washington, now at the University of Illinois.

[1] H. Staub and W. E. Stephens, Phys. Rev. **55**, 131–139 (1939).

[2] E. Hudspeth and H. Dunlap, Phys. Rev. **57**, 971–975 (1940).

most of whom agree that the half-width of the maximum is about 0.5 Mev and the height about a factor of five. Recently Staub and Tatel[3] have found a splitting of this resonance into two peaks, with an energy separation of 0.4 Mev. Now Primakoff and Goldsmith[4] and others have pointed out that if one assumes the equality of n-n and p-p forces, except for the Coulomb forces in the latter case, there should be a similar resonance in the scattering of protons by He but that the resonance should be nearer two than one Mev, the difference being due to the greater Coulomb energy of the compound Li^5 nucleus as compared to He^5.

Previous proton-helium scattering experiments have been carried out by Roberts and Heydenburg[5] but they had available only protons of one-Mev energy and the observations were consequently below the interesting region. In fact they were able to detect only a small departure from Coulomb scattering. Experiments on the scattering of α-particles by hydrogen yield the same information as those on the scattering of protons by helium and have been performed by several workers.[6] These have been done with α-particles of up to 8.5-Mev energy which corresponds to protons of up to 2.1 Mev. These energies are not sufficient to carry the observations over the resonance peak, as found in our proton-helium scattering experiments.

In the present experiments artificially accelerated protons of up to three-Mev energy have been used, so that an investigation of the entire predicted resonance region has been possible.

Apparatus

The protons used in this experiment were accelerated with our pressure electrostatic generator. A detailed description of the apparatus will be published in the future. The voltage was measured by means of a generating voltmeter calibrated in terms of the 0.867-Mev γ-ray resonance of fluorine and the 1.368-Mev γ-ray resonance of Al. The voltage on the electrostatic generator was manually monitored so that it did not fluctuate more than 50 kv during a run.

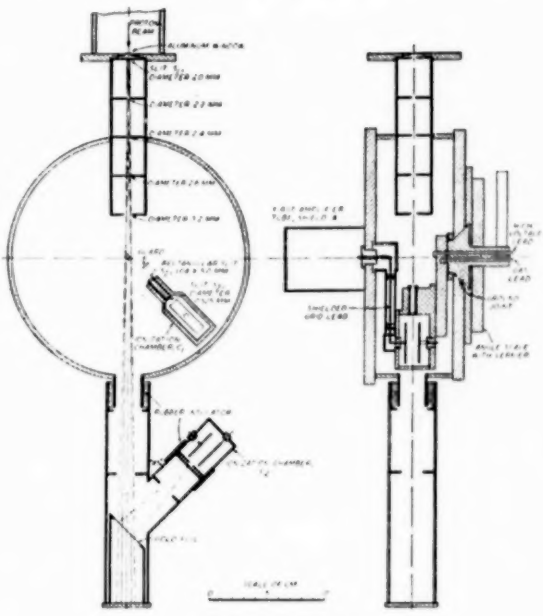

FIG. 1. Scattering chamber.

The scattering chamber used in these experiments was the same as that used by Heydenburg, Hafstad and Tuve in one of their proton-proton scattering experiments and has been described in detail by them.[7] A schematic diagram of the scattering chamber is given in Fig. 1. The magnetically analyzed proton beam from the electrostatic generator entered the scattering chamber through a thin aluminum window (0.0001-inch thick) and was defined by the indicated diaphragm system. The scattered protons entering slits S_2 and S_3 were detected by means of a parallel-plate ionization chamber C_1, connected to a linear amplifier and scale-of-eight counter. This chamber and attached defining diaphragms could be rotated from 0° to 140°. The guard shown in the diagram is to prevent protons scattered by the defining diaphragms from being counted. With the guard in, it was experimentally found that the number of counts in the absence of a scattering gas was negligible.

The beam was monitored by observing with the ionization chamber C_2 the number of protons

[3] H. Staub and H. Tatel, Phys. Rev. **58**, 820–828 (1940).
[4] H. Primakoff and H. H. Goldsmith, Phys. Rev. **55** 1117 (1939).
[5] N. P. Heydenburg and R. B. Roberts, Phys. Rev. **56**, 1092–1095 (1939).
[6] J. Chadwick and E. S. Bieler, Phil. Mag. **42**, 923–940 (1921); C. B. O. Mohr and G. E. Pringle, Proc. Roy. Soc. **160**, 190–206 (1937)
[7] N. P. Heydenburg, L. R. Hafstad and M. A. Tuve. Phys. Rev. **56**, 1078–1091 (1939).

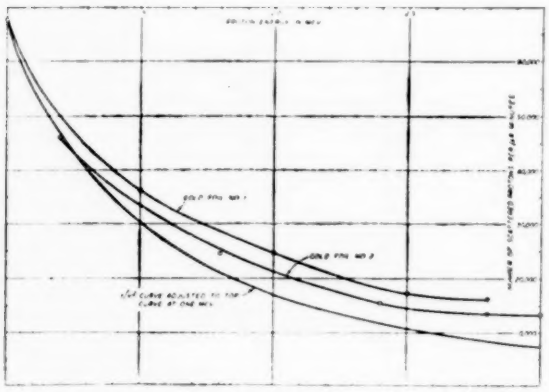

FIG. 2. Current calibration curve.

which were scattered from the gold leaf foil through an angle of about 135°. This gold foil count, however, was calibrated in microamperes of incident protons by simultaneously determining the average rate of counting of the monitor and measuring the current with an RCA amplifier microammeter when the scattering chamber was evacuated.

Most of the observations were made with helium of about ten-mm pressure in the scattering chamber. The helium pressure was measured with an Apiezon oil manometer. We used tank helium, purified by passing through a liquid-air-cooled charcoal trap. The helium in the chamber was tested for possible air impurity at the end of almost every run by a method which will be described in the next section.

PROCEDURE

At the beginning of the set of measurements, the scattering chamber was carefully aligned with respect to the beam direction. The generating voltmeter was calibrated in terms of the F and Al resonances at the beginning and end of the set of experiments.

During the observations the beam intensity was measured in terms of the number of protons scattered from the gold foil, but in a separate experiment this count was itself calibrated in terms of the number of microamperes of current entering the chamber when it was evacuated. This calibration was made for several proton energies between one and three Mev. The results are given in Fig. 2 for two different gold foils (foil No. 1 was damaged during the course of the experiments and was replaced by foil No. 2). While these two curves are similar in shape they are displaced, probably because of a difference in thickness and uniformity of the two foils. A Coulomb ($1/v^2$) curve, adjusted to fit the gold scattering curve No. 1 at one Mev, is also plotted. It is seen that the observed scattering is too large by about a factor of two at 2.8 Mev. This apparent anomalous scattering from gold was not expected and is probably not real. However, as the effect was reproducible and was repeated several different times in the course of the measurements, the curves of Fig. 2 were taken as a calibration of the number of microampere-minutes of current into the chamber corresponding to a given gold scattering count at different voltages. That this calibration was satisfactory was further verified by observing the proton scattering by argon at an angle of 30°. With the above calibration, the proton-argon scattering was found to be strictly Coulomb to within the experimental error of four percent for proton energies from 1.2 Mev to 2.8 Mev, the highest voltage for which these measurements were made.

As an additional check on the consistency of the apparatus, the angular distribution of protons scattered by He at one Mev was measured and found, in agreement with the earlier experiments of Heydenburg and Roberts,[5] to be purely Coulomb between 20° and 40°.

After these preliminary and consistency tests had been completed the actual observations were made by counting the number n_1 of protons scattered by the gas while another number n_2 was scattered from the gold. From these two numbers, from the measured voltage, from the gold scattering calibration, and from the geometry of the apparatus, the number N_S of protons scattered from the chamber per microampere per minute could be calculated. The method of calculation is the same as that of Heydenburg, Hafstad and Tuve[8] and, since the same scattering chamber was used, the geometrical constants are identical.

At the end of almost every run, the purity of the gas was tested by a simple scattering experiment. Since one-Mev protons scattered by He

[8] M. A. Tuve, L. R. Hafstad and N. P. Heydenburg, Phys. Rev. **50**, 806–825 (1936).

through 140° lost so much energy that they could not be counted, the only countable protons of such an energy scattered in this direction were necessarily due to the presence of a heavier scattering gas such as air. Hence, by determining the number of countable protons so scattered, the amount of impurity of the gas could be determined. All observations were rejected if the amount of impurity was sufficiently great for any scattering observations at an angle greater than 39° to be appreciably affected by the Coulomb scattering of the impurity.

TABLE I. *Results of the scattering experiments.*

θ	Energy Mev	Ratio He/Au Scat. $\times 10^3$	Obs. N_S per μA Min.	Coulomb N_S per μA Min.	Ratio N_S Obs. to N_S Coulomb
76°	1.2	3.49	16.3	5.60	2.91
	1.8	9.70	24.3	2.49	9.75
	2.4	21.6	33.5	1.40	23.9
	3.0	25.1	33.9	0.896	37.8
140	1.2	5.45	25.6	1.44	17.8
	1.4	10.7	40.0	1.06	37.7
	1.6	17.8	54.8	0.809	67.8
	1.8	28.4	71.1	0.639	111
	2.0	35.6	75.7	0.518	146
	2.2	39.8	71.5	0.428	167
	2.4	42.0	65.1	0.359	181
	2.6	35.3	49.5	0.306	162
	2.8	33.8	45.6	0.264	173
	3.0	30.3	40.8	0.230	177
20	1.5	315.0	1065	1640	0.65
40		12.53	42.4	57.9	0.73
60		6.47	21.9	9.34	2.34
80		8.70	29.4	2.97	9.90
100		11.0	37.1	1.44	25.8
120		9.90	33.5	0.974	34.4
140		13.2	44.6	0.921	48.5
20	2.0	236	500	923	0.54
40		52.7	112	32.5	3.45
60		18.7	39.7	5.26	7.55
80		13.1	27.8	1.67	16.6
100		14.9	31.6	0.808	39.1
120		19.2	40.7	0.548	74.2
140		32.7	69.4	0.502	138
20	2.5	612	1055	590	1.79
40		11.9	204	20.8	9.81
60		35.9	61.9	3.36	18.4
80		18.8	32.4	1.07	30.6
100		16.9	29.2	0.517	56.5
120		23.8	40.9	0.351	116.5
140		34.7	59.8	0.331	180.7
20	3.0	899	1215	410	2.96
40		145.4	196.4	14.5	13.5
60		53.8	72.7	2.34	31.1
80		21.1	28.4	0.743	38.2
100		16.5	22.3	0.359	62.1
120		21.5	29.1	0.244	119
140		33.7	45.4	0.230	197

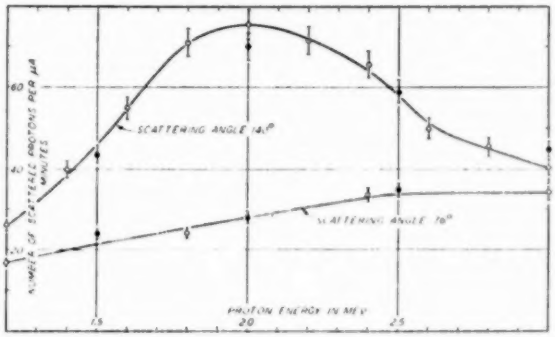

FIG. 3. Dependence of the amount of scattering upon voltage at fixed angles (points shown by solid circles are taken from curves in Figs. 4, 5 and 6).

RESULTS

The results of these experiments are given in Table I. In column (4) the observed N_S has been obtained from the ratios in column (3) by use of the gold foil calibration curves of Fig. 2. The calculated N_S gives the number of scattered protons to be expected from the Coulomb scattering law of Rutherford and Darwin for our scattering chamber dimensions. These results are plotted in Figs. 3, 4, 5 and 6, both the experimentally observed scattering and the theoretical Coulomb scattering being plotted. The calculated Coulomb scattering values given in column (5) and plotted in the figures have been multiplied by a $(1/\sin\theta)$ factor to take into account the change in the effective scattering volume with angle.[8]

Measurements were taken both at fixed angles as the voltage was varied and at fixed voltages as the scattering angle was varied. The results of the former type are shown in Fig. 3. These curves are at 140° and 76° in the laboratory system or at 149° and 90° in the center-of-gravity system. These angles are such that a pure p wave should show 75 percent of its maximum effect at 149° and none at 90°. The curves at fixed voltages as the scattering angle was varied are shown in Figs. 4, 5 and 6. Although these two sets of observations were made independently, they obviously overlap. Therefore, points obtained from Figs. 4, 5 and 6 have also been plotted on Fig. 3 to make clear the extent of the agreement between the two types of observations.

DISCUSSION OF RESULTS

From Fig. 3 it appears that the amount of scattering does pass through a maximum at

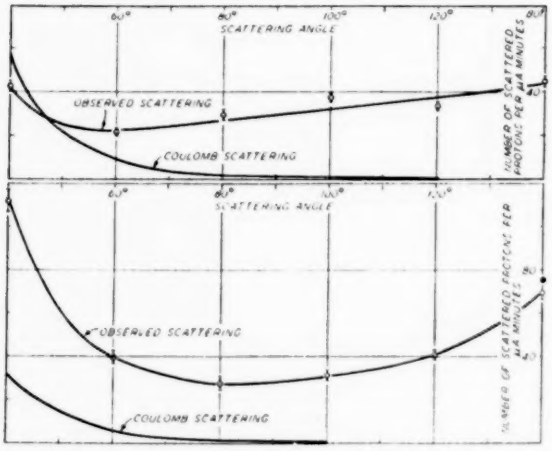

FIG. 4. (above) Angular distribution of 1.5-Mev protons scattered by helium.

FIG. 5. (below) Angular distribution of 2.0-Mev protons scattered by helium.

about two Mev as expected theoretically on the basis of the neutron-helium scattering results and the assumption of the equality of n-n and p-p forces. However, the height and narrowness of the maximum are much less than in the neutron-helium case, being only a factor of 2 instead of 5 in intensity, while the half-width is more than one Mev instead of about 0.5 Mev. Nevertheless, as Dr. Fano, Dr. Breit, and others have indicated, it is quite reasonable that the Li^5 resonance should be broader and less intense than the He^5.

This increased breadth of the resonance makes the interpretation of these results more difficult. In the first place it is more difficult to be certain that the maximum of the curve really is a resonance, since the amount of scattering could pass through a slight maximum merely due to the fact that the scattering cross section for a given type of scattering decreases with the increasing energy of the scattered particles. However, the maximum is probably sufficiently intense to justify at least the tentative assumption that the observed maximum is due to a resonance.

A second difficulty arising from the increased breadth of the curve is the difficulty in determining if there is a doublet structure to the curves. In the neutron-helium scattering experiments there has been disagreement among the observers as to whether there is a single or doublet structure of the resonance.[1,2] However, the more recent work of Staub and Tatel[3] seems to show conclusively that the resonance is a doublet. They have analyzed their data in terms of the theoretical equations given by Bloch[9] and find that their resonance curve can be fitted by assuming the $P_{3/2}$ and $P_{1/2}$ levels to be either an inverted or a normal level system depending on the values assigned to the constants occurring in the theoretical equation. They prefer the latter as being the correct interpretation when other considerations are taken into account. As proton experiments are in general less difficult than neutron ones, it was hoped for a time that it would be easier to determine the existence of a doublet structure in proton-helium scattering experiments than in n-He experiments. However, the greater width of the maximum in the p-He scattering makes it more, rather than less, difficult to detect a slight doublet structure in the

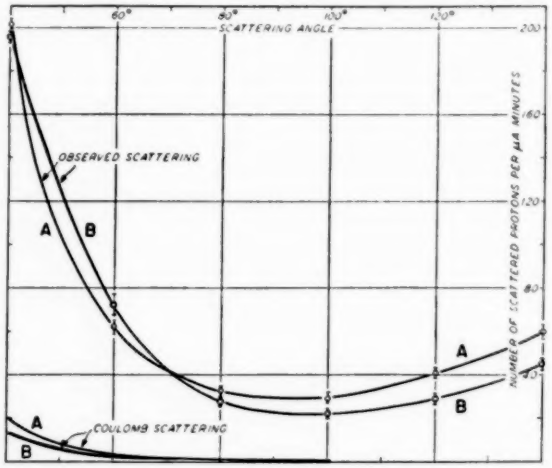

FIG. 6. Angular distribution of protons scattered by helium. Curve A, 2.5-Mev protons; curve B, 3.0-Mev protons.

curve. However, as far as our results yield information on the multiplicity of the resonance, there is no evidence for the existence of a resolvable doublet structure to the maximum in proton-helium scattering.

The authors wish to thank Dr. J. A. Fleming, Dr. M. A. Tuve, Dr. L. R. Hafstad, R. C. Meyer, and others of the Department of Terrestrial Magnetism staff for their friendly cooperation and assistance in this work.

[9] F. Bloch, Phys. Rev. **58**, 829–836 (1940).

The Acceleration of Electrons by Magnetic Induction

D. W. KERST*
University of Illinois, Urbana, Illinois
(Received April 18, 1941)

Apparatus with which electrons have been accelerated to an energy of 2.3 Mev by means of the electric field accompanying a changing magnetic field is described. Stable circular orbits are formed in a magnetic field, and the changing flux within the orbits accelerates the electrons. As the magnetic field reaches its peak value, saturation of the iron supplying flux through the orbit causes the electrons to spiral inward toward a tungsten target. The x-rays produced have an intensity approximately equal to that of the gamma-rays from one gram of radium; and, because of the tendency of the x-rays to proceed in the direction of the electrons, a pronounced beam is formed

IN the past the acceleration of electrons to very high voltage has required the generation of the full voltage and the application of that voltage to an accelerating tube containing the electron beam. No convenient method for repeated acceleration through a small potential difference has been available for electrons, although the method has been highly successful in the cyclotron for the heavier positive ions at velocities much less than the velocity of light.

Several investigators[1-4] have considered the possibility of using the electric field associated with a time-varying magnetic field as an accelerating force. This is a very attractive possibility because the magnetic field can be used to cause a circular or spiral orbit for the electron while the magnetic flux within the orbit increases and causes a tangential electric field along the orbit. The energy gained by the electron in one revolution is about equal to the instantaneous voltage induced in one turn of a wire placed at the position of the orbit. Since the electron can make many revolutions in a short time, it can gain much energy. The comparatively small momentum of a high energy electron requires correspondingly small values of Hr for high energy orbits. For example, the energy of an electron when $v\sim c$ is $KE=3\times10^{-4}Hr-0.51$ million electron volt. Thus with $H=3000$ oersteds and $r=5$ cm, the energy of the electron would be about 4 Mev, and the orbit could be held between the poles of a small magnet.

Because of the experimental experiences of previous investigators[1-3] with this method of acceleration, a rather detailed study of the focusing to be expected was made, and it is presented in the paper immediately following this one. With the results of this theoretical investigation to guide the design, it was possible to make an induction accelerator which produced x-rays of 2.3 Mev.[5,6] Briefly, in the focusing theory it is shown that:

1. The electrons have a stable orbit, "equilibrium orbit," where

$$\phi_0=2\pi r_0^2H_0. \tag{1}$$

ϕ_0 is the flux within the orbit at r_0, and H_0 is the magnetic field at r_0. Both ϕ_0 and H_0 are increased during the acceleration process. This flux condition holds for all velocities of the electrons, and it shows that if a maximum flux density of 10,000 gauss is allowed in the iron then 5000 oersteds is the maximum magnetic field which can be used at the orbit.

2. In the plane of their orbits the electrons oscillate about their instantaneous circles, circles for which $p=eHr/c$, with an increasing frequency

$$\omega_r=\Omega(1-n)^{\frac{1}{2}}, \tag{2}$$

where Ω is the angular velocity of the electron in its orbit, and ω_r is 2π times the radial focusing frequency. The number n is determined by the

* On leave at the General Electric Company Research Laboratory.

[1] G. Breit and M. A. Tuve, Carnegie Institution Year Book (1927–28) No. 27, p. 209.

[2] R. Wideröe, Arch. f. Electrotechnik **21**, 400 (1928).

[3] E. T. S. Walton, Proc. Camb. Phil. Soc. **25**, 469–81 (1929).

[4] W. W. Jassinsky, Arch. f. Electrotechnik **30**, 500 (1936).

[5] D. W. Kerst, Phys. Rev. **58**, 841 (1940).

[6] D. W. Kerst, Phys. Rev. **59**, 110 (1941).

radial dependence of the magnetic field, which we take to be of the form $H \sim 1/r^n$. For radial focusing n must be less than unity.

3. Axial oscillations, oscillations perpendicular to the plane of the orbit, have

$$\omega_A = \Omega n^{\frac{1}{2}}. \tag{3}$$

For axial stability n must be greater than zero. If the beam is to be smaller in an axial direction than it is in a radial direction then $n > \frac{1}{2}$.

4. Decrease of the amplitude of both axial and radial vibration occurs because of the increase of the restoring force with increasing magnetic field. At nonrelativistic velocities the damping is

$$da/a = -dE/4E, \tag{4}$$

where dE/E is the fractional increase of the kinetic energy of an electron and da/a is the fractional decrease in amplitude of the oscillation about the instantaneous circle. This holds for both axial and radial oscillations.

5. Instantaneous circles not coincident with the equilibrium orbit shrink or expand toward coincidence:

$$dx/x = -dE/2E, \tag{5}$$

where x is the displacement of the instantaneous circle from the equilibrium orbit and dx is the shift of the circle toward the equilibrium orbit while the electron's energy increases by the fraction dE/E.

Because of the shrinking or expansion of the instantaneous circle of a displaced electron toward the equilibrium orbit and the decrease of the amplitude of oscillation of an electron about its instantaneous circle, it was expected that a cathode or an electron injector placed outside of the equilibrium orbit could shoot in electrons which would miss the injector on successive revolutions around the magnet. Furthermore, since an instantaneous circle for electrons with a constant injection energy exists within the acceleration chamber for a small but finite interval of time while the magnetic field is increasing, a finite amount of charge should be captured in orbits not striking the walls. With constant potential on an injector the electrons first would hit the outer wall of the chamber before the magnetic field had grown large enough to give the electrons a radius of curvature less than the radius of the wall. Then as the field increased it would reach values which give instantaneous circles within the vacuum tube. Eventually the field would be so large that the electrons coming out of the injector strike the walls or spiral around in small circles.

From Eq. (2) it can be seen that the spreading rays from the injector will form injector images $\pi(1-n)^{-\frac{1}{2}}$ radian apart, since if each ray of the beam oscillates about the instantaneous circle, it also oscillates about the central ray from the injector.

Equations (4) and (5) indicate that for large da or dx it is desirable to use a small injection voltage E, and a high voltage per turn dE. A shift da in two revolutions or dx in one revolution of about 1 mm when the displacement of the injector from the equilibrium orbit is $x = a = 1.5$ cm would require $dE/E \backsimeq \frac{1}{8}$. It is not possible to decrease the injection voltage E indefinitely since scattering increases when this is done, and it may be that the beam would be lost by scattering through an angle greater than that which magnetic focusing can handle. Conservative estimates on the scattering out of a cone of 7° half-angle, which is about the focusing limit, showed that at 10^{-6} mm of Hg air pressure in the tube, a maximum $Hr = 15{,}000$ gauss cm, and $f = 600$ cycles/sec. for the frequency of oscillation of the magnetic field, the injection voltage must exceed 100 volts for less than a 20-percent loss of beam. This then requires that dE or the voltage per turn at the equilibrium orbit must be at least 12 volts at the time of injection. In the magnet which was built this condition was easily satisfied, for 25 volts per revolution could be attained. There is no trouble with energy loss by the electrons in their long paths through the residual gas in the vacuum tube. Wideröe[2] was aware of the flux requirement (1), but apparently he did not realize that the voltage gain per revolution could not be too small compared with the injection voltage, or that it would be necessary to inject the electrons nearly tangent to the equilibrium orbit.

After the injected electrons have orbits approximately coincident with the equilibrium orbit, they should remain close to r_0. A simple method was used to shift the equilibrium orbit so that the electrons struck a thin tungsten target.

A portion of the flux through the center of the orbit passed through disks cemented to the center of the pole faces and made of material which saturated easily. As saturation progressed, the electrons had to move inward to a smaller radius of curvature in order that $\phi = 2\pi r^2 H$. Eventually the electrons grazed past the target producing thin target x-radiation.

Space Charge Effects

It is difficult to estimate the effect of space charge within the beam on the formation of images, since there are two focusing oscillations, axial and radial, in general having different frequencies. However, an estimate can be made of the upper limit of current which the magnetic forces can hold.

At injection the magnetic forces are small so that the estimate should be made with the magnetic field at this time. The electrons at the edge of the beam, which is assumed to be a cylinder of radius Δ, determined by the distance between the equilibrium orbit and the injector, will experience a repulsive force of

$$F_e = (cQe)/(10\pi r_0 \Delta) \tag{6}$$

dynes. Q is the number of coulombs in the orbit, and r_0 is the radius of the orbit.

For radial unbalanced magnetic forces we get

$$F_m = e^2 H^2 (1-n)\Delta / mc^2 \tag{7}$$

dynes acting on the electrons toward r_0. If $F_e = F_m$ at the edge of the beam, then this balance will hold within the beam for all other distances δ smaller than Δ, because the Q of (6) is proportional to δ^2. Thus

$$I = 10\pi f e r_0 \Delta^2 H^2 (1-n)/mc^3. \tag{8}$$

Or in terms of the injection voltage E,

$$I = \pi \Delta^2 f E (1-n)/(15 r_0 c). \tag{9}$$

I is the target current in amperes, f the frequency of oscillation of the magnetic field, and n gives the dependence of the magnetic field on r. Since the value of E which can be used depends upon the voltage per turn dE, which is also dependent on the peak magnetic field reached or the output energy, and also upon the orbit shift da which is required to miss the injector, we get

$$I = 2\pi^3 \Delta^3 f^2 (KE + \tfrac{1}{2})(1-n)/(45 c da \times 10^4), \tag{10}$$

where KE is the final energy of the electrons in Mev. Inserting into (10) the constants of the machine which was built, we have $\Delta = 1.5$ cm, $f = 600$ cycles/sec., $KE = 2.3$ Mev, and $da \backsimeq 0.1$ cm. The target current should be about 0.03 microampere. This is fairly close to the lower limit of current as estimated from the x-ray output of the accelerator. This lower limit was found by using the thick target yield of Van Atta and Northrup[7] in the direction of the electron beam for comparison with the x-ray yield from the induction accelerator. It is found that the target current in the induction accelerator must be greater than 0.02 microampere. It is only possible to find the lower limit of this current since the output is thin target radiation.

A curious behavior which was immediately noticed when the apparatus began to work was that injection voltages much greater than the largest voltage which would allow the orbit to miss the injector could be used. In fact the yield increased greatly as this voltage was raised. This seems understandable on the basis of space charge forces spreading the beam away from the central ray of the injector.

At relativistic energies space charge forces are completely balanced by magnetic self-focusing of the beam, for the electric force on a stray electron at a distance Δ from the beam center is

$$e\mathcal{E} = 2\sigma e/\Delta, \tag{11}$$

where σ is the linear charge density in e.s.u./cm. The magnetic attraction due to the main current in the beam is

$$evH/c = (v/c)^2 2\sigma e/\Delta. \tag{12}$$

Thus it is evident that when $v \to c$, the magnetic pull of the beam for a stray electron just equals the electrostatic repulsion. Or, from the point of view of an observer on the electron, the spacing of the fixed number of electrons around the orbit will increase, since as $v \to c$ his yardstick becomes a smaller fraction of the circumference of the orbit.

[7] L. C. Van Atta and D. L. Northrup, Am. J. Roentgen. Rad. Ther. **41**, 633 (1939).

The Magnet

A photograph of the apparatus is shown in Fig. 1.

For the production of the rapidly changing magnetic field, with the proper dependence on the radius, finely laminated iron pole faces were made from 0.003-inch silicon steel sheets. The return magnetic circuit made from the same material was interleaved for mechanical strength; and the roughly circular central pole pieces were

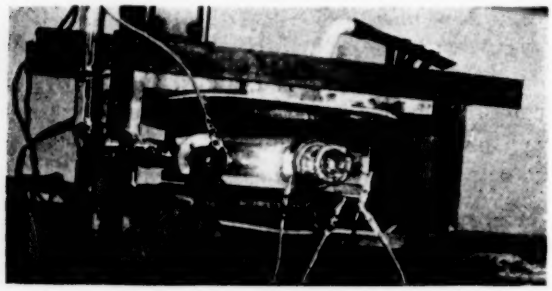

Fig. 1. The induction accelerator. The glass doughnut is between pole faces which are held apart by eccentric wedges.

formed by stacking with different widths of laminations as shown in Fig. 2. Each pole piece was capped by a disk of radially arranged laminations so that perfect circular symmetry was achieved at the pole surfaces (*B*, Fig. 2). The whole pole face was held together by a thick Transite or asbestos board ring about its perimeter, with cement of water glass and flint dust filling the cracks between the laminations and hardened by baking. The pole caps were held against the pole pieces by eccentric wedges between the Transite rings.

To supply the flux within the orbit which was necessary to hold the electrons out at the equilibrium orbit, two disks about two inches in diameter, each made of pressed iron dust of permeability about eight, were cemented onto the flat center portions of the pole faces. The thickness of these disks was chosen so that the equilibrium orbit was formed at about 7.5 centimeters radius, and the final adjustment of the position of the equilibrium orbit was made by painting a mixture of water glass and iron filings, or the turnings from the compressed iron dust disks, onto the surface of the iron dust disks so that the reluctance of the gap was correct. Since the iron particles in these disks are separated, the flux density through them is greater than the average flux density through the disks. This causes the saturation which shrinks the equilibrium orbit down to the target.

Because of the large leakage flux the main coil of the magnet had to be highly subdivided. Two hundred strands of No. 20 double enameled wire were made into a cable approximately 10 yards long which was twisted about ten times and which had its inside wires interchanged with its outside wires several times. This was formed into a 10-turn coil with about $\frac{1}{32}$ inch of insulation between turns. Two such 10-turn coils were made and fitted with large lugs of 1-inch copper tubing. The coils were wrapped with cotton tape, dipped in Bakelite varnish and baked. Figure 3 shows the circuit with the coils connected to a total of eighty 5-microfarad Pyranol condensers which were rated at 660 volts a.c. Energy was supplied to this resonating circuit by a 2-turn primary of stranded enameled wire around the pole pieces. The r.m.s. electromotive force in this primary

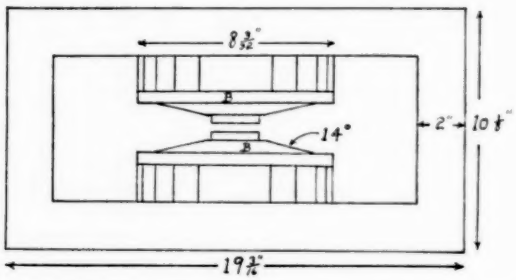

Fig. 2. Dimensions of the magnet. Parts *B* are the pole caps made with all laminations placed in a radial direction. The iron dust disks supply the central flux. Outside of the 14° conical surface a flat rim on the pole face tends to prevent too rapid decrease of the field at the edge of the gap.

could be run up above 100 volts, but 60 to 80 volts were usually used in operation since this was sufficient to saturate the powdered iron and to collapse the orbit. Power was supplied by a 4-kilowatt 600-cycle alternator driven by a direct-current motor with an adjustable speed.

To determine how the magnetic field decreased with r a small search coil was arranged so that it could be held between the poles at different radial distances from the center. The e.m.f. from

this search coil was bucked against the e.m.f. from a voltage divider connected across a 1-turn coil about the leg of the magnet, equality of e.m.f. being determined by no deflection of the beam of an oscillograph. Since the wave form of the voltage on the search coil differed slightly from the wave form from the coil around the core, balance could be obtained only at one phase, and the phase of interest was that of zero magnetic field. The use of the oscillograph as a null instrument in this way proved to be sufficiently accurate. The pole faces gave a field following the $1/r^3$ law between a radius of 4.5 centimeters and 9.25 centimeters when the separation between the flat central portions of the pole faces was 2.8 centimeters. At $r=10$ cm the law was $1/r$.

To determine the position of the equilibrium orbit use was made of a concentric system of seven 1-turn coils set in grooves in a Bakelite disk which fit snugly around one of the iron dust disks. Relative values for the e.m.f.'s induced in these coils were determined by the same null method which was used for determining the shape of the field. These data could be used in several ways to find r_0. The simplest method is to find the radius of minimum electric field, since this will be r_0.

The Acceleration Chamber

It was desirable to have the volume available for electron orbits as large as possible. This required a doughnut-shaped glass vessel with walls parallel to the conical pole faces. The outer diameter was 20 cm, and the center of the doughnut was 7 cm in diameter. The glass work for this vessel required great skill.[8] A 20-cm spherical bulb with a wall thickness of 2.5 mm was flattened and dished conically on both sides so that it would fit between the magnet poles. The central 7-cm hole of the doughnut was formed by pushing the centers of the dished faces together and picking out the glass.

The inside of this bulb was coated with a thin conducting layer by chemical silvering. This coating is necessary to prevent stray charges from building up potentials on the walls. Contact is made to the silver coating which is then grounded outside of the tube. Resistances of the silver coat between 20 ohms and 300 ohms between test probes put in the side arms were used.

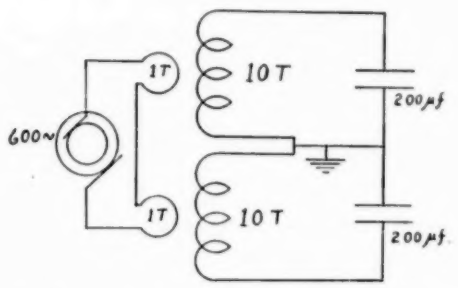

FIG. 3. The resonant circuit which energizes the magnet. Losses are supplied by a 4-kilowatt 600-cycle-per-second generator.

Both target and injector were mounted on the glass pinch seal which was waxed to a flare on the doughnut. The target was a piece of 0.015-inch tungsten sheet folded to present an edge of large radius of curvature to the electron orbit which shrinks inward toward it. Thin tungsten is used so that eddy currents will not be excessive. The injector was made of thin molybdenum sheets and a cylindrically spiraled tungsten wire for the filament. The whole assembly is shown in Fig. 4.

Fortunately the presence of this much metal near the orbit does not seem to disturb the local magnetic field too much. However, the orbits are destroyed if a piece of metal is brought up to the side of the glass doughnut while the machine is running. This was observed when a block of beryllium was put near the tube for experiments with photo-disintegration. The x-ray yield disappeared when the beryllium was too close. The original injector was arranged to send a beam of electrons in both directions around the magnet so that both directions of field could be used. Thus two beams of x-rays oppositely directed were produced.

Operation

Although the focusing theory shows that for the present design of the accelerator electrons should be injected at approximately 200 volts, it was found that the yield increased with voltage and that it was still increasing at 600 volts. Likewise the negative voltage on the small focusing plates G beside the filament gave an

[8] I am indebted to the Vacuum Tube Department of the General Electric X-Ray Corporation for producing a correctly shaped tube.

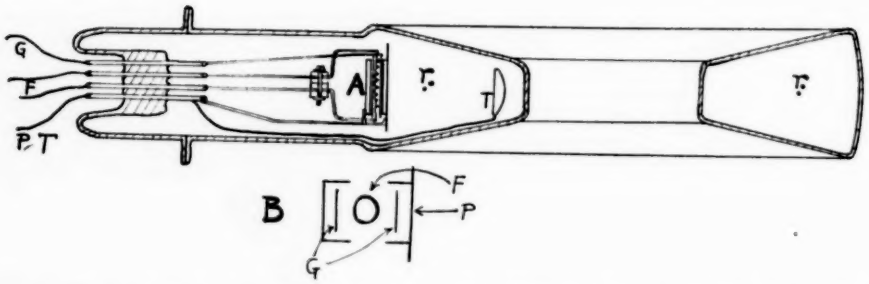

FIG. 4. Cross section of the doughnut-shaped acceleration chamber. The equilibrium orbit is at r_0, T is the tungsten target, A is the injector, B is a top view of the injector. A ribbon beam of electrons from the filament F is shot out through slots in the positive plates P. G are negative focusing electrodes.

increasing yield as it was raised to 200 volts. The beam from the injector was allowed to pour into the vacuum tube continuously.

Initially the yield obtained was approximately equivalent to 10 millicuries of radium when measured in a direction from the target at right angles to the electron beam as it strikes the target, and the yield was approximately ten times greater in the direction of the electron beam. Later the yield in the direction of the beam was increased to the equivalent of one gram of radium.

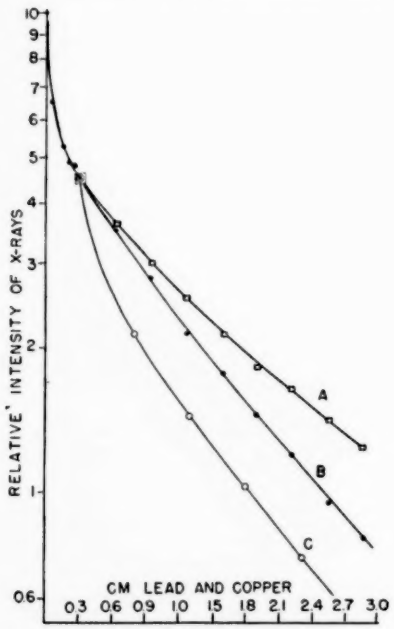

FIG. 5. The relative intensity of x-rays from the induction accelerator as a function of absorber thickness. A is absorption in copper. The absorption coefficient is 0.454 cm^{-1} which gives a monochromatic equivalent of 1.35 Mev for the x-rays. B is the curve for lead. The coefficient is 0.62 cm^{-1}, which corresponds to 1.4 Mev monochromatic equivalent. C is the lead absorption curve of Van Atta and Northrup for x-rays produced by 2.0-Mev electrons striking a thick target.

Figure 5 shows an absorption curve of the radiation as it passes through lead, and the comparison with two-million-volt x-rays from the M. I. T. electrostatic machine[7] shows that the energy reached in the induction accelerator is approximately 2.0 million electron volts and that the radiation produced is thin target radiation. With other iron dust disks cemented on the pole faces, absorption coefficients indicating 2.3-Mev x-rays have been obtained. By means of a collimated Geiger-Müller counter the source of the x-rays was shown to be the target. A large lead block with a small hole in it let an abundant amount of x-rays through to the Geiger-Müller tube only when it was pointed at the target and not when it was pointed at the injector or other portions of the vacuum tube. By connecting the vertical deflection plates of an oscillograph to the Geiger-Müller counter and the horizontal deflection plates to a 1-turn coil around one leg of the magnet, the phase of the magnetic field at which electrons struck the target could be determined. As was expected it was found that the greater the excitation of the dynamo which energizes the magnet, the earlier in the cycle the iron dust saturated and brought the beam in to the target. Lowering the primary voltage postponed sufficient saturation in the iron dust until the peak of the magnetic field was reached. The Geiger-Müller counter then gave x-ray pulses at the center of the oscillograph screen. This indicated a path length of about sixty miles from injector to target. If the primary voltage was lowered beyond this point, the yield disappeared, for the

electrons were not drawn in to the target but were slowed down by the decreasing magnetic field. Fortunately the operation of the accelerator is not sensitive to the alignment of the pole faces. No difference in the output can be detected when the pole faces are placed off axis as far as a thirty-second of an inch. It is also surprising that vacuum requirements are not as severe as was expected. No rigorous outgassing is necessary and the apparatus has been run with a vacuum as poor as 10^{-5} mm Hg. The tube can be opened for changes and operated three-quarters of an hour after sealing shut.

At present, low flux densities have been used at the orbit. When these are increased, it should be possible to go to 5 million volts even with this small model. One of the promising possibilities for the induction accelerator as a research tool is that the electrons from the beam can come out through the glass walls of the doughnut after they strike the target. They should be fairly homogeneous in energy provided that the target has a high atomic number. The great increase in bremsstrahlung production with rising electron energy in addition to the concentration of this radiation in a cone of solid angle mc^2/E about the original electron direction gives the induction accelerator the possibility of providing an intense source of x-radiation for nuclear investigations. Since there is no evident limit on the energy which can be reached by induction acceleration, it may soon be possible to produce some small scale cosmic-ray phenomena in the laboratory.

I am indebted to Professor H. M. Mott-Smith and Professor R. Serber for many discussions of the theoretical aspects of this problem and to Mr. R. P. Jones for assistance in the construction of the magnet.

JULY 1, 1941 PHYSICAL REVIEW VOLUME 60

Electronic Orbits in the Induction Accelerator

D. W. KERST* AND R. SERBER
University of Illinois, Urbana, Illinois

(Received April 18, 1941)

The first section gives a general account of the principles of operation of the electron induction accelerator. The second section gives the more detailed analysis of the orbits of the electrons which was undertaken to serve as a guide in the design of the accelerator.

I. INTRODUCTION

THE construction and operation of an induction accelerator for electrons has been discussed in the preceding paper.[1] The idea of using the principle of electromagnetic induction for the production of high energy particles has been entertained by a number of investigators,[2] but has hitherto met with little success in application. It was therefore felt necessary to carry out a more careful analysis of the orbits of electrons in changing magnetic fields for the double purpose of determining whether such a device was practicable, and to serve as a guide in its design.

The basic idea of the accelerator is a simple one. An electron started in a radially symmetric magnetic field at the proper position and with the right velocity will move in a circle of radius given by

$$p = eHr/c. \tag{1}$$

If now the magnetic flux enclosed by the orbit, ϕ, is increased, a tangential electric field will be produced at the orbit, $E_\varphi = \dot{\phi}/2\pi rc$, which will accelerate the electron. If the magnetic field is so arranged that p and H increase proportion-

* On leave at the General Electric Company Research Laboratory.

[1] Also D. W. Kerst, Phys. Rev. **58**, 841 (1940); *ibid.* **59**, 110 (1941).

[2] G. Breit and M. A. Tuve, Carnegie Institution Year Book (1927–28) No. 27, 209. R. Wideröe, Arch. f. Electrotechnik **21**, 400 (1928); E. T. S. Walton, Proc. Camb. Phil. Soc. **25**, 469–81 (1929); W. W. Jassinsky, Arch. f. Electrotechnik **30**, 500 (1936).

ately, the radius of the orbit will remain unchanged; the electron continues to move in the equilibrium orbit ($r=r_0$), but with momentum constantly increasing as H is increased.

The condition for the existence of such an equilibrium orbit is readily found. The rate of increase of momentum is

$$\dot{p}=e\dot{\phi}/2\pi r_0 c,$$

which gives

$$p=e(\phi-\phi_1)/2\pi r_0 c.$$

Using (1), with $r=r_0$, we find

$$H=(\phi-\phi_1)/2\pi r_0^2. \qquad (2)$$

Thus the change in flux through the orbit must be twice that which would obtain if the magnetic field were uniform in space. To satisfy this requirement one must have a strong central field to supply the necessary flux, and a weaker field to hold the electron in its circular orbit.

The energies which can be obtained by this means are quite high. The Illinois accelerator ($r_0=7.5$ cm, $H_{\max}=1200$ gauss) should give, according to (1), electrons of 2.2 Mev. It will be observed that, since the phase of the electron in its orbit is immaterial to the operation of the accelerator, the relativistic change of mass with velocity causes no difficulty for a machine of this type.

However, the very fact that such high velocities are attained brings with it new difficulties which at first sight seem rather formidable. Since, during most of the time the electron is being accelerated, its velocity is very nearly the velocity of light, its path length in the machine is very great. The magnet of the Illinois machine was activated by 600-cycle a.c., and the acceleration took place during a quarter-cycle. In this time the electrons traveled nearly 100 kilometers and made about 200,000 revolutions. It is therefore essential, to obtain any appreciable beam intensity and to overcome the effects of scattering by the residual gas and of space charge, that there be strong focusing forces to hold the electron in its equilibrium orbit.

The focusing requirements impose additional restrictions on the form of the magnetic field. Consider first the radial focusing, that is, the motion in the plane of the orbit. The equilibrium Eq. (1) is just the condition for the balancing of the magnetic and centrifugal forces. If the electron is displaced from the equilibrium radius, an unbalanced force will act, and, since the centrifugal force is proportional to $1/r$, this force will be directed towards the equilibrium radius provided the magnetic field falls off less rapidly than $1/r$. The electron, when displaced, will then oscillate around the equilibrium orbit. We shall see that this is a damped oscillation;[3] its amplitude is proportional to $H^{-\frac{1}{2}}$. The focusing

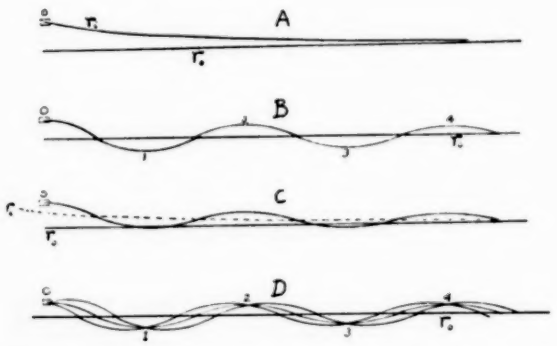

FIG. 1. The figures represent the developed paths of electrons. r_0 is the position of the equilibrium orbit, and r_i is the position of the instantaneous circle. The injector is at 0. (A) Path of an electron injected tangentially on its instantaneous circle. It approaches r_0 without oscillation. (B) Path of an electron with an instantaneous circle coincident with the equilibrium orbit. Oscillation occurs about r_0. (C) Path of an electron whose instantaneous circle does not pass through 0 at the time of injection but is between 0 and r_0. The oscillation is about r_i while r_i approaches r_0. (D) A real beam from the injector showing image formation at 1, 2, 3 and 4. The instantaneous circle is coincident with the equilibrium orbit.

is thus most effective at small velocities, where scattering and space charge effects are most important. Figure 1(B) shows such a damped oscillation about the equilibrium radius. There will also be vertical focusing, forces tending to drive the electron back to the plane of the orbit, provided the magnetic field strength is decreasing with increasing r. The restoring force here is due to the curvature of the magnetic field near the median plane; the focusing action is similar to the magnetic focusing effective in

[3] This can be shown in the following way. The energy of oscillation is $E=J\nu_r$, where J is the action variable, ν_r the frequency of oscillation. The amplitude of oscillation a is given by $E=\frac{1}{2}M(2\pi\nu_r)^2a^2$, with M the transverse mass. Thus $a^2=J/2\pi^2M\nu_r$. The frequency of rotation of the electron in its orbit is $\nu=p/2\pi rM$, so, writing $n_i=\nu_r/\nu$, $a^2=Jr/\pi n_i p$. It follows from the adiabatic invariance of the action variable that $a\sim(r/n_i p)^{\frac{1}{2}}\sim(1/n_i H)^{\frac{1}{2}}$. For $H\sim 1/r^n$, n_i turns out to be a constant.

the cyclotron. The vertical oscillations are similarly damped. Thus both radial and vertical focusing can be obtained, for a magnetic field which in the region of the orbit is of the form $H \sim 1/r^n$, within the limits $0 < n < 1$.

The injection of electrons into the machine is a problem which also has its difficulties. It is obviously not possible to inject the electrons at the position of the equilibrium orbit. Nor is it possible to shoot them into the magnetic field from an external source as was attempted by Wideröe; for, unless the magnetic field were increasing extremely rapidly, the orbits would be nearly symmetric around the point where the radial velocity vanished: the electrons would shoot right out again. Thus the electrons must be injected at a point within the magnetic field, either inside or outside the equilibrium orbit (in the following we shall suppose it outside).

The analysis of the paths of the electrons is greatly simplified by the fact that the magnetic field increases little during one revolution of the electron. The adiabatic theorem can therefore be applied: it states that under these circumstances the motion is very nearly the same at each instant as if the magnetic field were held fixed at its instantaneous value. Consider now an electron injected tangentially with a given momentum p, at radius r. As the magnetic field is increased from zero there will come a time when p, H, and r satisfy the relation (1). An electron injected at this time would, if the magnetic field remained constant, travel in a circle. The adiabatic theorem tells us that at any later time, even though the field is increasing, the position of the electron will still be given by (1); at each instant the electron is moving on its "instantaneous circle." Since the injection radius is larger than the radius of the equilibrium orbit, the flux within the instantaneous circle is less than that necessary to hold the electron at r. Momentum is gained less rapidly than necessary to keep the radius of the orbit constant, and the instantaneous circle shrinks towards the equilibrium orbit. The actual orbit of the electron will thus be a spiral which approaches the equilibrium orbit asymptotically as shown in Fig. 1(A).

This contraction of the instantaneous orbit in itself provides relatively little clearance for the injection electrodes. The contraction is fastest for small velocities, but it is inadvisable to use too small injection energies because of relatively large space charge forces and scattering. In the University of Illinois accelerator (at injection energy 180 v, injection radius 9 cm, $r_0 = 7.5$ cm) the instantaneous circle shrinks 1 mm during the first revolution of the electron. However, electrons injected not quite tangentially, or a little too early or too late, so that at the time of injection their instantaneous circle lies outside or inside the injection radius, will, as the discussion of focusing shows, oscillate with decreasing amplitude about the appropriate spiral orbit. This situation is shown by Fig. 1(C). The period of these oscillations is different from the period of revolution, so that the electron will, in general, execute several decreasing oscillations before the maximum displacement occurs near the starting electrodes. There is thus a considerable range of starting angles and times which allow capture into the equilibrium orbit, even though the electrons are injected at constant energy. In Fig. 1(D) the paths of divergent rays from an injector are shown. The formation of an image occurs at intervals of half an oscillation. In addition to these magnetic effects, the space charge spreading of the beam can also play a role in causing electrons to clear the injector.

After the electrons have been accelerated a variety of devices can be employed to bring them to strike a target, all of them based, of course, on destroying the relation (2) at the appropriate time. A simple method was used in the Illinois accelerator to accomplish this. A small amount of iron dust in an insulating cement made up a part of the magnetic circuit which fed flux through the center of the orbit. These dust particles saturate before the iron core does. When saturation sets in, p increases less rapidly than the magnetic field at the orbit. The electrons then spiral inward until they hit the target.

II. The Electronic Orbits

The position of the electron will be specified by the cylindrical coordinates (r, φ, z). We shall first consider the motion in the median plane

$(z=0)$, in which the magnetic field has only a z component, $H_z=H(r,t)$. This field can be derived from a vector potential, $A_\varphi=A(r,t)$, by the relation

$$H_z=r^{-1}\partial(rA)/\partial r=A/r+\partial A/\partial r. \tag{3}$$

There is a concomitant electric field $E_\varphi=-\dot{A}/c$.

The Hamiltonian function is

$$\mathcal{H}=c(m^2c^2+p_r^2+p^2)^{\frac{1}{2}}, \quad p=p_\varphi/r+eA/c.$$

Here p_φ is the canonical angular momentum, defined by the relation

$$p=mr\dot{\varphi}/(1-v^2/c^2)^{\frac{1}{2}},$$

and is a constant of the motion.

For any p_φ, the radius r_i of the instantaneous circle is determined by the condition $\dot{p}_r=0$, or, since $\dot{p}_r=c^2pp'/\mathcal{H}$, by

$$p'_i=-(p_\varphi/r^2-eA'/c)_i=0. \tag{4}$$

We use a prime to denote partial differentiation with respect to r. The subscript i indicates that the quantity is to be evaluated at $r=r_i$; the subscript 0 will be used for $r=r_0$. Since an electron moving on the instantaneous circle has a momentum p_i, we see, using (3), that (4) is another expression of the relation (1).

The condition for motion in the equilibrium circle ($r_i=r_0$, a constant independent of time) is then

$$p_\varphi=0, \quad A'_0=0, \tag{5}$$

since p_φ/r_0^2 is independent of time, and we take A of the form[4] $A(r,t)=f(r)h(t)$.

It can readily be shown that the condition $A'_0=0$ is equivalent to (2). We have

$$\phi=\int\mathbf{H}\cdot d\boldsymbol{\sigma}=\int \mathrm{curl}\mathbf{A}\cdot d\boldsymbol{\sigma}=\int\mathbf{A}\cdot d\mathbf{s}=2\pi r_0A_0,$$

and from (3), $H_0=A_0/r_0$. Thus on the equilibrium circle, $\phi_0=2\pi r_0^2H_0$.

It may be remarked that for a magnetic field *everywhere* of the form $H=b/r^n$ (and thus lacking the central field necessary to satisfy the flux condition (2)) the vector potential is $A=b/(2-n)r^{n-1}$, and (4) gives $er_i^2H_i/c=(2-n)p_\varphi/(1-n)$, or, from (1), $p_ir_i=$constant. In such a field the electron spirals rapidly towards the center as its momentum increases.

[4] The case in which there is a time independent flux ϕ_1 through the center of the orbit is also of interest. It can be represented by $A(r,t)=f(r)h(t)+\phi_1/2\pi r$, which necessitates only replacing p_φ, in (5), by $p_\varphi+e\phi_1/2\pi c$.

Radial focusing

In order to take advantage of the adiabatic theorem, we write $r=r_i+x$, and suppose $x\ll r_i$. If we introduce x and $p_x=p_r$ as new canonical variables, and in the new Hamiltonian function, $\mathcal{H}_1=\mathcal{H}-p_x\dot{r}_i$, retain only terms not higher than quadratic in x and p_x we obtain

$$\mathcal{H}_1=\epsilon+\tfrac{1}{2}c^2p_x^2/\epsilon+\tfrac{1}{2}p_ip''_ix^2/\epsilon-p_x\dot{r}_i. \tag{6}$$

Here $\epsilon=c(m^2c^2+p_i^2)^{\frac{1}{2}}$ is the energy of an electron moving on the instantaneous circle.

The equations of motion are

$$\begin{aligned}\dot{x}&=c^2p_x/\epsilon-\dot{r}_i,\\ \dot{p}_x&=-c^2p_ip''_ix/\epsilon,\end{aligned} \tag{7}$$

which, by eliminating p_x, give

$$\ddot{x}+\dot{\epsilon}\dot{x}/\epsilon+c^4p_ip''_ix/\epsilon^2=-\ddot{r}_i-\dot{\epsilon}\dot{r}_i/\epsilon. \tag{8}$$

The forcing terms on the right represent the nonadiabatic corrections to the motion.

If we write $x=(mc^2/\epsilon)^{\frac{1}{2}}u$, and omit the forcing terms for the moment, (8) becomes

$$\begin{aligned}&\ddot{u}+\omega_r^2u=0,\\ &\omega_r^2=c^4p_ip''_i/\epsilon^2-\tfrac{1}{2}\ddot{\epsilon}/\epsilon+\tfrac{1}{4}\dot{\epsilon}^2/\epsilon^2\sim c^4p_ip''_i/\epsilon^2,\end{aligned} \tag{9}$$

since the second and third terms of ω_r^2 are smaller than the first by a factor of order $(cp_m/\epsilon)^2f^2/\nu^2$, where f is the frequency of the magnetic field, ν the frequency of revolution of the electron, and p_m is the maximum momentum attained by the electron. If we write

$$p''_i=n_i^2p_i/r_i^2, \tag{10}$$

Eq. (9) takes the simple form

$$\omega_r=n_iv/r_i.$$

The frequency of radial oscillation is thus just n_i times the frequency of rotation of the electron in its orbit. In general n_i will be a slowly varying function of r, but for $H\sim 1/r^n$, n_i is independent of r, $n_i=(1-n)^{\frac{1}{2}}$. We also see that for focusing oscillations to occur we must have $p''_i>0$, which, on the equilibrium circle, reduces to $A''_0>0$, in virtue of (5). The equilibrium circle is thus the point of minimum electric field.

If we choose $t=0$ when $A=0$, we require the solution of (9) only for $\omega_rt\gg 1$, since this condi-

tion is already met at the time of injection of the electron. The asymptotic form of the solution for $\omega_r t \gg 1$ is

$$u = a(c/r_0\omega_r)^{\frac{1}{2}} \sin\left[\int_0^t \omega_r dt + \gamma\right],$$

or

$$x = a(mcr_i/n_i p_i r_0)^{\frac{1}{2}} \sin\left[\int_0^t \omega_r dt + \gamma\right], \quad (11)$$

with a and γ arbitrary constants. The amplitude of the radial oscillations is thus damped by a factor $(p_i/r_i)^{-\frac{1}{2}} = (eHI_i/c)^{-\frac{1}{2}}$.

Injection of the electron

An electron injected on its instantaneous circle, will, in the adiabatic limit, continue to move on this circle as it shrinks down to the equilibrium orbit. The rate of contraction of the instantaneous circle can be obtained by differentiating (4),

$$\dot{r}_i = -e\dot{A}'_i/cp''_i = -\dot{A}'_i/(A''_i + 2A'_i/r_i).$$

For $r_i - r_0$ small this reduces, in virtue of (5), to $\dot{r}_i = -(r_i - r_0)\dot{A}''_0/A''_0$. The shift of the instantaneous circle toward the equilibrium orbit produced by a change $\delta H I$ of the magnetic field is thus given by

$$\delta r_i/(r_i - r_0) = -\delta H I/H I. \quad (12)$$

An electron injected not on the instantaneous circle, but in its neighborhood, will oscillate about the instantaneous circle; its motion is described by (11). Since the instantaneous circle is simultaneously approaching the equilibrium orbit, the resultant motion is that shown in Fig. 1(C).

Both the damping of the oscillation about the instantaneous circle and the shrinking of the instantaneous circle toward the equilibrium orbit are used to cause the electrons to miss the injector on successive revolutions. In terms of the voltage gain per revolution δV, and the injection voltage V, the damping is expressed by

$$\delta a/a = -\tfrac{1}{4}\delta V/V, \quad (13)$$

where $\delta a/a$ is the fractional decrease in the amplitude of oscillation. Similarly the shrinking described by (12) is

$$\delta r_i/(r_i - r_0) = -\tfrac{1}{2}\delta V/V. \quad (14)$$

We may verify that the wandering from the instantaneous circle caused by the nonadiabatic correction terms in (8) is in fact very small. The term $\dot{\epsilon}\dot{r}_i/\epsilon$ is of order $\ddot{r}_i v^2/c^2$, and will be neglected. Let t_I be the time of injection. The asymptotic solution of (8) for $\omega_r t \gg 1$ can be written down with the aid of the solutions (11). It is

$$x = -\int_{t_I}^t \left\{\frac{n_i(s)p_i(s)r_i(t)}{n_i(t)p_i(t)r_i(s)}\right\}^{\frac{1}{2}} \frac{\ddot{r}_i(s)}{\omega_r(s)} \sin\left[\int_s^t \omega_r dt'\right] ds$$

$$= \left\{\frac{n_i(t_I)p_i(t_I)r_i(t)}{n_i(t)p_i(t)r_i(t_I)}\right\}^{\frac{1}{2}} \frac{\ddot{r}_i(t_I)}{\omega_r(t_I)^2} \times \cos\left[\int_{t_I}^t \omega_r dt'\right] - \frac{\ddot{r}_i(t)}{\omega_r(t)^2}.$$

The maximum displacement is

$$x_m = -2\ddot{r}_i(t_I)/\omega_r(t_I)^2.$$

In the interesting case, near the beginning of the acceleration when the field is increasing linearly with time, differentiation of (12) gives $\ddot{r}_i = -2\dot{r}_i\dot{H}/H$. If δH and δr_i are the increments of H and r_i during one revolution of the electron, we then have

$$x_m = \delta r_i \delta H/\pi^2 n_i^2 H,$$

all quantities being evaluated at $t = t_I$.

Vertical focusing

Near the median plane the magnetic field has a radial component determined by $\partial H_r/\partial z = \partial H_z/\partial r$. The vector potential then takes the form

$$A_\varphi = A(r, t) - \tfrac{1}{2}A_1(r, t)z^2,$$

where

$$A_1(r, t) = \partial H_z/\partial r|_{z=0} = (c/e)[(rp)'/r]'_i.$$

For small deviations from the median plane, the Hamiltonian (6) must be supplemented by the terms

$$\mathcal{H}_z = \tfrac{1}{2}c^2 p_z^2/\epsilon - \tfrac{1}{2}c^2 p_i[(rp)'/r]'_i z^2/\epsilon.$$

The equations of motion are

$$\dot{z} = c^2 p_z/\epsilon, \quad \dot{p}_z = c^2 p_i[(rp)'/r]'_i z/\epsilon,$$

which differ from (7) only in the absence of a forcing term, and in the replacement of p''_i by

$-[(rp)'/r]'_i$. The solutions are thus the same as (11), but with ω_r and n_i replaced by $\omega_A = m_i v/r_i$ and m_i, defined by

$$-[(rp)'/r]'_i = m_i^2 p_i/r_i^2. \tag{15}$$

Choice of the field shape

It has been shown that there must be a position of minimum electric field (i.e., $A'_0=0$, $A''_0>0$) for radial stability, and that the field must decrease with increasing distance from the axis for axial stability of the electrons. If the field in the region of the electron's orbit is of the form

$$H_z = H_0(t)(r_0/r)^n,$$

the vector potential is given by

$$A = \frac{H_0(t)}{2-n}\left[\frac{r_0^n}{r^{n-1}} + (1-n)\frac{r_0^2}{r}\right].$$

The second term in the bracket gives an electric field, but no magnetic field at the position of the orbit; it represents the effect of the strong central magnetic field required to satisfy the flux condition (2).

Evaluating (10) and (15) for this potential we find

$$n_i^2 = (1-n), \quad m_i^2 = n.$$

The conditions for radial and vertical focusing, $n_i^2>0$, $m_i^2>0$, thus demand $0<n<1$, as we have already seen.

An electron deflected from its instantaneous circle by a small angle scattering will execute oscillations of amplitude proportional to the transverse velocity imparted by the scattering divided by the initial frequency of oscillation. The ratio of radial to vertical amplitude will thus be

$$x/z = [n/(1-n)]^{\frac{1}{2}}.$$

Since in the Illinois accelerator the vertical clearance was smaller than the horizontal, it was desired to have vertical focusing stronger than horizontal focusing. The pole pieces were accordingly shaped to give a field with $n=\frac{2}{3}$.

JULY 1, 1941 PHYSICAL REVIEW VOLUME 60

The Resonance Energy of the Thorium Capture Process

LISE MEITNER
Forskningsinstitutet för Fysik, Stockholm, Sweden

(Received May 20, 1941)

IN a paper dealing with the capture cross section for thermal neutrons in thorium[1] it was pointed out that the pure capture process in thorium has a resonance character with a large contribution from thermal neutrons.[2] The following experiments were carried out in order to determine the resonance energy of this process.

As the neutron source available was only 100 mg Ra+Be, it was not possible to determine the resonance energy in the usual way, i.e., by measuring the absorption coefficient of boron for the resonance neutrons with thorium 233 as detector. We therefore made use of a less direct method by measuring the absorption in thorium for various neutron resonance groups picked out by suitable detectors. If there are found neutron groups having absorption coefficients whose ratio is not inversely proportional to the ratio of the respective velocities, one can expect that a resonance group of the thorium capture process is lying within the range of the energies under investigation.

Since the large contribution of thermal neutrons to the capture process in Th suggested that the resonance energy might be rather low, Au ($E_r=3.5$ ev),[3] In ($E_r=0.9$ ev)[4] and Rh, which has the same resonance energy as In were used as

[1] L. Meitner, Nature **45**, 422 (1940).
[2] L. Meitner, O. Hahn and F. Strassmann, Zeits. f. Physik **109**, 538 (1938).
[3] O. R. Frisch, Kgl. Danske Vid. Selsk. Math.-Phys. Medd. **14**, Nr. 5.
[4] C. P. Baker and R. F. Bacher, Phys. Rev. **57**, 1076 (1940).

detectors. The resonance energy of these three elements is rather well-determined and their resonance levels are known to be single. In addition, use could be made of the absorption coefficient of Th for thermal neutrons known from our earlier experiments. As already mentioned, there can be no doubt that the resonance energy of Th is beyond the energy of the neutrons strongly absorbed by Cd, hence the $1/v$ law will be valid for the absorption of thermal neutrons.

The experimental arrangement was generally as follows: The neutron source was placed inside a block of paraffin wax 3.4 cm below the surface. The detectors were placed 1.4 cm above the surface and shielded in all experiments by 0.44 mm Cd on both faces. The face opposite to the source was screened by a thick foil of the material under investigation. Between the detectors and the paraffin surface the thorium absorber (13.4 g/cm² of metallic Th), or other absorbers, could be inserted. The contribution to the activity of the detectors from neutrons beyond the resonance region was determined by carrying out the irradiation with absorbers of the same material and sufficiently thick to cut off practically all the resonance neutrons. One set of experiments was carried out inside paraffin with the same arrangement as had been applied for the determination of the capture cross section of thermal neutrons in Th.[1] When account is taken of the slightly changed geometrical conditions, the values found were the same as those obtained with the arrangement described above. All activity measurements were followed over several half-life periods in order to get a higher accuracy, and every experiment was repeated at least three times.

Because of the arrangement used—the detector being placed directly on the absorber of nearly equal size—one can expect that only a small part of the scattering cross section enters into the measurements. If, however, the capture cross section is small itself, the effect of scattering might be very important. Since it was not possible to determine this contribution for Th as absorber, the absorption of the resonance neutrons of In in lead was measured under the same experimental conditions. The lead absorber had the same dimensions and, within 2 percent, the same number of absorbing nuclei per cm² as the thorium absorber. The capture cross section for thermal neutrons in lead is known[5] to be $\overset{\text{Pb}}{\sigma_{\text{cap}}} = 2.5\times10^{-24}$ cm², and there are good reasons to suppose that the $1/v$ law is holding for lead. So the difference between the cross section found experimentally and that one computed according to the $1/v$ law can be regarded as the contribution from scattering within the whole range of energies under investigation. However, the scattering effect implies a change in the primary directional distribution of the neutrons. In order to evaluate this influence, the relative number of neutrons indicated behind an absorber of 23.8 mg/cm² boron was measured with and without the lead absorber in position. With the Pb absorber inserted, the apparent absorption coefficient of boron was 10 percent larger than that one found without the lead. After applying the corresponding obliquity correction, the contribution of scattering in lead was found to be $\sigma_s = 1.2\times10^{-24}$ cm².

From the results given below it can be seen that the scattering is important only for the absorption of the resonance neutrons of gold in Th. On account of the low absorption coefficient, these measurements are not very accurate, the difference in scattering to be expected for Pb and Th is negligible. The same holds for In and Rh, as the scattering effect is small compared to the capture process. So the absorption coefficients found experimentally for Th were corrected for the scattering contribution found with lead.

In calculating the absolute values of capture cross sections, obliquity corrections (angles up to about 70° were involved) were made according to the curves for thin, compared to thick, detectors given by Frisch,[3] without taking into account any influence of the change in the directional distribution caused by the scattering effect. We are interested only in the ratio of these cross sections to the cross section for thermal neutrons, which, as far as the latter is corrected in the same way, is independent of the applied correction. The results are given in Table I. The last column gives the cross sections calculated by assuming the validity of the $1/v$ law and by taking the capture cross section for thermal neutrons as a basis ($\overset{\text{Th}}{\sigma_{\text{th}}} = 6.0\times10^{-24}$ cm²).

[5] R. Fleischmann and W. Bothe, Ergeb. d. exakt. Naturwiss. **16**, 37 (1937). L. Meitner, reference 1.

TABLE I. *Data on cross section values.*

DETECTORS	RESONANCE ENERGY	$\sigma^{Th}_{exp.} \times 10^{24}$ CM²	$\sigma^{Th}_{cal.} \times 10^{24}$ CM²
In	0.9 ev	3.5±0.7	1.0
Rh	0.9 ev	3.5±0.7	1.0
Au	3.5 ev	~0.3	0.5

In the calculation we set $E_{th}=0.026$ ev.

The results show that, for $E=0.9$ ev, the experimental cross section is much larger than the calculated cross section, while for $E=3.5$ ev the experimental cross section appears to be somewhat smaller than that calculated according to the $1/v$ law. On account of the poor accuracy of the results it seems meaningless to calculate the exact resonance energy from the values obtained by assuming the existence of a single resonance level. Hence one can conclude only that thorium has a resonance level between 0.2 ev (cut-off energy of Cd) and 3.5 ev, and probably in the neighborhood of 2 ev.

We attempted to get additional information by carrying out some experiments with the resonance neutrons of silver ($E_r=2.5$ ev). The activities due to the resonance neutrons were, however, so low even without any absorber that it was not possible to obtain any reliable results.

The absorption of the In resonance neutrons in thin layers of boron was found to correspond to a resonance energy of 0.92±0.06 ev, if for the boron absorption coefficient of thermal neutrons the value $\overset{B}{\mu}_{th}=28$ cm²/g is taken.

I wish to thank the Academy of Sciences in Stockholm for a grant and Professor G. Borelius and Doctor J. Tandberg for the indium and rhodium foils kindly put at my disposal.

Letters to the Editor

PROMPT publication of brief reports of important discoveries in physics may be secured by addressing them to this department. Closing dates for this department are, for the first issue of the month, the eighteenth of the preceding month, for the second issue, the third of the month. Because of the late closing dates for the section no proof can be shown to authors. The Board of Editors does not hold itself responsible for the opinions expressed by the correspondents.

Communications should not in general exceed 600 words in length.

On a Theory of Particles with Half-Integral Spin

WILLIAM RARITA AND JULIAN SCHWINGER
Department of Physics, University of California, Berkeley, California
June 18, 1941

FIERZ and Pauli[1] have developed a general theory of particles with arbitrary spin, both integral and half-integral. The quantities describing particles of integral spin are tensors of suitable rank; half-integral spins are described by spinors of multiple order. It is the purpose of this note to suggest an alternative formulation of the theory on half-integral spins which avoids the complicated spinor formalism of Fierz and Pauli. The fundamental quantities of this theory $\Psi_{\mu_1\ldots\mu_k}$, have the mixed transformation properties of a Dirac four-component wave function, and of a symmetric tensor of rank k. (The Dirac index is suppressed.) The equations, which describe a particle of spin $k+\frac{1}{2}$ are:

$$(\gamma_\tau\partial_\tau+\kappa)\Psi_{\mu_1\ldots\mu_k}=0, \quad \gamma_\alpha\Psi_{\alpha\mu_2\ldots\mu_k}=0. \tag{1}$$

The usual supplementary conditions of the integral spin theory:

$$\partial_\alpha\Psi_{\alpha\mu_2\ldots\mu_k}=0, \quad \Psi_{\alpha\alpha\mu_3\ldots\mu_k}=0, \tag{2}$$

appear as consequences of these equations.

The verification that such wave fields are indeed associated with a particle of spin $k+\frac{1}{2}$ may proceed either by demonstrating that the number of independent plane wave solutions of definite energy and momentum is $2(k+\frac{1}{2})+1$, or by a direct proof that the square of the intrinsic angular momentum has the value $(k+\frac{1}{2})(k+\frac{3}{2})$ in the rest system. (It will not have this value in an arbitrary reference system.) The spin multiplicity is an invariant and is easily calculated in the rest system. Since each Ψ obeys the Dirac equation, the "small" components vanish and the two "large" components altogether form $2(k+3)!/k!3!$ quantities. The second equation of (1) provides the information that the $\Psi_{4\mu_2\ldots\mu_k}=0$, which are $2(k+2)!/(k-1)!3!$ in number, and that $\sigma_i\Psi_{i\mu_2\ldots\mu_k}=0$ $(\mu_s\neq 4)$ which constitute $2(k+1)!/(k-1)!2!$ relations among the Ψ's. The total number of independent components is, therefore, $2(k+1)$, as desired. The operator of total spin consists of the sum of the k infinitesimal rotation operators associated with the tensor indices in addition to the spin operator $\frac{1}{2}\boldsymbol{\sigma}$ of the Dirac theory. The proof that the spin possesses the correct eigenvalue is an elementary consequence of the condition $\sigma_i\Psi_{i\mu_2\ldots\mu_k}=0$.

The special case of spin $\frac{3}{2}$ has been treated in detail by Fierz and Pauli employing a method that necessitated the adjunction of auxiliary spinors in order to produce the proper subsidiary conditions from a variational principle. It is an advantage of the new formalism that a suitable Lagrangian can be constructed without the intervention of additional fields. One of a class of possible Lagrangians is

$$L=\bar{\Psi}_\mu(\gamma_\tau\partial_\tau+\kappa)\Psi_\mu-\tfrac{1}{3}\bar{\Psi}_\mu(\gamma_\mu\partial_\nu+\gamma_\nu\partial_\mu)\Psi_\nu + \tfrac{1}{3}\bar{\Psi}_\mu\gamma_\mu(\gamma_\tau\partial_\tau-\kappa)\gamma_\nu\Psi_\nu. \tag{3}$$

Although the Lagrangian is not unique in the absence of external fields, the form (3) is the only one which permits a relatively simple expression of the equations of motion in the presence of electromagnetic fields. The four-vector of charge and current, obtained by the usual prescription, is

$$\begin{aligned} j_\nu&=\bar{\Psi}_\mu\gamma_\nu\Psi_\mu-\tfrac{1}{3}(\bar{\Psi}_\mu\gamma_\mu)\Psi_\nu-\tfrac{1}{3}\bar{\Psi}_\nu(\gamma_\mu\Psi_\mu) \\ &\quad+\tfrac{1}{3}(\bar{\Psi}_\sigma\gamma_\sigma)\gamma_\nu(\gamma_\tau\Psi_\tau) \\ &=\bar{\Psi}_\mu\gamma_\nu\Psi_\mu \end{aligned} \tag{4}$$

in the absence of external electromagnetic fields. Although the charge density is not a positive definite form, the total charge is necessarily definite since $\Psi_4=0$ in the rest system. In the exceptional case of zero rest mass the wave function admits a gauge transformation,

$$\Psi_\mu'=\Psi_\mu+\partial_\mu\varphi, \quad \gamma_\tau\partial_\tau\varphi=0,$$

which leaves all physical quantities invariant.

The method here presented for developing the theory of spin $\frac{3}{2}$ thus contains many of the features of both the Proca and the Dirac theory. This is particularly evident in the application to β-decay which Mr. Kusaka[2] has discussed in an accompanying letter.

[1] M. Fierz and W. Pauli, Proc. Roy. Soc. **A173**, 211 (1939).
[2] S. Kusaka, Phys. Rev. **60**, 61 (1941), this issue.

β-Decay with Neutrino of Spin $\frac{3}{2}$

SHUICHI KUSAKA
Department of Physics, University of California, Berkeley, California
June 13, 1941

ALL current theories of β-decay assume the neutrino to have the spin $\frac{1}{2}$ although there is no *a priori* reason for this choice, except that of simplicity. Recently Oppenheimer[1] has suggested the possibilities of neutrinos with different masses and spins, and it is of some interest to find what distribution laws, energy-lifetime relations, and selection rules for β-decay are possible with a neutrino of spin $\frac{3}{2}$. The results show that for any coupling involving the neutrino wave function, or its first derivative, the spectrum distribution is predominantly of the Konopinski-Uhlenbeck type, and that, correspondingly, the energy-lifetime relation for high energy is given by the seventh-power law. Further, for neutrino of non-zero mass, both the Fermi and the Gamow-Teller selection rules are possible; while for neutrino of zero mass, only the latter is permitted. Now, since the energy-lifetime relations for the observed β-spectra agree better with the fifth-power

law given by the Fermi distribution rather than the seventh-power law, we have experimental grounds for ruling out the possibility of neutrino with spin $\frac{3}{2}$.

The wave equation for a particle of spin $\frac{3}{2}$ has been developed by Rarita and Schwinger.[2] The wave function ψ_μ consists of a four-vector, each component of which is a Dirac spinor, and satisfies the supplementary conditions $\partial_\mu\psi_\mu=0$ and $\gamma_\mu\psi_\mu=0$. The plane wave solutions can be built up from the polarization vectors

$$\mathbf{e}_1=\frac{1}{\sqrt{2}}(1, i, 0), \quad \mathbf{e}_2=\frac{1}{\sqrt{2}}(1, -i, 0), \quad \mathbf{e}_3=\frac{\mathbf{P}}{p}=(0, 0, 1),$$

where the z axis is taken in the direction of the momentum, and the solutions ψ_{+1} and ψ_{-1} of the Dirac equation for the spin parallel and antiparallel to the momentum. If we separate the space and time components of ψ_μ by writing $\mathbf{\Phi}=(\psi_1, \psi_2, \psi_3)$ and $i\varphi=\psi_4$, the four independent solutions for positive energy are

$$\mathbf{\Phi}^{(1)}=\mathbf{e}_1\psi_{+1}, \qquad \varphi^{(1)}=0,$$
$$\mathbf{\Phi}^{(2)}=\mathbf{e}_2\psi_{-1}, \qquad \varphi^{(2)}=0,$$
$$\mathbf{\Phi}^{(3)}=\frac{1}{\sqrt{3}}\mathbf{e}_3\psi_{+1}-\sqrt{\tfrac{2}{3}}\frac{E}{\mu}\mathbf{e}_3\psi_{-1}, \quad \varphi^{(3)}=-\sqrt{\tfrac{2}{3}}\frac{p}{\mu}\psi_{-1},$$
$$\mathbf{\Phi}^{(4)}=\frac{1}{\sqrt{3}}\mathbf{e}_1\psi_{-1}+\sqrt{\tfrac{2}{3}}\frac{E}{\mu}\mathbf{e}_3\psi_{+1}, \quad \varphi^{(4)}=\sqrt{\tfrac{2}{3}}\frac{p}{\mu}\psi_{+1}.$$

They are orthogonal, normalized, and satisfy the supplementary conditions.

Following the usual recipe, the interaction between the heavy and light particles can be written down. Because of the supplementary conditions, there is no scalar coupling term. The vector coupling term is

$$i\psi_P^\dagger\gamma_\mu\psi_N\psi_e^\dagger\psi_\mu,$$

which gives in the non-relativistic limit for the heavy particle

$$\psi_P^*\psi_N\psi_e^*\beta\varphi.$$

The tensor and the pseudo-vector coupling terms can similarly be written down.

Since the plane wave solutions have terms with the factor E/μ or p/μ, the square of the matrix elements contains a factor of the form $E+a\mu$ where a is a numerical constant depending on the type of coupling. Hence, for high energy, this theory gives the seventh-power law for the relation between the lifetime and the energy. It has actually been verified, by calculating the transition probability for the most general type of interaction, that there is no possible choice of the constants which would lead to a cancellation of the energy and momentum terms and so give the Fermi law.

When the mass of the neutrino is taken to be zero, the wave function admits a gauge transformation. Now it is easily seen that any interaction involving the neutrino wave function is not gauge invariant: in fact the only interactions satisfying this condition are those involving the curl of the wave function. Thus only the tensor and the pseudo-vector couplings are possible, and hence only the Gamow-Teller selection rule is permitted. However the energy-lifetime relation is still given by the seventh-power law since there remains only the first two of the plane wave solutions given above,[3] and the differentiation introduces the momentum factor.

In conclusion, the author wishes to thank Professor J. R. Oppenheimer and Dr. Julian Schwinger for helpful discussions on this subject.

[1] J. R. Oppenheimer, Phys. Rev. **59**, 908 (1941).
[2] W. Rarita and J. Schwinger, Phys. Rev. **60**, 61 (1941), this issue. The author is greatly indebted to Drs. Rarita and Schwinger for letting him make use of their theory before publication.
[3] This is a special case of the general theorem due to M. Fierz, Helv. Phys. Acta **13**, 45 (1940), that for a particle of zero mass and any spin, there are only two independent, non-trivial solutions.

Observations Bearing on Stellar Collapse

DEAN B. MCLAUGHLIN
The Observatory, University of Michigan, Ann Arbor, Michigan
May 19, 1941

THE recent publication, by G. Gamow and M. Schoenberg,[1] of an ingenious theory of the cause of nova outbursts makes it of interest to examine the observational facts concerning pre-nova and post-nova stars.

About pre-nova stars, we know only that their *photographic* luminosities are comparable with that of the sun, and that one and only one of them had its spectrum recorded feebly before outburst. The faint record of Nova Aquilae 1918 was classified by Miss Cannon on the basis of violet extent of the spectrum, and not from spectral lines, as "resembling classes *B* and *A*."[2] Actually class *O* would also be a possibility, since the violet extents of *O* and *B* spectra look alike when photographed with *glass* prisms.

Some years after outburst, all stars which have been studied (sixteen in all) show continuous spectra with great violet extent and no absorption lines. Some have bright lines of hydrogen, HeII, CIII, and other elements which indicate temperatures similar to those of class *O* stars.[3] Of special importance is the fact that the *photographic* luminosities are equal to those of the pre-nova objects. No observational fact clearly contradicts the working hypothesis that the physical conditions of pre- and post-nova stars are nearly identical. The burden of proof thus rests with those who postulate that stars change from normal to degenerate configurations at the time of outburst.

The collapse theory encounters grave difficulties in the attempt to reconcile radical changes of radius and temperature with the observed equality of pre- and post-nova brightness in a narrow range of wave-lengths, the common photographic region.

To fix ideas, suppose a normal main sequence star collapses to a sub-dwarf or white dwarf configuration such that the *bolometric* luminosity is unchanged. Then, assuming blackbody radiation, we must have

$$R_0^2T_0^4=R_c^2T_c^4,$$

where R_0 and T_0 are the original radius and temperature, and R_c and T_c refer to the collapsed star. If we take $T_0=6000°\text{K}$ (equal to that of the sun) and $T_c=50{,}000°\text{K}$ (estimated from spectra of old novae), we find $R_c=0.014R_0$, and the density would obviously be increased by a factor of 3×10^5. These figures are characteristic of the known white dwarfs. Of more direct application here is the result

that the *photographic* luminosity of the collapsed star should be roughly three magnitudes fainter than its pre-nova value. Put differently, since such a large bolometric reduction results from the change of temperature, we conclude that the observed equality of pre- and post-nova stars requires that the end product be three magnitudes brighter bolometrically than before outburst. To the writer, at least, this appears to be a *reductio ad absurdum*. More details are given in a paper now in press in *Popular Astronomy*.

It is, of course, possible to object that the assumption of equal bolometric luminosities is incorrect. This is granted as a likely possibility. It is, therefore, of interest to determine in which direction it may be expected to fail. Appealing to observation, we see that while main sequence stars in general fit the mass-luminosity relation, the white dwarf companion of Sirius is too faint for its mass. This is just opposite to the direction of failure which would be required to account for the equality of the pre- and post-nova photographic luminosities on the hypothesis of collapse.

We must, of course, admit the existence of a remote possibility that a star could collapse, with radical changes of all its physical parameters except mass, and vary the energy distribution in its spectrum so as to keep the photographic radiation the same. This would imply almost a diabolical intent to deceive the observer! And, as one of my colleagues has remarked, it would take a pretty "cagey" star to do the trick.

The above remarks apply only to the common novae, and are not meant to include the supernovae. There are reasons for believing that the latter originate in a different way from the former, and because the energy liberated in these greater explosions is of the order of magnitude to be expected from stellar collapse, it appears quite possible that the theory of neutrino emission would apply there. The pre-outburst state of supernovae is entirely unknown, and the preceding arguments, therefore, cannot be applied to them.

[1] G. Gamow and M. Schoenberg, Phys. Rev. **59**, 539 (1941).
[2] Harvard Annals **81**, 179 (1920).
[3] M. Humason, Astrophys. J. **88**, 228 (1938).

Classical and Quantum Reflections of X-Rays

C. V. Raman and P. Nilakantan
Department of Physics, Indian Institute of Science, Bangalore, India
May 7, 1941

In a series of papers[1] published in April and May, 1940, we presented evidence proving conclusively that the lattice planes in a crystal give a second kind of geometric reflection of x-rays which we designated as the modified or quantum reflection, to distinguish it from the unmodified or classical reflection discovered by Laue and his collaborators in 1912. The process which results in the modified reflection was clearly established by the experimental results in the specific cases studied by us. In the language of classical optics, a modified reflection by the lattice planes results from the dynamic variation of their structure amplitude consequent on an oscillation, relative to each other, of the interpenetrating lattices in the structure of the crystal. In the act of such reflection, the primary x-ray frequency is altered by the addition or subtraction of one or another of the characteristic infra-red frequencies of the crystal. In the language of quantum mechanics, the modified reflection represents an inelastic collision of the photon with the crystal in which the two exchange energy. The probability of such transition, and therefore also the intensity of reflection, is determined by the principles of quantum mechanics and not by classical dynamics. The theory of the effect has been discussed in further papers.[2]

The view has been put forward in some recent papers[3–5] that the phenomenon dealt with by us may be explained as "diffuse maxima in the scattering of x-rays by elastic waves of thermal origin." We desire energetically to contradict this suggestion. The theory of the thermal scattering of x-rays has been fully discussed by Laue[6] in 1926. It is therefore possible to anticipate the results to be expected on the basis of such scattering. It may be stated at once that they are quite incapable of explaining the phenomena actually observed by us.

In the first place, the intensity of the scattering of x-rays by elastic waves of thermal origin comes out proportional to N, the number of scattering atoms in the crystal, and not to N^2. The absolute intensity of scattering is therefore very small, and the effects due to it would be perceptible only when large volumes of the crystal are operative. The present effect, on the other hand, though decidedly feebler than the classical reflections, can be recorded under precisely the same experimental conditions as the latter, that is to say, with fine x-ray beams and the thinnest crystal plates.

The so-called maxima in scattering arise from the presence of a factor in the expression for its intensity proportional to the square of the wave-length of the elastic waves which are effective. However, it is only when the direction of scattering coincides exactly with that of the classical reflection, and is therefore unobservable, that this multiplying factor becomes important. For other settings of the crystal, the "peak" disappears and is replaced by broad humps of relatively small intensity in the curve of intensity of scattering. These cannot explain the discrete reflections actually observed over a wide range of settings of the crystal. The (111) reflection by a crystal of diamond, for example, is remarkably sharp and may be readily photographed with crystal settings, in which it appears displaced by as much as 10° on either side of the Laue spot. No significant changes are observable either in its size or in its definition over the whole of this range.

Thirdly, exact measurements of the position of the (111) reflection by diamond over a wide range of settings have been made. They fit perfectly into the Raman-Nath formula, the inclination of the phase waves to the lattice planes coming out as half the tetrahedral valence angle. On the other hand, considered over the whole of this range, the Faxén formula is not even a rough approximation to the truth.

Finally, a crucial test is provided by the low temperature results with the (111) reflections by diamond. As

Laue has shown, a change of frequency occurs also in the scattering by elastic waves. According to the "scattering" theory, the intensity maxima correspond to elastic waves of maximum wave-length and minimum frequency. In such a case, therefore, the transition probabilities should be given correctly by the classical dynamics. The intensity maxima should fall off in proportion to the absolute temperature, the more exactly, the nearer the "scattering" maximum is to the Laue spot. Actual observations show, however, that the intensity is practically unaffected by cooling the crystal down to liquid-air temperatures, and this is true irrespective of the setting of the crystal. The observations thus clearly show that the transitions involved correspond to the high frequency infra-red levels and not to the low frequency acoustic ones. They also prove that the modified reflection is a quantum-mechanical effect.

[1] C. V. Raman and P. Nilakantan, Current Science **9**, 165 (1940); Proc. Ind. Acad. Sci. **11**, 379, 389, 398 (1940).
[2] C. V. Raman and N. S. N. Nath, Proc. Ind. Acad. Sci. **12**, 83, 427 (1940); Raman, Proc. Ind. Acad. Sci. **13**, 1 (1941).
[3] W. H. Zachariasen, Phys. Rev. **59**, 207 (1941).
[4] S. Siegel, Phys. Rev. **59**, 371 (1941).
[5] H. A. Jahn and K. Lonsdale, Nature **147**, 88 (1941).
[6] M. v. Laue, Ann. d. Physik **81**, 877 (1926).

JULY 1, 1941 PHYSICAL REVIEW VOLUME 60

Proceedings of the Ohio Section of the American Physical Society

THE fourth meeting of the Ohio Section of the American Physical Society was held at Muskingum College, New Concord, Ohio, on March 29, 1941. About fifty-five members and guests were present at the luncheon. Fourteen papers were scheduled for presentation, though weather conditions curtailed the programme; abstracts of five are appended.

The fifth meeting of the Ohio Section was held at Cleveland, in the buildings of the Case School of Applied Science and the Western Reserve University, on May 10, 1941; it was a joint meeting with the Ohio Academy of Science. One hundred members and guests were present. Nineteen papers were scheduled for presentation; of these the abstracts of five are appended. It was voted to cooperate with the Ohio Academy in sponsoring the programme of the Junior Academy for the creation of further interest in science in secondary schools, and five members (J. Albright, F. L. Berger, H. J. Kersten, H. P. Knauss, H. H. Roseberry) were chosen to collaborate in the various parts of the state. A symposium on "Light and Lighting" is planned for the meeting intended to be held in Cleveland in October 1941.

Newly elected officers of the Section for the season 1941–42 are the following: Chairman, W. E. Forsythe; Vice Chairman, P. B. Taylor; Secretary-Treasurer, R. H. Howe.

RICHARD H. HOWE, *Secretary*
Denison University, Granville, Ohio

ABSTRACTS OF PAPERS PRESENTED AT THE MUSKINGUM MEETING

1. The Vibrational Spectrum of the Potassium Chloride Crystal Lattice. L. L. FOLDY, *Case School of Applied Science.* (Introduced by R. S. Shankland.)—The methods of Born, v. Kármán, and Blackman for the investigation of the thermal vibrations of crystal lattices are applied in detail to an atomic model representative of a potassium chloride crystal. The potential interaction between ions, assumed of equal mass, is represented as a Coulomb interaction for any ion and its eighty nearest neighbors, a van der Waals attractive interaction varying as the inverse sixth power of the distance between nearest neighbors, and an exponential repulsive interaction also between nearest neighbors. Explicit solutions of the secular equation for the frequencies, which is of the third order, are obtained for waves traveling in certain directions in the crystal. The calculated principal restrahlen frequency was found to be about 10 percent lower than the observed value. The dispersion for short longitudinal waves traveling normal to the 111 planes of the crystal was found to be so great that the frequency increases with wave-length for wave-lengths less than about four and one-half times the distance between nearest neighbors. This extreme behavior was not manifested for transverse waves traveling normal to the 111 planes or for any waves traveling normal to the 110 and 100 planes.

2. The Harmonic Analysis of Geiger Counter Pulses. ROBERT S. SHANKLAND AND RICHARD H. BLYTHE, *Case School of Applied Science.*—The discharge of a Geiger-Müller counter results in a sudden drop in the potential of the wire electrode, followed by a more gradual return of this potential to its normal value. The time variation of potential constitutes a voltage pulse of which the shape and duration depend on both the discharge mechanism in the counter itself and upon the values of the electrical elements that compose the counter circuit. Thus the voltage

pulses observed on a cathode-ray tube may be analyzed to give information about the nature of the counter discharge and the behavior of the circuit. The present method of analysis gives the Fourier integral components making up the pulse in the form of a frequency spectrum of the amplitudes and phases. This is accomplished by charting the pulse to several scales of abscissae and analyzing the resulting curves by means of the Henrici harmonic analyzer according to a method previously described.[1] The pulses analyzed include an idealized pulse and those characteristic of counters used with the Neher-Harper circuit, the Neher-Pickering circuit, and a circuit employing a series resistance.

[1] R. S. Shankland, J. Acous. Soc. Am. **12**, 383–386 (1941).

3. Heat Transfer Across Horizontal Air Spaces. LOUIS B. YOUNG, *Marietta College.*—Heat transfer across horizontal air spaces is encountered in problems involving the calculation of heat transmission through floors and ceilings. Much of the transfer results from radiation exchange between the boundary surfaces; the remainder is due to convection. Convection in the case of upward heat flow, as in winter, is much greater than in the case of downward heat flow, as in summer. In both cases the actual transfer exceeds the possibility of ideal conduction as a transfer mechanism. Test apparatus was a two-foot guarded hot plate. Heat flow was calculated from the temperature gradient through a cork slab of known conductivity which was placed "in series" with the air space. The data enable computation of heat transmission through various floor and ceiling constructions incorporating different methods of insulation. The transfer is the sum of convection, following the five-fourths power law, and radiation exchange, following a modified Stefan's law.

4. Some Observations on an A.C. Resonant Pendulum. DAVID K. WEIMER.—A condenser and an air core inductance in series are tuned to resonance at 60 cycles. A pendulum bob of iron suspended so as to swing into the coil is thereby kept moving at its own frequency. Measurements were made on the current and voltage as the bob swung in and out of the coil in an effort to determine the nature of the driving force acting on the pendulum. It was found that the current is greater as the bob entered the coil than it is in the corresponding position as the bob leaves the coil for the greater part of the cycle of the pendulum.

5. Motion of the Walls of a Cornet. HAROLD P. KNAUSS, *Ohio State University.*—Vibrations of the metal walls of a cornet were studied by using a crystal pick-up in contact with the metal. The cathode-ray oscillograph showed wave forms which are complex for the lower tones of the cornet and sinusoidal for the higher tones. By substituting for the sweep voltage the output of a microphone responding to air-borne vibrations, a kind of Lissajous figure was obtained, which was quite irregular for the lower tones and elliptical for the higher tones. For a range of about half an octave it was shaped like a figure 8, indicating that in this range the metal vibrates at half the frequency of the air column.

ABSTRACTS OF PAPERS PRESENTED AT THE CLEVELAND MEETING

1. Observation of "Forbidden" Bands in the Infra-Red. C. H. TINDAL, *Ohio State University.*—According to the simple theory of tetrahedrally symmetric molecules there are four different normal frequencies designated as ν_1, ν_2, ν_3, and ν_4. The first two of these are optically inactive and are non-degenerate and twofold degenerate, respectively. The latter two are optically active, are threefold degenerate, and should appear as bands with sharp lines forming *P*, *Q*, and *R* branches. While this is essentially true for ν_3 it is not so for ν_4. The complex structure in ν_4 has been explained by Jahn[1] as due to a resonance Coriolis interaction between ν_4 and inactive ν_2, which are only about 100 cm^{-1} apart. Because of this interaction, the wave functions for ν_2 and ν_4 become sufficiently "mixed" so that ν_2 becomes active in the infra-red. The region from 9μ to 13μ has been resolved for SiH_4 and GeH_4 so that rotational lines are clearly distinguishable in two overlapping bands. The two bands are identified as ν_2 and ν_4, the *Q* branches folding in opposite directions as predicted by the theory of Jahn. The weaker band is identified as ν_2 and the other as ν_4. This identification is further verified since the rotational line spacing satisfies the relation presented by Teller:[2]

$$\Delta\nu_3+\Delta\nu_4=1\tfrac{1}{2}\Delta\nu_2.$$

[1] H. A. Jahn, Proc. Roy. Soc. **A168**, 469, 495 (1938).
[2] E. Teller, *Hand- und Jahrbuch der Chemischen Physik*, Vol. 9, No. 2, p. 152.

2. Absorption Bands of GeH_4 and SiH_4 in the Near Infra-Red. JOSEPH W. STRALEY, *Ohio State University.*—The fundamental vibration-rotation bands J_2, J_3, and J_4 of GeH_4 and SiH_4 have been carefully measured and the moments of inertia and the $X-Y$ distances calculated. Measurements of combination bands J_1+J_4 and J_3+J_4 in SiH_4 have also been made. The discrepancy in the appearance of the satellite structure in GeH_4 reported by Steward and Nielsen[1] with that reported by Lee and Sutherland[2] can now be attributed to difference in the absorbing layers of gas used by these observers. The recent measurements indicate the intensity of the satellites is not more than 10 percent of that of the principal rotation lines. The moments of inertia in g-cm^2 in the various states are as follows—

	I_0	I_2	I_3	I_4
SiH_4	0.986×10^{-39}	0.974×10^{-39}	0.993×10^{-39}	0.993×10^{-39}
GeH_4	1.030	1.021	1.032	1.039

[1] W. B. Steward and H. H. Nielsen, Phys. Rev. **48**, 861 (1935).
[2] E. Lee and G. B. B. M. Sutherland, Proc. Camb. Phil. Soc. **35**, 341 (1939).

3. Studies of Metallic Friction. R. I. STROUGH AND W. E. RUPP, *Case School of Applied Science.*—For the purpose of studying metallic friction under varying conditions of speed and normal load, a rotary testing apparatus was constructed. In this apparatus a flat disk-shaped sample of one material to be tested was mounted on a faceplate and

rotated in contact with three small pads of the other material. These pads were held in place by another stationary faceplate arranged so that the torque acting on it through friction between the samples could be measured. From this the coefficient of friction was computed. Friction phenomena of copper sliding dry on steel were studied with the above apparatus. Both kinetic and static coefficients of friction were observed to be higher for ground (crystalline) surfaces than for polished (non-crystalline) surfaces. Friction was observed to increase uniformly with the number of rotations of the disk for both types of surfaces until a critical point was reached where galling occurred and the coefficient of friction rose rapidly to a high value. Polished surfaces withstood about three times as many rotations as ground surfaces under similar conditions before galling occurred. The coefficient of friction was observed to be independent of sliding speed from speeds of 20 cm per second to the limit of the apparatus (200 cm per second) throughout the experiments.

4. Charge and Mass of Electronic Particles. ALFRED LANDÉ, *Ohio State University.*—The problem of explaining the empirical formula $e^2=ch/137$ is attacked from various angles that gradually seem to yield a reasonable picture of how the electronic charge is determined by quantum theory and relativity. From the *classical* point of view an electron can be characterized (1) by its rest energy E_0 proportional to its mass m, (2) by its "radius," or, better, by a characteristic time period t_0 inversely proportional to the mass. The customary radiation theory yields the wrong result that the energy is infinitely large and the radius is infinitely small. In order to get finite results a change of the theory is indispensable. We have suggested a formal change of the energy expression, analogous to the energy reduction due to radiative damping of a vibrating electron. The resulting finite energy E_0 is connected with a finite "damping radius" r_0 and with a finite time period $t_0=3mc^3/4\pi e^2$ characteristic for the damping. From the *quantum* point of view the product E_0t_0 can have only certain selected values that are obtained by a quantization in the energy-momentum space of Einstein's equation $E^2-(pc)^2=E_0^2$, and in a corresponding space $t^2-(r/c)^2=t_0^2$. The smallest eigenvalue of E_0t_0 turns out to be $\approx h/210$. This together with $E_0=mc^2$ and with the value of t_0 yields $e^2\approx hc/140$. A correction is necessary because t_0 was calculated for infinitely weak fields as against the actually finite self-field.

5. Determination of Mercury Arc Temperatures by X-Rays. CARL KENTY AND W. J. KARASH, *General Electric Co. and Case School of Applied Science.*—Molybdenum radiation at 32,000 volts, filtered through zirconium dioxide was used. Data for a graph of transmission *vs.* moles of Hg per sq. cm in the path of the beam were obtained by measuring transmissions of tubes with known amounts of Hg vapor. Direct-current temperature data were obtained for a hollow electrode, quartz lamp of 20-mm diameter and 29.0-cm arc length. Hg pressures, appendix controlled, were measured with a quartz pressure gauge.[1] Axial transmissions were measured. End corrections were determined by thermocouple measurements of wall temperatures, and pyrometer measurements of electrode temperatures. Axial temperatures were calculated from the perfect gas law. For a constant pressure of 1.0 atmosphere, the axial temperature varied approximately as the 20th root of the input, from 5950 deg. K at 30.7 watts per cm to 6100 deg. K at 58.5 watts per cm. For a constant input of 30.7 watts per cm, the axial temperature increased from 5950 deg. K at 0.22 atmosphere to 6450 deg. K at 0.40 atmosphere and then decreased to 5950 deg. K at 1.0 atmosphere. The probable error of the temperatures is estimated as 150 deg. K.

[1] Carl Kenty, Rev. Sci. Inst. **11**, 377 (1940).